General Disclaimer

One or more of the Following Statements may affect this Document

- This document has been reproduced from the best copy furnished by the organizational source. It is being released in the interest of making available as much information as possible.

- This document may contain data, which exceeds the sheet parameters. It was furnished in this condition by the organizational source and is the best copy available.

- This document may contain tone-on-tone or color graphs, charts and/or pictures, which have been reproduced in black and white.

- This document is paginated as submitted by the original source.

- Portions of this document are not fully legible due to the historical nature of some of the material. However, it is the best reproduction available from the original submission.

Produced by the NASA Center for Aerospace Information (CASI)

DEVELOPMENT OF SPUTTERED TECHNIQUES FOR THRUST CHAMBERS

INTERIM REPORT

March 1975

by: J. R. Mullaly, R. J. Hecht, T. E. Schmid,
and
C. T. Torrey

Pratt & Whitney Aircraft
Division of United Technologies Corporation
Contract NAS3-17792
National Aeronautics and Space Administration
Nasa-Lewis Research Center

J. M. Kazaroff, Program Manager

AUG 1975
RECEIVED
NASA STI FACILITY
INPUT BRANCH

10

1. Report No. NASA CR-134824	2. Government Accession No.	3. Recipient's Catalog No.

4. Title and Subtitle	5. Report Date August 1975
Development of Sputtered Techniques for Thrust Chambers, Interim Report	6. Performing Organization Code

7. Author(s) J.R. Mullaly, R.J. Hecht, T.E. Schmid, C.T. Torrey	8. Performing Organization Report No. FR-6924
	10. Work Unit No.

9. Performing Organization Name and Address Pratt & Whitney Aircraft Division of United Technologies Corporation Florida Research and Development Center P.O. Box 2691 West Palm Beach, Florida 33402	11. Contract or Grant No. NAS3-17792
	13. Type of Report and Period Covered Contractor Report
12. Sponsoring Agency Name and Address National Aeronautics and Space Administration Washington, D.C. 20546	14. Sponsoring Agency Code

15. Supplementary Notes

16. Abstract

The purpose of this program was to develop and evaluate techniques and materials for the fabrication and coating of advanced, long life, regeneratively cooled thrust chambers. The program was divided into five work tasks.

In Task I, five materials were evaluated as fillers for sputter application of OFHC copper as a closeout layer to channeled inner structures. Of the materials evaluated, aluminum was found to provide the highest bond strength and be the most desirable for chamber fabrication. The methods of filling with aluminum by flame spraying and slurry techniques were found to be unacceptable. CERROTRU®, a low melting Bi-Sn alloy, could be cast into channeled structures with low porosity levels. However, bond contamination during closeout layer application resulted in lower closeout bond strength than attained with a flame sprayed aluminum filler.

Task II of the program evaluated the structure and properties of thick sputtered OFHC copper, 0.15 Zr-Cu (AMZIRC®), Al_2O_3-Cu and SIC-Cu. In sputtering from a hollow (cathode) target configuration using a diode discharge (at the conditions evaluated), high substrate temperatures and low deposition rates were required to generate dense deposits of OFHC copper and be the most desirable for chamber fabrication. The use of substrate bias and a triode discharge in a hollow cathode was effective in generating dense deposits of 0.15 Zr-Cu at low substrate temperatures and moderately high deposition rates. However, deposits produced at these conditions were brittle. Post heat treatment was found effective in increasing the ductility of these deposits. In co-sputtering Al_2O_3 and Cu or SIC and Cu, it was not apparent that a true dispersion strengthened alloy was formed. However, co-sputtered deposits of both systems resulted in deposit strength over twice that of OFHC copper, and the highest of those evaluated in this task. The increased strength of the Al_2O_3-Cu and SIC-Cu was attributed to solid solution strengthening mechanisms.

In Task III layered structures of OFHC copper and 0.15 Zr-Cu were investigated as means of improving chamber inner wall fatigue life. Deposits having four layers, with increasing hardness from substrate to surface, were produced by sputtering from a post cathode. With the structures evaluated the OFHC copper layered structure did not affect low cycle fatigue properties over unlayered wrought OFHC copper. With the four layer 0.15 Zr-Cu structure of graded hardness low fatigue properties resulted. However, a thick 100% sputtered 0.15 Zr-Cu comprised of thirteen layers of constant hardness exhibited excellent fatigue properties.

The evaluation of sputtered Ti-5Al-2.5Sn, NASA IIb-11, aluminum and Al_2O_3-Al alloys as high strength chamber outer jackets was performed in Task IV. Of the materials evaluated, the NASA IIb-11 provided the highest tensile strength, as deposited. The aluminum and Al_2O_3-Al materials, as sputtered, exhibited tensile strengths over double that of wrought aluminum.

In Task V, techniques for refurbishing degraded thrust chambers with OFHC copper and coating thrust chambers with protective ZrO_2 and graded ZrO_2-copper thermal barrier coatings were developed. No decrease in fatigue strength was observed with OFHC copper sputtered to the inner wall surface of simulated chamber segments. Adherent ZrO_2 coatings were obtained by sputtering from a post cathode using a floating RF bias. Using sputter fabricated targets, techniques were developed to apply graded ZrO_2-copper coatings.

17. Key Words (Suggested by Author(s)) Sputtering CERROTRU© Thrust Chambers AMZIRC® OFHC Copper Coatings Flame Spraying	18. Distribution Statement Unclassified-Unlimited

19. Security Classif. (of this report) Unclassified	20. Security Classif. (of this page) Unclassified	21. No. of Pages 162	22. Price* $3.00

* For sale by the National Technical Information Service, Springfield, Virginia 22151

TABLE OF CONTENTS

TABLE OF CONTENTS (Continued)

LIST OF ILLUSTRATIONS

INTRODUCTION

In the development of advanced chambers for programs such as the Space Tug Experimental Engine Program, new fabrication techniques and/or materials will be needed to meet the projected chamber requirements. Of the techniques currently available for fabrication, deposition by sputtering offers the most potential of meeting the demands of the advanced designs. The application of sputtering techniques to the fabrication of thrust chambers permits relative freedom in materials selection for the chamber designer. Not being limited by the inability to electrodeposit a material and not having to sacrifice the material properties by elevated temperature joining operations, the chambers can be fabricated from practically any alloy or combination of alloys desired. Furthermore, the improved bonding obtainable with sputtering provides increased low-cycle fatigue life through improved materials and an elimination of joining materials at the bond interface. Previous work by McClanahan, Busch and Moss[1] has shown that precipitation-hardened and dispersion-strengthened copper alloys synthesized by sputtering offer potential as materials for fabricating regeneratively cooled thrust chambers. Furthermore, it was shown that a sputtered copper-0.15 zirconium alloy can be stronger than the same alloy produced by conventional primary forming techniques.

The proposed method for chamber fabrication involves the sputtering of an inner chamber wall, which is machined to a ribbed wall configuration. The chamber channels are then filled with a suitable material and the final closeout layer applied. Fabrication by this approach requires that the filler material be compatible with the vacuum sputtering environment. The filler must be capable of being applied to the channeled configuration and completely removed without degrading the chamber material properties. The inner wall structure and closeout layer could be (1) an alloy such as copper-0.15 zirconium; (2) a dispersion-strengthened, high-strength copper alloy; or (3) made of graded layers to promote improved fatigue capabilities. The sputter application of a high strength alloy outer chamber structure, with or without wire reinforcement, may permit further increases in chamber pressure to be attained, as indicated by the work of McCandless and Davies[2]. Refurbishment or surface protection by sputtering of inner wall coatings are further concepts for extending chamber life. It was the objective of this program to develop sputtering techniques for evaluating these concepts for advanced chamber fabrication and coating.

The investigation performed in this program was divided into five work tasks. Task I involved the application of an OFHC copper closeout layer to a ribbed wall cylinder to yield a cylindrical structure representative of regeneratively cooled thrust chambers. Within this task an evaluation of five materials to fill the grooved cylinder passages and selection of predeposition processing and sputtering deposition parameters compatible with the filler materials were performed. With the techniques developed, a cylindrical channeled structure was fabricated and was submitted to NASA-LeRC. In Task II, fabrication and evaluation of bulk sputtered OFHC Cu, Cu-0.15Zr, Al_2O_3-Cu, and SiC-Cu were performed. With the deposits fabricated, an investigation of structure, morphology, and tensile properties of each alloy was performed. The purpose of Task III was to investigate laminated cylindrical structures. The materials for this task were selected by NASA-LeRC from those evaluated in the second task of this program. One cylinder was sputter deposited with four layers of

OFHC copper and the other cylinder with four layers of Cu-0.15Zr. Each layer of the deposit was of different hardness. Each cylinder was evaluated for layer hardness, structure and bond integrity. Higher strength outer structures were evaluated in Task IV. Four sputtered alloys, NASA IIb-11, Ti-5Al-2.5Sn, aluminum, and Al-Al$_2$O$_3$ were evaluated for tensile properties. Task V of the program investigated techniques to refurbish and coat the inner surface of the thrust chambers. Inner surfaces of 7.6 cm (2.6 in.) internal diameter OFHC cylinders were sputtered with OFHC copper, ZrO$_2$ and graded OFHC copper-ZrO$_2$ coatings. These were evaluated for bond quality, structure and fatigue characteristics.

This report covers all the work performed in Tasks I through V of the program. This report includes the work that was separately reported in the Task I final report (NASA CR-134629).

TASK I

INTEGRAL COOLANT PASSAGE FILLER MATERIAL

The objective of this task is the evaluation of five candidate materials for use as fillers for the subsequent application by sputtering of the closeout layer to the inner structure of regeneratively cooled thrust chambers.

EQUIPMENT AND PROCEDURES

The equipment used for sputter deposition is shown schematically in figure 1. The vacuum chamber was of welded stainless steel construction, with elastomer sealed main flanges. All other flanges were metal sealed. The vacuum pumping system consisted of an air-driven aspirator pump, two liquid-nitrogen-cooled sorption pumps, and a 0.270 m^3/s ion pump. The target, substrate, and anode power supplies were all unfiltered fullwave-rectified DC supplies with a nominal 4.5% ripple. The filament current was provided by an AC power supply.

Except for the initial depositions, which used research grade argon, research grade 99.99% pure krypton[4] was employed as the sputtering gas. Pressure during sputtering was measured with a Pirani gauge, and the gauge reading corrected to the approximate krypton pressure. A Schultz-Phelps gauge was employed to detect rapid changes in pressure and served as a back-up gauge. The ion pump current was used to indicate pumpdown pressure.

For the closeout layer depositions, the targets, machined from Certified Grade 101 OFHC copper,[3] were 14.6 cm long with an outside diameter of 12.7 cm. Target internal diameters of 10.2, 11.4 and 11.7 cm were employed in the depositions performed. The targets were supported in a water-cooled stainless steel holder. The cylindrical substrates were held on a stainless steel or OFHC copper holder, water-cooled through a coaxial support tube.

The substrates were machined from Certified Grade 101 OFHC copper[3] tubing. Two configurations of cylindrical substrates were fabricated: fully grooved (figure 2) and quarter-grooved (figure 3). The blank cylinder was mounted on an aluminum arbor affixed to an indexing head. The grooves were machined using an 0.159-cm wide cutter. The cylinder was approximately 2.5 cm longer and 0.025 cm larger in diameter than the final dimensions desired. The excess length and diameter were machined off after filling to provide a clean surface on the ribs. The final machining and finishing operations were an integral part of the filler material evaluation and will be separately discussed.

The operational characteristics of the sputtering device did not depend, to first order, on substrate diameter. The selected substrate diameter of 6.1 cm was within the 5.1 to 7.6 cm requirement and minimized the machining required on the starting substrate material.

A general procedure was used for all depositions performed in this evaluation. The substrate with the desired surface finish was cleaned, installed on the substrate holder, and loaded into the vacuum chamber. The system was then rough pumped with an air-driven aspirator pump and sorption pump and ion pumped to high vacuum. The time required to reach a low base pressure was dependent on the filler material being evaluated.

3
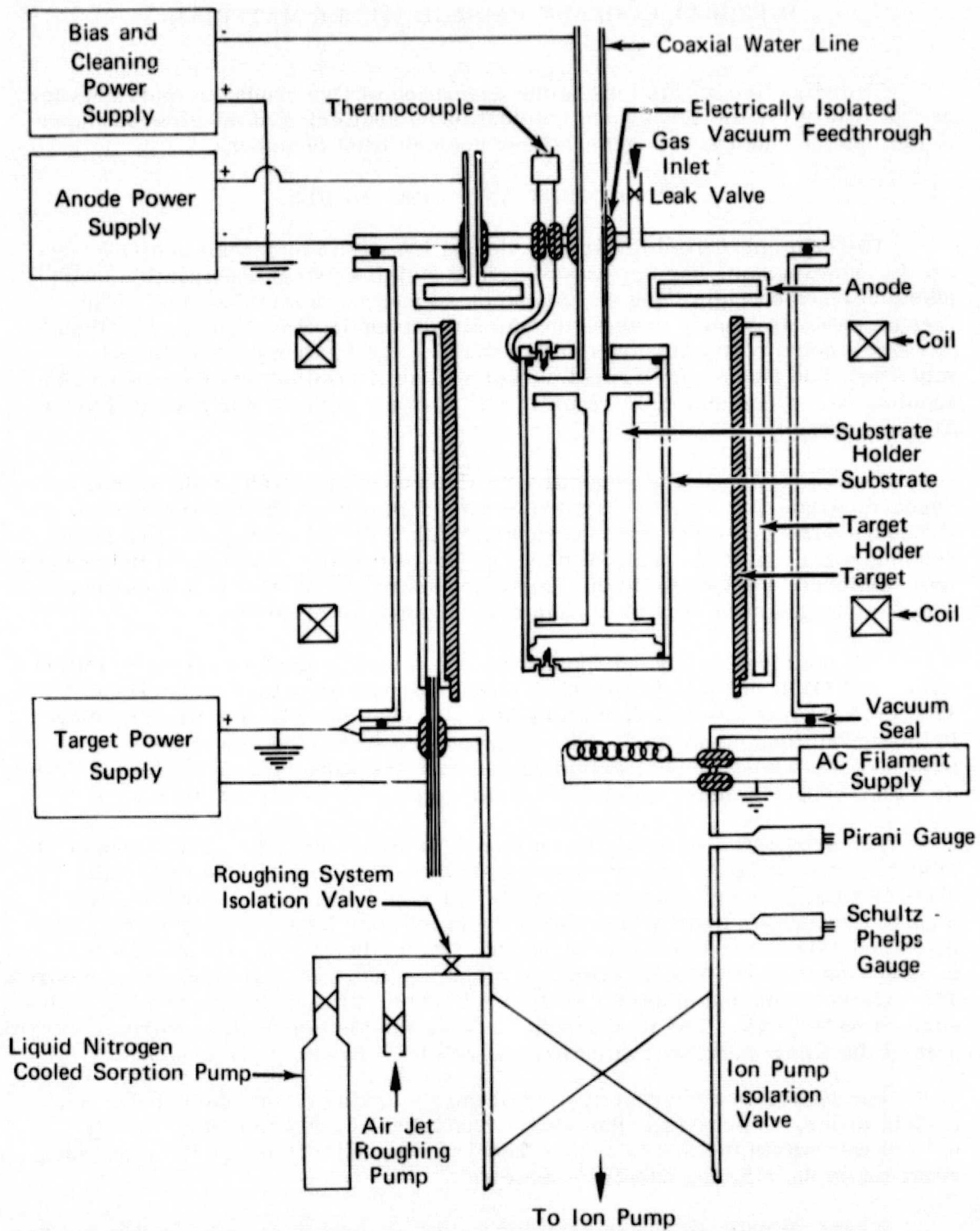
Figure 1. Schematic of Hollow Cathode Coater   FD 78478A
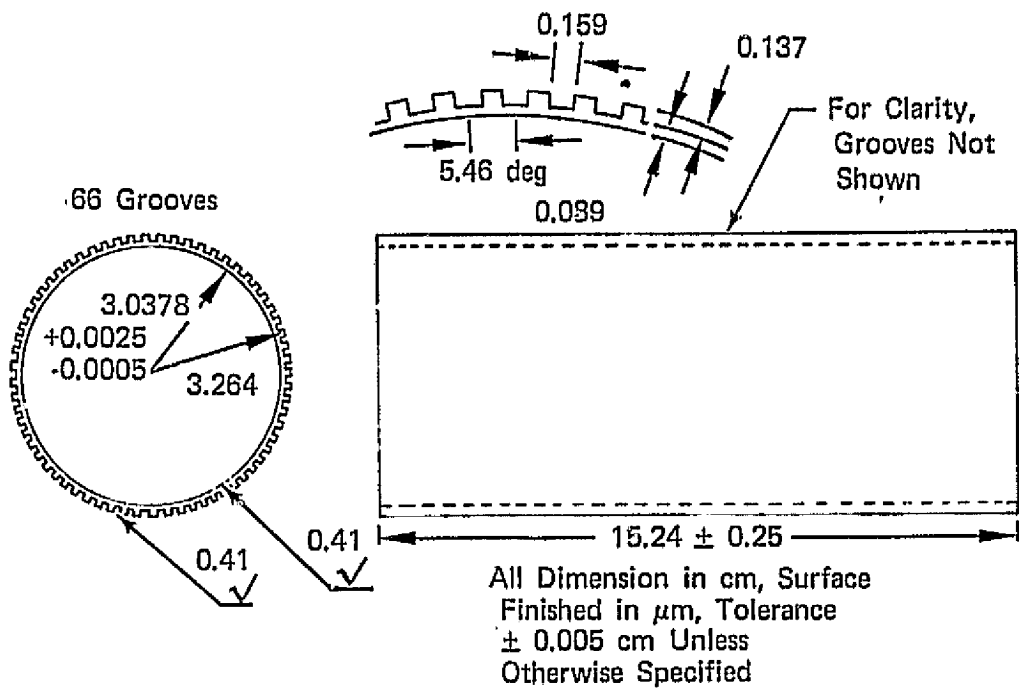
Figure 2. Fully Grooved OFHC Copper Substrate   FD 78464
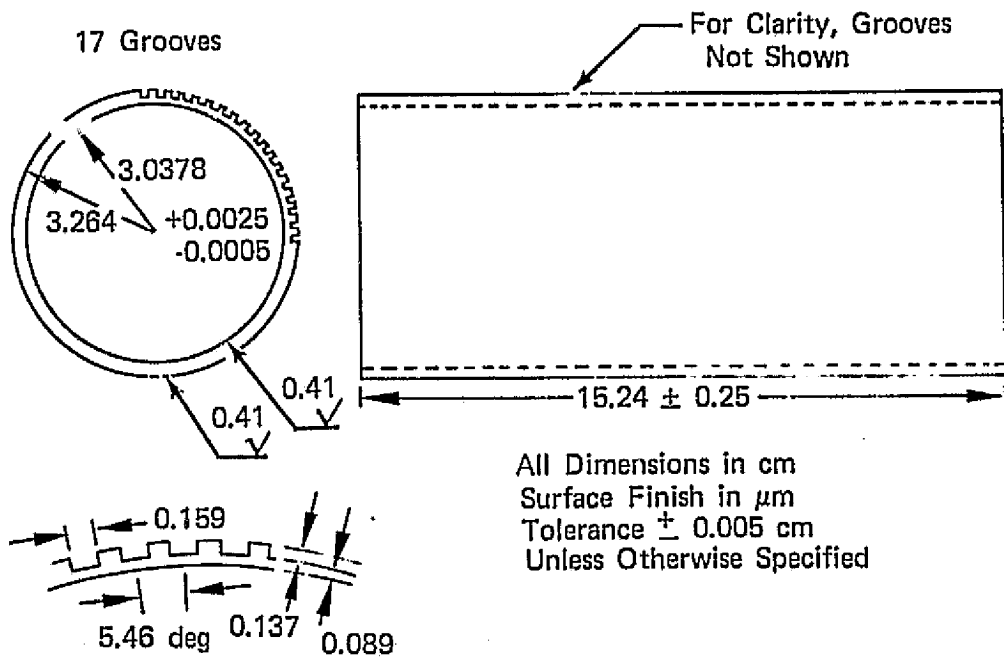
Figure 3. Quarter-Grooved OFHC Copper Substrate   FD 78465A

5

After pumping to high vacuum, argon or krypton was bled into the system and sputter cleaning (back sputtering) of the substrate started. Argon was used during the initial experiments (runs I-1 through I-9) because krypton was not available. Krypton was used in the latter runs because of the higher deposition rates resulting when this gas is used. During sputter cleaning, the magnetic field was established and a high negative substrate bias voltage applied. The purpose of the sputter cleaning is to remove gases and other contaminants from the substrate surface so that a high strength substrate-closeout layer bond is achieved. Substrate cleaning was usually accomplished by several cycles of ion bombardment, followed by pumping to high vacuum. Sputter cleaning the substrate also accomplished a partial clean-up of the target. During the final cleaning cycle, the target was sputtered simultaneously with the substrate. The cleaning cycles were continued until no increase in pressure was noted when the discharge was initiated.

To start deposition, the voltage and current to the target were increased to the desired level. Usually, target power was kept low at the start of deposition to minimize substrate heating and outgassing or vaporizing of the filler material.

· From the completed cylinder of each deposition, sections were removed for metallographic examination. These were typically mounted in clear epoxy and polished to a 1μ finish. Etching was performed exclusively with a solution of 5g $FeCl_3$, 10-ml HCl, 50-ml glycerin, and 30-ml water.

When closeout layer bond strength was to be determined, 2.5 by 2.5 cm square sections were removed for tensile testing. After removal of the filler material, these sections were bonded to tensile fixtures (figure 4) with EA951 Structural Adhesive[5] (450°K, 4.5-ks air cure) and pulled in tension normal to the bond interface at a strain rate of 8.3×10^{-5} cm/cm/s (0.005 in./in./min). Where high bond strengths were anticipated, the ribs on each side of the segment were cut to reduce bond area.

FILLER MATERIALS

Selection

The filler materials chosen for this evaluation (table I) included materials that could be applied by casting, flame or plasma spraying, or slurry techniques. Casting was to be limited to materials whose melting point was less than 450°K (177°C). Three low melting alloys CERROTRU®, CERROCAST®, and CERROBEND® [6] were selected for evaluation. CERROBEND was chosen for its low melting point and ease of application, while CERROCAST was selected because of its stability after casting and its noneutectic composition providing a nonunique freezing temperature. CERROTRU was selected because its net expansion upon freezing would provide a tighter mechanical bond to the groove walls.

The SERMETEL® 481 material[7] was selected because of the ease of application. This material is applied as a slurry and dried at 353°K (196°F). Usually, this material is then baked at 811°K (1000°F) to sinter the particles together to form a continuous aluminum matrix. This heat treatment was not to be performed, since this exposure would result in annealing the OFHC copper substrate.

6
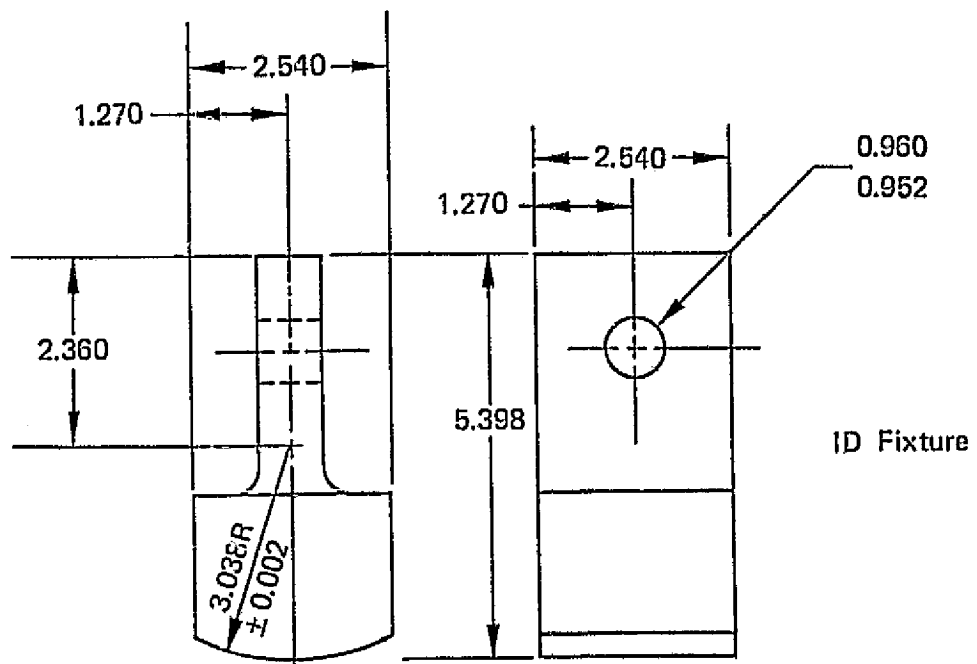
All Dimensions in cm
All Tolerances ± 0.005 cm
Unless Otherwise Specified
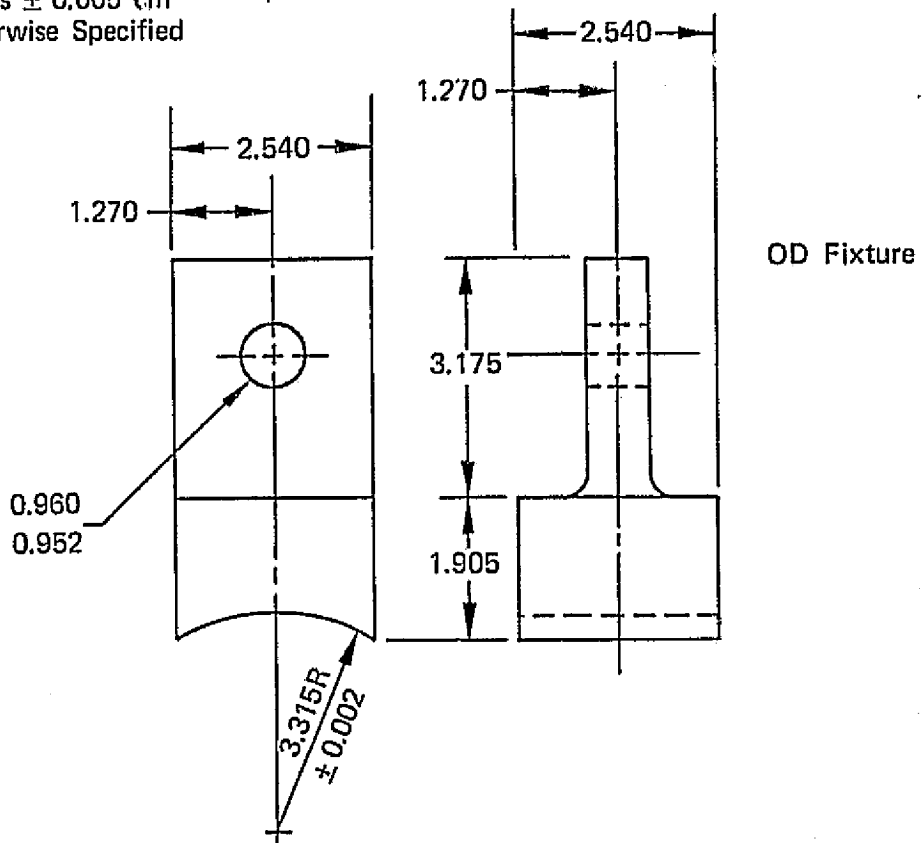
ID Fixture

OD Fixture

Figure 4. Tensile Fixtures for Determination of   FD 80757A
Closeout Layer Bond Strength

Table I. Filler Materials

Material	Melting Temperature, °K	°F	Composition, Percent by Weight
CERROBEND®	343	158	50Bi-26.7Pb-13.3Sn-10Cd
CERROCAST®	411-443	281-338	40Bi-60Sn
CERROTRU®	411	281	58Bi-42Sn
Aluminum	933	1220	99.9Al
SERMETEL® 481	933	1220	45Al-54.5NaSiO$_4$-0.5ZnO

Pure aluminum, applied by flame spraying, provided the final filler material examined. Ranging in density from 85 to 90% of theoretical density, this material could be easily machined and easily removed by leaching in a NaOH solution. Aluminum and SERMETEL 481 allowed higher substrate temperatures to be maintained during deposition of the closeout layer.

Filling Techniques

All CERRO® Alloys examined in this program as possible filler materials were cast into the grooves using the same technique. (See figure 5.) The technique consisted of three steps: preparation of the cylinder, casting of the CERRO Alloy, and removal of the cylinder from the casting.

Typically, the cylinder was prepared by vapor blasting or sanding the grooves to remove burrs and contaminants and washed with methanol. The ends of the cylinder were tightly plugged. The cylinder was then tightly wrapped with 0.0127-cm Ti-6Al-4V sheet so that it extended slightly beyond the copper cylinder ends. The titanium alloy sheet was secured with 0.025-cm diameter wire at two positions along the cylinder length. This assembly was then preheated for 2 to 3 min in an air furnace at 477 ± 10°K (399.2 ±20°F).

Approximately 3.9 kg of CERRO Alloy was melted in a PYREX® container and the molten alloy skimmed to remove floating contaminants. The preheated cylinder was pushed vertically into the molten CERRO Alloy so that the top edge of the copper cylinder was below the surface of the molten CERRO Alloy. Since a difference in pressure exists, the molten CERRO Alloy is forced up the passages formed by the titanium alloy sheet and the grooved copper cylinder. Vibrating the assembly assisted the movement of entrapped bubbles up the grooves and assured complete filling of the passages. The whole assembly was then allowed to cool to room temperature.

After removing the outer glass container, the excess CERRO Alloy was broken away, and the titanium-alloy sheet and the end plugs removed to complete the process. The filled grooves were visually examined for entrapped porosity and subsequently machined to final dimensions. This entailed removal of 2.54 cm from the cylinder length and 0.0254 cm from the outside diameter.
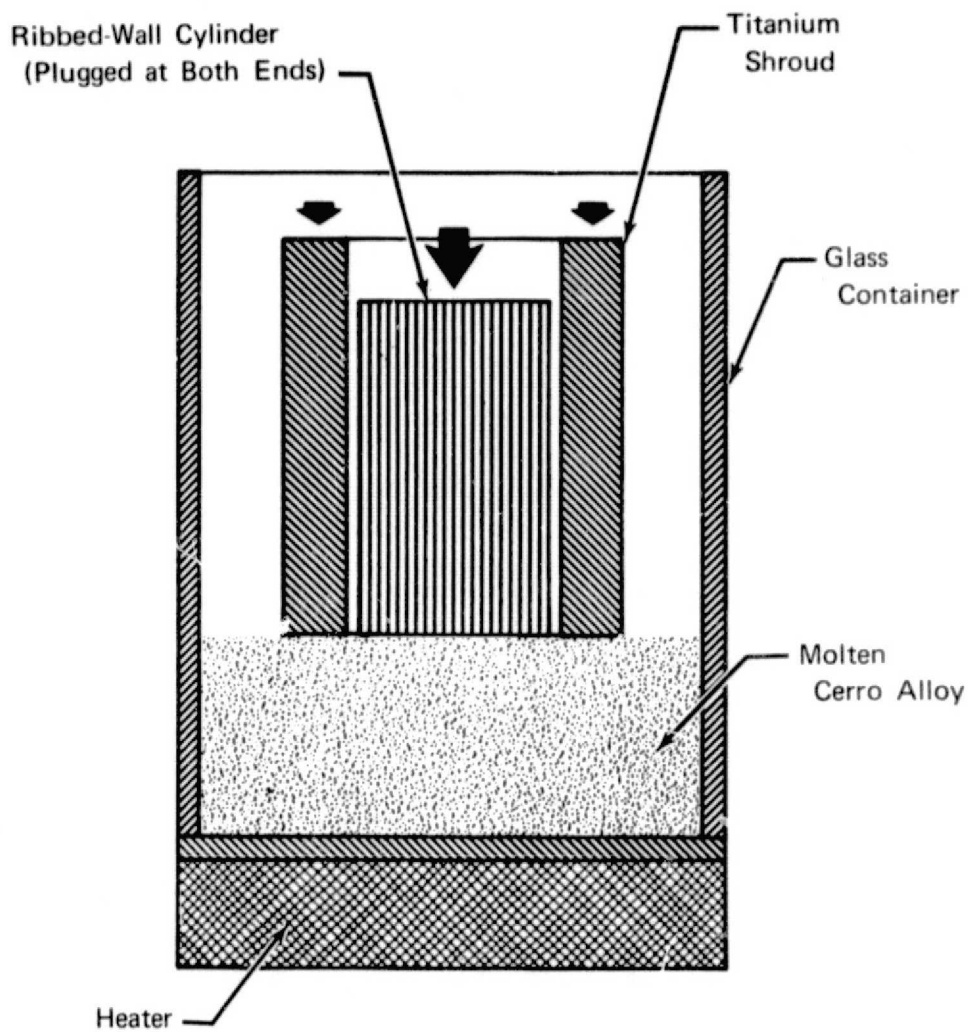
A. Preheated Cylinder and Shroud Pushed Vertically Into Molten Cerro Alloy
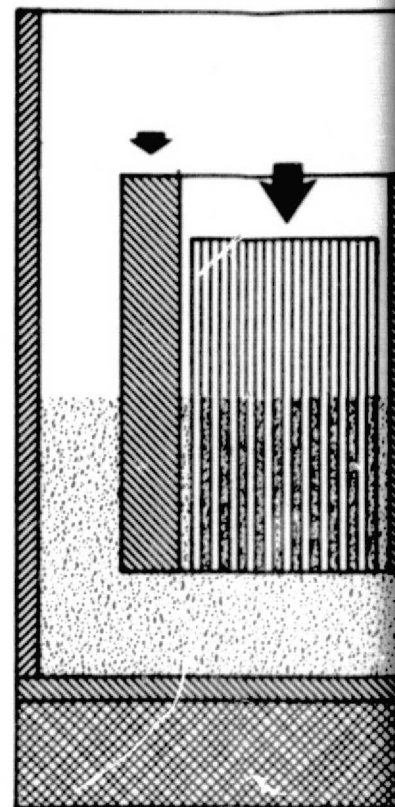
B. Cerro Alloy is Forced up The C...
Rate Immersion Into The Molte...

Figure 5. Procedure for Filling Ribbed Wall Cylinder With CERRO® Alloys
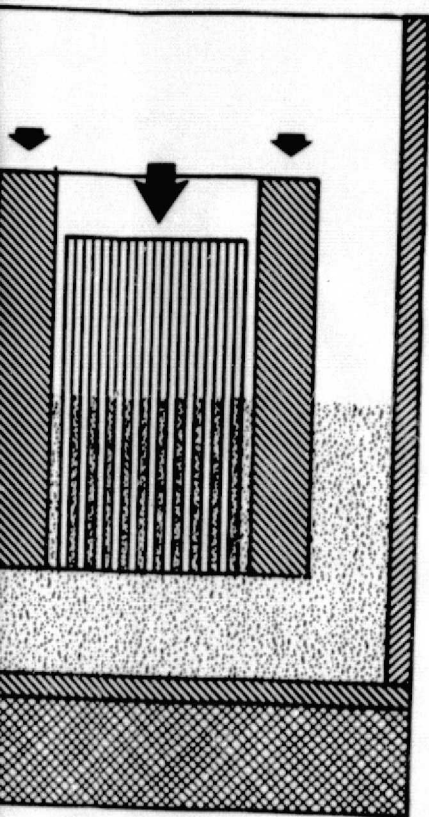
is Forced up The Grooved During Slow
rsion Into The Molten Pool
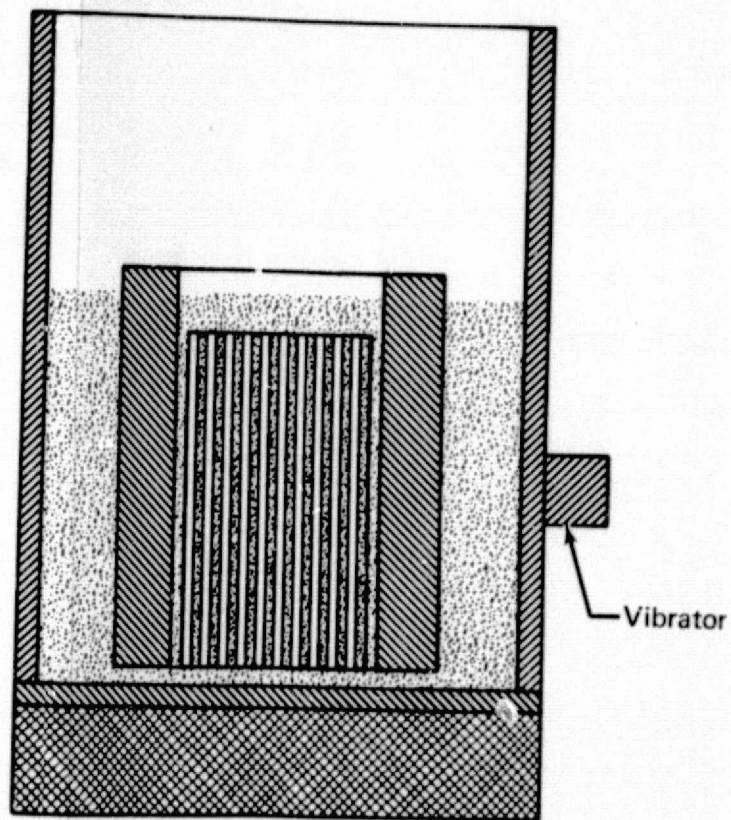
C. Upon Complete Immersion and Filling The Grooves, The
   Cylinder is Vibrated to Remove Entrapped Bubbles. The
   Cerro Alloy is Then Allowed to Solidify. The Outer
   Glass Container, Excess Cerro Alloy, and Titanium
   Shroud are Removed and The Filled Cylinder
   Machined to Final Dimensions.

FD 91445

The aluminum filler material was applied to the vapor-blasted cylinder by flame spraying. After approximately 0.025 cm of aluminum was applied, the excess was removed from the ridges between the grooves. This procedure was continued until the flame-sprayed aluminum completely filled the grooves. The cylinder was then machined to final dimensions.

The SERMETEL 481 filler was trowelled into the grooves and baked at 353°K (176°F) for approximately 1 hr. The filled cylinder was then machined to final dimensions.

Machining Operations

The removal of the final 0.025 cm from the diameter of the cylinders after filling was performed using a variety of machining techniques. These included: the normal lathe turning operation, longitudinal surface grinding, longitudinal milling, and bidirectional dry machining. The several techniques were tried in an attempt to minimize smearing of the filler material onto the rib lands and to eliminate the formation of cracks along the grooves due to the filler material being pulled away from one side of the groove. Each operation is described in some detail in the following paragraphs.

Normal Lathe Machining – The filled cylinder was mounted on an aluminum arbor, rotated axially at 3 rev/s. Using a carbide cutting tool, traversing at 0.005 cm per revolution, approximately 0.013 cm was removed from the radial dimension per pass during the initial rough machining and approximately 0.002 cm was removed from the radial dimension per pass during the final finishing operation. No lubricants were used at any time during this machining operation. Trimming to length was performed as the final operation in this and all subsequent machining techniques to be discussed.

Longitudinal Surface Grinding – The filled cylinder was mounted on an aluminum arbor attached to an indexing fixture. The surface grinding operation was performed using an AF-1226 grinding wheel, rotating at about 40 rev/s and traversing the specimen lengthwise at 0.1 cm/s. Removal of 0.0013 cm per pass resulted in a flat surface approximately 0.3 cm wide. After each pass the cylinder was rotated 5.46 deg. A water soluble lubricant was used throughout the surface grinding operation.

Longitudinal Milling – The basic setup for the longitudinal milling operation was the same as that used for the surface grinding operation. In this operation, a 1.9-cm diameter carbide end mill rotating at 5 rev/s traversed the cylinder at 0.1 cm/s. The axis of rotation of the end mill was parallel to the tangent plane of the surface being milled and orthogonal to the cylinder axis. The cylinder was rotated 5.46 deg after each pass. After milling, the cylinder had 66 flats approximately 0.3 cm wide about the circumference. A water-soluble lubricant was used in this machining operation.

Bidirectional Dry Machining – The dry machining operation was performed on a reversing lathe with the cylinder mounted on an aluminum arbor and rotated at 2.3 rev/s. Using a TGB 431 cutting tool, traversed at 4.5×10^{-3} cm per revolution, approximately 0.0025 cm was removed per pass. The lathe rotation was reversed for the final two passes. The cylinder was then polished with 600-grit SiC paper in both directions on the lathe to complete the process. No lubricants were used at any time during the dry machining operation.

11

Finishing Operations

Several techniques were employed throughout this program to either eliminate the smearing of the filler material onto the rib lands, reduce the surface porosity of the filler materials, eliminate the pulling of the filler away from one side of the grooves, or affect the surface finish of the substrate. These operations included shot peening, vapor blasting, glass bead peening, chemical polishing, and mechanical polishing, and, in some cases, a sequence of several of these.

Shot Peening - The shot peening was performed using SAE 170 cast steel shot at a carrier air pressure of 0.210 MN/m^2 (30 psi). The orifice was held 3 to 7 cm from the surface. The flow was directed normal to the surface and traversed in such a way that a given point experienced 3 to 5 sec of peening.

Vapor Blasting - The vapor blasting operation was performed using a water slurry of 325-grit NOVACULITE® with a water pressure of 0.55 to 0.69 MN/m^2 (80 to 100 psi). Typically, the nozzle was held approximately 20 cm from and 45 deg inclined to the surface of the cylinder. Vapor blasting was performed until the desired surface finish was achieved.

. Glass Bead Peening - The glass bead peening operation was performed using 0.0177- to 0.0296-cm diameter glass beads impinging normal to the surface from a nozzle held 5 to 10 cm from the surface. Typically, the peening operation was performed with a water carrier operating at a line pressure of 0.55 to 0.69 MN/m^2 (80 to 100 psi). The nozzle was traversed at such a rate that a given point on the surface experienced approximately 5 sec of peening.

Chemical Polishing - Chemical polishing was accomplished by placing the work piece in a solution consisting of equal portions of H_3PO_4, CH_3COOH. and HNO_3 for 5 sec. The solution was typically heated to 348 ±5°K. Immersion in distilled water followed by an ethanol rinse completed the process.

Mechanical Polishing - Mechanical polishing was performed using a hand-held, air-operated tool. The polishing media, 6μ paste, was applied to the MICROCLOTH® disk affixed to the polishing tool. A VARSOL® carrier was liberally applied to the work piece throughout the polishing operation. Polishing pressure and direction were left to the discretion of the operator performing the polishing.

The surfaces of many cylinders were finished by sanding with 600-grit SiC paper using no lubricants. Both lengthwise and circumferential sanding were employed, although both were not necessarily used on every cylinder. The sanding operation was continued until the desired surface finish was achieved.

Sputter Cleaning and Closeout Layer Deposition

After the filled cylinder had been machined to final dimensions and the surface finished to the desired degree, a final cleaning was performed prior to insertion in the vacuum chamber. Sputter cleaning (back sputtering) was employed to remove surface contaminants that could degrade the interface between the substrate and the closeout layer. (See table II.) The deposition cycle (table III) immediately followed the sputter cleaning operation. In some cases, the two processes were performed simultaneously, i.e., while one was being phased in the other was being phased out. Whenever the deposition was stopped for any significant period of time, a sputter cleaning cycle was performed prior to re-initiating the deposition cycle.

12

Table II. Summary of Cylinder Preparation and

Run Number	Cylinder Number	Cylinder Configuration	Filler Material	Machining, Finishing Treat Preparation, and Primar
I-1	None	–	None	Lathe machined, light vapor bl distilled water rinse, methanol
I-2	None	–	None	Lathe machined, heavy vapor b distilled water rinse, methanol
I-3	C-1	Fully grooved	CERROBEND[R]	Lathe machined, light vapor bl distilled water rinse, methanol
I-4	C-3	Fully grooved	CERROBEND[R]	Lathe machined, degreased, A distilled water rinse, methanol
I-5	C-1	Fully grooved	CERROBEND[R]	Lathe machined, 25% 6μ polish peen, 50% vapor blast, degreas water rinse, methanol rinse
I-6	C-4	Quarter grooved	CERROTRU[R]	Lathe machined, 90% vapor bla polish, degrease, methanol rin
I-7	C-5	Quarter grooved	CERROTRU[R]	Lathe machined, vapor blast, rinse, methanol rinse
I-8	C-9	Quarter grooved	SERMETEL[R] 481	Lathe machined, vapor blast, rinse, methanol rinse
I-9	C-7	Quarter grooved	Aluminum	Lathe machined, vapor blast, rinse, methanol rinse
I-10	C-8	Quarter grooved	Aluminum	Lathe machined, vapor blast, rinse, methanol rinse
I-11	C-4	Quarter grooved	CERROTRU[R]	Lathe machined, glass bead po water rinse, methanol rinse
I-12	C-12	Quarter grooved	Aluminum	Surface ground, sanded No. 12 followed by No. 325 paper, vap distilled water rinse, methanol
I-13	C-10	Quarter grooved	Aluminum	Milled lengthwise, glass bead water rinse, methanol rinse
I-14[2]	C-14	Quarter grooved	Aluminum	Milled lengthwise, vapor blast peen, vapor blast, distilled wa methanol rinse

...ng, Finishing Treatment, Surface ...ration, and Primary Cleaning	Sputter Cleaning			Pressure,	
	Voltage, V	Current, mA	Duration, s	N/m^2	μ
...ined, light vapor blast, AJAX[R] scrub, ...ter rinse, methanol rinse	–	None	–	–	–
...ined, heavy vapor blast, AJAX[R] scrub, ...ter rinse, methanol rinse	–	None	–	–	–
...ined, light vapor blast, AJAX[®] scrub, ...ter rinse, methanol rinse	–300	50	300	1.3	10
...ined, degreased, AJAX[®] scrub, ...ter rinse, methanol rinse	–450	50	300	4.5	34
...ined, 25% 6μ polish, 25% glass bead ...apor blast, degrease, distilled ..., methanol rinse	–450	50	300	4.0	30
...ined, 90% vapor blast, 10% 6μ ...rease, methanol rinse	–450	50	300	3.1	23
...ined, vapor blast, distilled water ...anol rinse	–500	50	300	3.6	27
...ined, vapor blast, distilled water ...anol rinse	None–system would not pump down due to filler outgassing				
...ined, vapor blast, distilled water ...anol rinse	–900 / –600	300 / 300	60 / 60	5.5	41
...ined, vapor blast, distilled water ...anol rinse	–700 / –750	300 / 300	60 / 300	3.3	25
...ined, glass bead peen, distilled ..., methanol rinse	–700 / –700	300 / 300	60 / 60	3.9	29
...und, sanded No. 120 paper ...No. 325 paper, vapor blast, ...ter rinse, methanol rinse	–650 / –750	300 / 300	60 / 900	3.9	2.9
...hwise, glass bead peen, distilled ..., methanol rinse	–675	300	660[1]	3.9	2.9
...hwise, vapor blast, glass bead ...blast, distilled water rinse, ...nse	–250	300	1620[3]	1.2	9

Table II. Summary of Cylinder Preparation and Sputter Cle

Run Number	Cylinder Number	Cylinder Configuration	Filler Material	Machining, Finishing Treat Preparation, and Primar
I-15[4]	C-11	Quarter grooved	None	No machining, 25% sanded No. vapor blast, 25% glass bead pe distilled water rinse, methanol
I-16	C-17	Quarter grooved	Aluminum	Milled lengthwise, glass bead (54 hr) vacuum bake, vapor bl soak (ultrasonic)
I-17	C-14	Quarter grooved	CERROTRU[R]	Milled lengthwise, 50% sanded paper, 50% chemical polish[6], rinse, methanol rinse
I-18	C-19	Quarter grooved	CERROTRU[R]	Milled lengthwise, sanded leng paper, ethyl alcohol rub
I-19	C-15	Quarter grooved	Aluminum	Milled lengthwise, shot peened lengthwise, sanded lengthwise AJAX[R] scrub, methanol rub,
I-20	C-18	Quarter grooved	Aluminum	Dry milled lengthwise, dry ma lengthwise No. 600 paper, AJA methanol rub, ethyl alcohol ri
I-21	C-21	Fully grooved	CERROTRU[R]	Dry machined, sanded lengthwi AJAX[R] scrub, ethyl alcohol ri
I-22	C-22	Fully grooved	Aluminum	Dry machined, sanded lengthw AJAX[R] scrub, methanol rub,
I-23	C-20	Fully grooved	CERROTRU[R]	Dry milled lengthwise, machin wise No. 600 paper, AJAX[R] s ethyl alcohol rinse
I-24	C-22	Quarter grooved	Aluminum	Dry milled lengthwise, etched (3 hr) vacuum bake, methanol
I-25	C-20	Fully grooved	CERROTRU[R]	Dry machined, sanded lengthw AJAX[R] scrub, methanol rub,

Notes:

[1] 120 s, 240 s, and 300 s cleaning cycle with pump down between cycles

[2] Triode operation during cleaning; filament at 7.5V (108A), anode at +40V (5A)

[3] 60 s, 180 s, 600 s, 480 s, and 300 s cleaning cycle with pump down between cycles

[4] Triode operation during cleaning cycle; filament at 7V (110A), anode at +40V (7.2A)

[5] 60 s, 120 s, 180 s, 300 s and 120 s cleaning cycle with pump down between cycles + 180s t

[6] 1/3 HNO_3, 1/3 H_3PO_4, 1/3 CH_3COOH heated to 348°K

[7] 225 mA substrate current for first few seconds.

...ning, Finishing Treatment, Surface ...paration, and Primary Cleaning	Sputter Cleaning			Pressure, N/m^2	μ
	Voltage, V	Current, mA	Duration, s		
...ing, 25% sanded No. 600 paper, 25% ...t, 25% glass bead peen, 25% untreated, ...ater rinse, methanol rinse	−500	500	1200	2.2	17
...gthwise, glass bead peen, 800°F ...cuum bake, vapor blast, methanol ...sonic)	−800	300	960[5]	3.9	29
...gthwise, 50% sanded lengthwise No. 600 ...% chemical polish[6], distilled water ...thanol rinse	−500	60	1200	3.6	27
...gthwise, sanded lengthwise No. 600 ...yl alcohol rub	−500	70	840	3.6	27
...gthwise, shot peened, dry milled ..., sanded lengthwise No. 600 paper, ...rub, methanol rub, methanol rinse	−500	65	600	3.6	27
...l lengthwise, dry machined, sanded ...No. 600 paper, AJAX® scrub, ...rub, ethyl alcohol rinse	−500	70	600	3.3	25
...ned, sanded lengthwise No. 600 paper, ...rub, ethyl alcohol rinse	−500	70[7]	300	3.3	25
...ned, sanded lengthwise No. 600 paper, ...rub, methanol rub, ethyl alcohol rinse	−500	100	1020	3.3	25
...lengthwise, machined, sanded length-...00 paper, AJAX® scrub, methanol rub, ...ol rinse	−500	55	240	3.3	25
...lengthwise, etched dilute HNO_3, 400°F ...um bake, methanol rub	−1000	100	1200	2.7	20
...ned, sanded lengthwise No. 600 paper, ...rub, methanol rub, ethyl alcohol rinse	−500	70	1200	3.9	29

...0V (5A)

...ween cycles

...t +40V (7.2A)

...een cycles + 180s target phase in cycle

Table III. Summary of Deposition

Run Number	Cylinder Number	Cylinder Configuration	Filler Material	Substrate Voltage, V	Current, mA	Target Voltage, V	Current, A	Magnetic Coils Current, A	Separ...
								TARGET A - 10.2	
I-1	None	--	None	Ground	-	-600	5.0	7.0	6.4
I-2	None	--	None	Ground	-	-530	5.1	7.7	6.4
I-3	C-1	Fully Grooved	CERROBEND®	-125	3	-450	4.0	7.7	6.4
				Ground	-	-450	4.0	7.7	6.4
I-4	C-3	Fully Grooved	CERROBEND®	-250	5	-430	3.0	7.5	7.6
								TARGET B - 10.2	
I-5	C-1	Fully Grooved	CERROBEND®	-100	65	-620	1.0	5.0	7.6
				-100	65	-690	1.5	6.0	7.6
				Ground	-	-670	1.5	6.0	7.6
I-6	C-4	Quarter Grooved	CERROTRU®	-35	6	-500	4.0	7.5	7.6
I-7[1]	C-5	Quarter Grooved	CERROTRU®	-50	45	-690	1.5	5.0	7.6
				Ground	-	-690	1.5		
I-8	C-9	Quarter Grooved	SERMETEL® 481	No deposition; system would not pump down due to filler outgassing
I-9	C-7	Quarter Grooved	Aluminum	-200	140	-700	1.2	5.0[2]	7.6
				-100	140	-700	2.0	7.0	7.6
I-10	C-8	Quarter Grooved	Aluminum	-300	250	-725	1.8	5.0	7.6
I-11	C-4	Quarter Grooved	CERROTRU®	-250	215	-800	1.9	5.0	7.6
								TARGET C - 10.2	
I-12[3]	C-12	Quarter Grooved	Aluminum	-250	175	-850	2.0	7.0	3.8
				-250	175	-1000	0.8	7.0	3.8
								TARGET D - 11.5	
I-13	C-10	Quarter Grooved	Aluminum	-500	250	-750	1.5	5.0	7.0
I-14	C-13	Quarter Grooved	Aluminum	Ground[4]	0	-500	0.8	0.0	7.0
				-350	120	-650	1.3	5.0	7.0
				-150	59	-650	1.3	5.0	7.0
I-15[5]	C-11	Quarter Grooved	None	Ground	0	-720	1.9	5.0	7.
				-100	60	-720	1.9	5.0	7.
				-200	100	-720	1.9	7.5	7.
				-200	194	-750	4.4	7.5	7.
				-100	84	-750	4.4	7.5	7.
I-16	C-17	Quarter Grooved	Aluminum	-500	140	-500	1.0	5.0	7.
				-250	60	-570	1.4	5.0	7.
				-250	89	-670	2.0	5.0	7.
				-250	89	-650	2.0	5.0	7.
				-150	89	-650	4.8	7.5	7.
I-17	C-14	Quarter Grooved	CERROTRU®	-500	86	-450	1.0	5.0	7.
				-250	75	-615	2.0	5.0	7.
				-100	84	-905	4.0	5.0	7.

PRECEDING PAGE BLANK NOT FILMED

FOLDOUT FRAME)

	Magnetic Coils		Time,		Substrate Temperature,		Maximum Closeout Layer Thickness,		Maximum Deposition Rate,		Pressure,	
nt,	Current, A	Separation, cm	ks	hr	°K	°F	mm	mils	nm/s	mil/hr	N/m²	μ
TARGET A – 10.2 cm ID												
	7.0	6.4	25.2	7.0	322	120	0.533	21.0	21.1	3.0	1.3	10
	7.7	6.4	23.4	6.5	341	155	0.584	23.0	24.9	3.5	0.9	7
	7.7	6.4	7.2	2.0	336	145	0.558	22.0	30.9	4.4	1.5	11
	7.7	6.4	10.8	3.0								
	7.5	7.6	18.0	5.0	350	170	0.407	16.0	22.6	3.2	1.5	11
TARGET B – 10.2 cm ID												
	5.0	7.6	7.2	2.0	350	170	0.173	6.8	8.0	1.1	4.0	30
	6.0	7.6	7.2	2.0	358	185						
	6.0	7.6	7.2	2.0	358	185						
	7.5	7.6	18.0	5.0	341	155	NM	NM	NM	NM	1.7	13
	5.0	7.6	16.2	4.5	380	225	0.170	6.7	7.5	1.1	3.6	27
			6.3	1.75	526	487						
own due to filler outgassing												
	5.0[2]	7.6	16.2	4.5	339	151	0.142	5.6	7.5	1.1	5.3	40
	7.0	7.6	2.7	0.75	354	178					7.2	54
	5.0	7.6	18.9	5.25	324	124	0.173	6.8	9.1	1.3	4.5	34
	5.0	7.6	21.6	6.0	349	169	0.241	9.5	11.1	1.6	3.9	29
TARGET C – 10.2 cm ID												
	7.0	3.8	10.8	3.0	383	231	0.127	5.0	8.8	1.3	5.6	42
	7.0	3.8	3.6	1.0	362	192						
TARGET D – 11.5 cm ID												
	5.0	7.6	40.5	11.25	355	180	0.280	11.0	6.9	1.0	3.9	29
	0.0	7.6	20.7	5.75	656	722	0.231	9.1	5.1	0.8	1.1	8
	5.0	7.6	10.8	3.0		–					3.9	29
	5.0	7.6	13.5	3.75		–					3.9	29
	5.0	7.6	8.1	2.25	566	560	0.295	11.6	10.9	1.6	3.6	27
	5.0	7.6	7.2	2.0								
	7.5	7.6	7.2	2.0								
	7.5	7.6	0.9	0.25								
	7.5	7.6	3.6	1.0								
	5.0	7.6	1.8	0.5	482	408	0.580	22.8	12.9	1.8	3.9	29
	5.0	7.6	2.7	0.75								
	5.0	7.6	14.4	4.0								
	5.0	7.6	9.7	2.75								
	7.5	7.6	16.2	4.5								
	5.0	7.6	14.4	4.0	364	195	0.052	2.0	3.6	0.5	3.6	27
	5.0	7.6	14.4	4.0			0.129	5.1	9.0	1.3		
	5.0	7.6	22.5	6.25			0.493	19.4	21.9	3.1		

Table III. Summary of Deposition Pa

Run Number	Cylinder Number	Cylinder Configuration	Filler Material	Substrate		Target		Magnetic Coils	
				Voltage, V	Current, mA	Voltage, V	Current, A	Current, A	Separa cn
								TARGET E - 11.7	
I-18	C-19	Quarter Grooved	CERROTRU®	-500	60	-470	0.5	5.0	7.6
				-500	60	-450	0.5	5.0	7.6
				-500	90	-615	1.0	5.0	7.6
				-500	155	-800	3.0	7.0	7.6
				-0.6	73	-730	3.0	7.0	7.6
				-25	18	-760	4.0	7.5	7.6
I-19	C-15	Quarter Grooved	Aluminum	-500	70	-450	0.7	5.0	7.6
				-250	42	-450	0.8	5.0	7.6
				-250	40	-450	0.8	5.0	7.6
				-250	50	-600	1.1	5.0	7.6
				-250	53	-600	1.1	5.0	7.6
				-100	63	-1000	2.0	5.0	7.6
I-20	C-18	Quarter Grooved	Aluminum	-500	70	-450	0.7	5.0	7.6
				-250	54	-600	1.1	5.0	7.6
				-100	65	-1000	2.1	5.0	7.6
I-21	C-21	Fully Grooved	CERROTRU®	-500	75	-450	0.9	5.0	7.6
				-500	80	-500	1.1	5.0	7.6
				-500	160	-1000	2.4	5.0	7.6
I-22	C-22	Fully Grooved	Aluminum	-50	0	-350	0.9	6.5	7.6
				-50	0	-250	0.9	6.5	7.6
				-25	10	-600	4.2	6.5	7.6
I-23	C-20	Fully Grooved	CERROTRU®	-500	65	-350	0.7	5.0	7.6
				-500	60	-350	0.5	5.0	7.6
				-500	80	-450	1.2	5.0	7.6
				-500	100	-550	1.8	5.2	7.0
				-500	155	-800	3.3	5.0	7.6
				-500	140	-1000	2.0	4.0	7.6
				-25	21	-1000	2.3	4.0	7.6
				-25	25	-1000	5.0	5.0	7.6
				-250	90	-1000	5.0	4.8	7.6
I-24[6]	C-16	Quarter Grooved	Aluminum	-500	140	-800	4.0	4.7	7.6
				-25	21	-1000	4.0	4.1	7.6
				0	0	-1000	3.4	4.5	7.6
				0	0	-1000	2.5	4.5	7.6
				0	0	-800	3.5	7.5	7.6
				0	0	-700	4.5	8.0	7.6
								TARGET F - 11.7	
I-25	C-23	Fully Grooved	CERROTRU®	-900	50	-400	0.6	5.0	7.6
				-400	84	-550	1.1	5.0	7.6
				0	0	-700	1.0	5.0	7.6
				0	0	-1000	1.7	5.0	7.6
				0	0	-1000	3.2	6.0	7.6

NOTES:

[1] Operated in triode mode last 1.75 hr

[2] For first hour of operation, 5A coil current was used

[3] Discharge unstable during entire run

[4] Triode operation with filament at 8.5 v (115a) and anode at +40v (15a) for first 5.75 hr

[5] Filament operated without anode to heat substrate throughout run

[6] After 5.5 hr, system evacuated, 5 min back sputter 1000 v (230 mA) at 25μ pressure

NM - Not Measured

	Magnetic Coils		Time,		Substrate Temperature,		Maximum Closeout Layer Thickness,		Maximum Deposition Rate,		Pressure,	
ent,	Current, A	Separation, cm	ks	hr	°K	°F	mm	mils	nm/s	mil/hr	N/m²	µ
	TARGET E - 11.7 cm ID											
	5.0	7.6	14.4	4.0	NM		0.021	0.8	1.5	0.2	3.3	25
	5.0	7.6	15.3	4.25			0.024	0.9	1.6	0.2		
	5.0	7.6	19.8	5.50			0.078	3.1	4.0	0.6		
	7.0	7.6	6.3	1.75			0.099	3.9	15.7	2.2		
	7.0	7.6	2.7	0.75			0.037	1.4	13.7	1.9		
	7.5	7.6	26.1	7.25			0.550	21.6	21.1	3.0		
	5.0	7.6	1.8	0.5	NM		0.003	0.1	1.7	0.2	3.2	24
	5.0	7.6	5.4	1.5			0.013	0.5	2.4	0.4		
	5.0	7.6	18.0	5.0			0.083	3.3	4.6	0.7		
	5.0	7.6	9.0	2.5			0.021	0.8	2.3	0.3		
	5.0	7.6	4.5	1.25			0.024	0.9	5.3	0.8		
	5.0	7.6	21.6	6.0			0.238	9.4	11.0	1.6		
	5.0	7.6	21.6	6.0	NM		0.074	2.9	3.4	0.5	3.3	25
	5.0	7.6	48.5	13.5			0.249	9.8	5.1	0.7		
	5.0	7.6	28.8	8.0			0.025	1.0	0.9	0.1		
	5.0	7.6	27.9	7.75			0.056	2.2	2.0	0.3	3.3	25
	5.0	7.6	46.7	13.0			0.191	7.5	4.1	0.6		
	5.0	7.6	27.9	7.75			0.332	13.1	11.9	1.7		
	6.5	7.6	19.8	5.5			0.038	1.5	1.9	0.3	3.3	25
	6.5	7.6	3.6	1.0			-	-	-	-		
	6.5	7.6	20.7	5.75			0.356	14.0	17.2	2.4		
	5.0	7.6	13.5	3.75	NM		0.017	0.7	1.3	0.2	3.3	25
	5.0	7.6	18.0	5.0			0.020	0.8	1.1	0.2	3.3	25
	5.0	7.6	18.0	5.0			0.068	2.7	3.7	0.5	3.3	25
	5.2	7.6	43.2	12.0			0.284	11.2	6.7	0.9	3.3	25
	5.0	7.6	7.2	2.0			0.101	4.0	14.0	2.0	3.3	25
·	4.0	7.6	9.0	2.5			0.094	3.7	10.4	1.5	1.6	12
	4.0	7.6	7.2	2.0			0.094	3.7	13.1	1.9	1.6	12
	5.0	7.6	3.6	1.0			0.094	3.7	26.1	3.7	1.6	12
	4.8	7.6	3.6	1.0			0.094	3.7	26.1	3.7	1.6	12
	4.7	7.6	5.4	1.5	NM		0.292	11.5	20.6	2.9	2.7	20
	4.1	7.6	1.8	0.5							2.7	20
	4.5	7.6	7.2	2.0							0.7	5
	4.5	7.6	4.5	1.25			0.420	16.5	16.7	2.4	0.7	5
	7.5	7.6	11.7	3.25							0.5	4
	8.0	7.6	9.0	2.5							0.5	4
	TARGET F - 11.7 cm ID											
	5.0	7.6	18.0	5.0	NM		1.015	40.0	10.7	1.4	3.6	29
	5.0	7.6	9.0	2.5							3.3	25
	5.0	7.6	5.4	1.5							1.6	12
	5.0	7.6	37.8	10.5							1.6	12
	6.0	7.6	30.6	8.5							1.6	12

Techniques were established for removal of the CERROTRU and aluminum fillers. Removal of the flame-sprayed aluminum by leaching with NaOH was found to be most rapid between 6.0 and 7.0 molarity. (See figure 6.) Ultrasonic vibration and tilting of the sample did not result in significant increases in the rate of removal. A maximum rate of 1.3×10^{-4} m/s (0.48 cm/hr) was obtained using 7.0 molar NaOH at 348 to 353°K (167 to 176°F) without ultrasonic vibration. Removal of the CERROTRU was accomplished by placing one end of the cylinder in a pool of molten CERROTRU at 453°K (356°F) for about 300 seconds and withdrawing slowly. Final removal of the last remnants of the CERROTRU was accomplished by etching in a concentrated HCl solution.
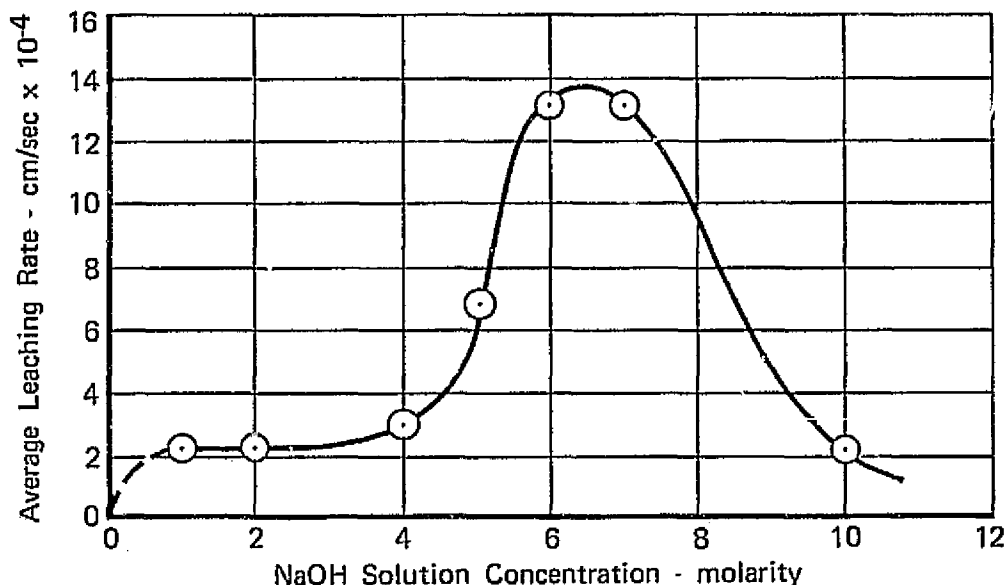
Figure 6. Effect of NaOH Solution Molarity on the Average Leaching Rate of the Flame-Sprayed Aluminum Filler at Ambient Temperatures   FD 78193A

RESULTS AND DISCUSSION

The closeout layer thickness was measured throughout the program to evaluate the geometrical characteristics of the selected sputtering configuration and to determine if thickness distribution was changing as a result of nonuniform target depletion. Typically, the circumferential distribution at the cylinder center varied between ±5% of the average coating thickness. (See figure 7.) This variation in coating thickness was attributed to deviations from perfect symmetry of the target, substrate, and magnetic field during deposition. The longitudinal closeout layer thickness distributions obtained in all runs were typical of those shown in figure 8. The basic shape of the distribution over the cylinder length was a consequence of the similar length of substrate (12.7 cm) and target (14.6 cm). The change in longitudinal distribution with deposition was attributed to the change in target geometry due to the nonuniform sputter removal of material. Similar distribution profiles with a similar type device have been previously observed and described by Gill and Kay. [8]

21

PRECEDING PAGE BLANK NOT FILMED

The distributions obtained were acceptable for the filler material evaluation to be performed since the required deposit thickness was relatively small. Where thicker deposits would be required longer targets, modification of the target ends or shaping of magnetic field would have to be performed. The various filler materials, processing techniques and deposition parameters are discussed separately in the following sections.

Effects of Filler Materials

Of the filler materials evaluated, CERROCAST, CERROBEND, and SERMETEL 481 were found to be unacceptable for use in the fabrication of thrust chambers by sputtering. The high shrinkage characteristics of CERROCAST resulted in incomplete filling of the grooves after repeated filling attempts. The casting technique being used with the low melting alloys would require modification to allow for the shrinkage of the CERROCAST. Application of this filler in contoured thrust chambers would be extremely difficult. Although, the casting of CERROBEND into the grooves resulted in adequate filling, this use of this filler resulted in severe bond contamination. The closeout layer removed from the rib lands of run I-3 exhibited discoloration indicative of CERROBEND contamination. This was qualitatively identified by spark source emission spectrography to contain Cd, Bi, Sn, and Pb, the constituents of CERROBEND. Bond contamination also resulted in the cylinders produced in runs I-4 and I-5. The SERMETEL 481 filler was found to be unacceptable due to continuous outgassing in the vacuum environment. Without using the high temperature curing cycle (3.6 ks at 813°K) which would anneal the OFHC copper substrate, the SERMETEL 481 was porous and contained entrapped gases that prevented acceptable vacuum levels to be obtained. Furthermore, the surface could not be densified sufficiently to yield a smooth surface.
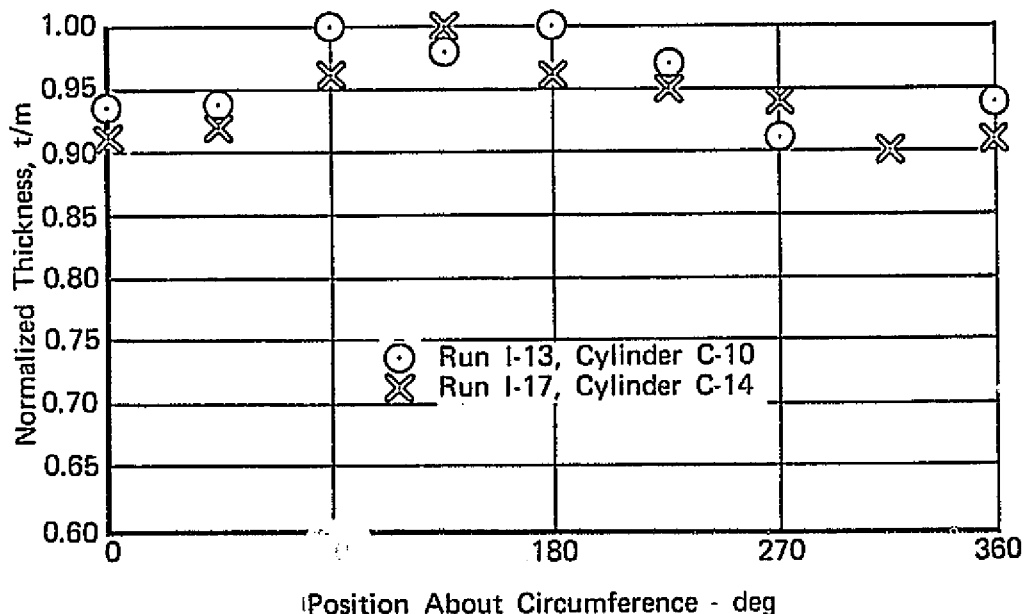
Figure 7. Circumferential Closeout Layer   FD 78481A
         Thickness Distribution at Cylinder
         Center
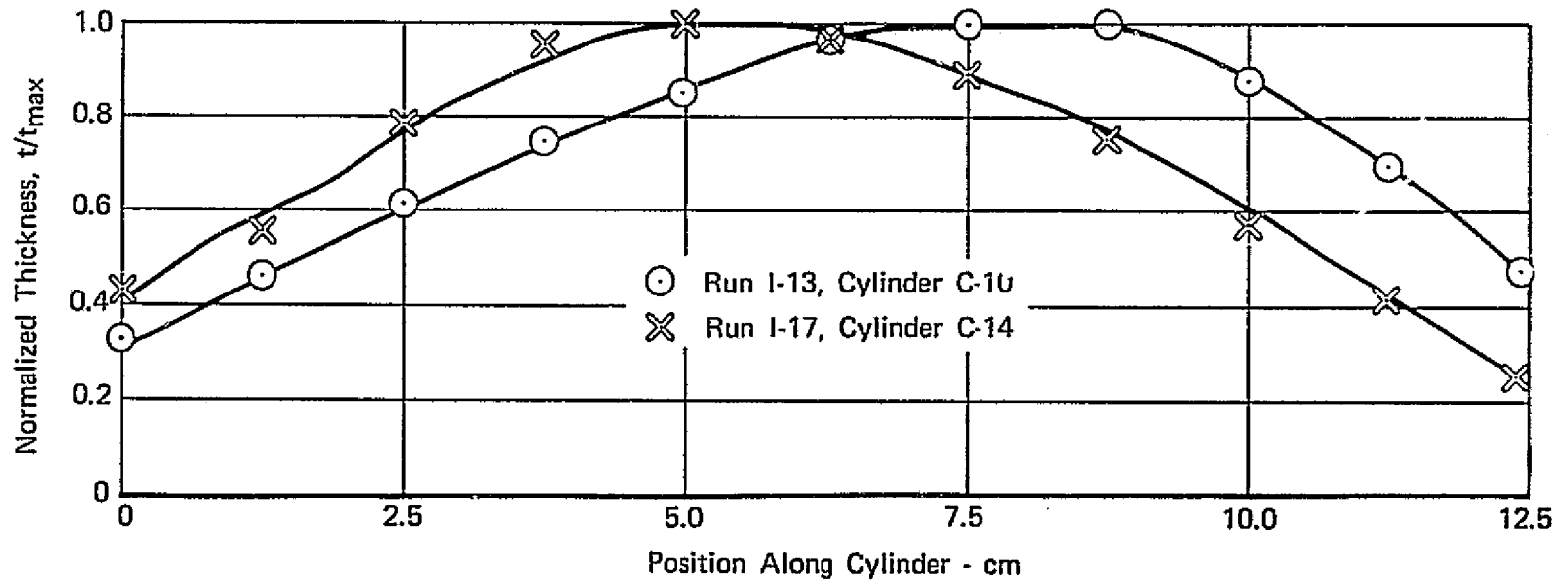
Figure 8. Closeout Layer Thickness Distribution Along Cylinder Length

FD 78482A

Aluminum was found to be the most suitable filler for thrust chamber fabrication. However, the method of application by flame-spraying was found to be unacceptable. The application by flame-spraying resulted in a porous structure (figure 9), which exhibited extensive outgassing. System contamination was the most excessive in the experiments in which this filler material was used. A direct result of the contamination was the oxide layer at the bond interface observed in runs I-14 and I-16. Whether the oxide layer formed entirely during the sputter cleaning, the in-situ bakeout cycles, or the initial stages of the deposition cycle could not be determined from the experiments performed.

Of the filler materials investigated, aluminum was the most easily removed and provided the highest bond strengths. The investigation of other techniques for applying the aluminum filler, such as vapor deposition, ion plating, or sputtering, was beyond the scope of this program.

The CERROTRU filler was used in eight of the experimental depositions, with some measure of success. Contamination of the interface between the closeout layer and the rib surfaces resulted in lowering the bond strength. The degree to which the interface was contaminated seemed to depend on the severity and duration of the sputter cleaning operation. A technique for the application of CERROTRU was developed that provided a complete filling of the grooves. Removal of the last remnants of the CERROTRU was usually accomplished by etching in a concentrated HCl solution. This procedure sometimes resulted in embrittling the closeout layer. The embrittlement was attributed to the openness of the closeout layer.

Effects of Predeposition Processing

From the initial depositions performed on cylinders prepared by normal lathe machining techniques, it was observed that this method of machining tended to smear the filler and substrate and result in the formation of a large burr on one side of the rib edge. On the nonburred side of the rib edge, the filler material was pulled away from the rib wall. The sputtered closeout layer persistently exhibited cracks extending from the nonburred side of the groove. (See figure 10.) Longitudinal surface grinding was evaluated in run I-12 as a means of forming burrs on both sides of the grooves. The grinding technique introduced deep machining marks into substrate, which required excessive sanding for removal. Longitudinal milling did not result in deep machining marks, but did yield significant burring along both sides of the grooves. As is apparent in figure 11, burring the groove sides did not in itself eliminate the cracking problem, although a reduction in severity of the cracking was noted.

Suspecting that the machining lubricants trapped in the filler material during milling also contributed to the crack formation through the introduction of contaminants, dry milling was used in run I-19. Though the outgassing rate of the aluminum filler was significantly reduced, the cracking problem persisted. Dry machining using a reversing cutting technique resulted in minimal cracking at the rib wall and reduced the extent of cracking in the closeout layer. (See figure 12.)

24
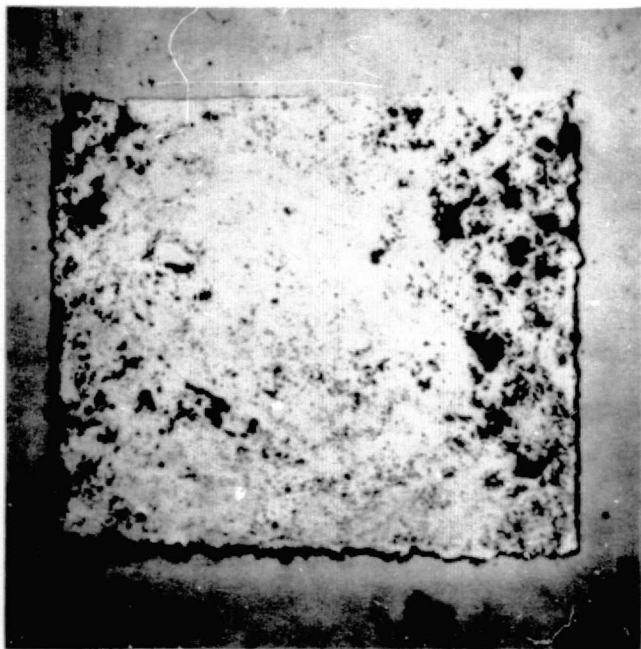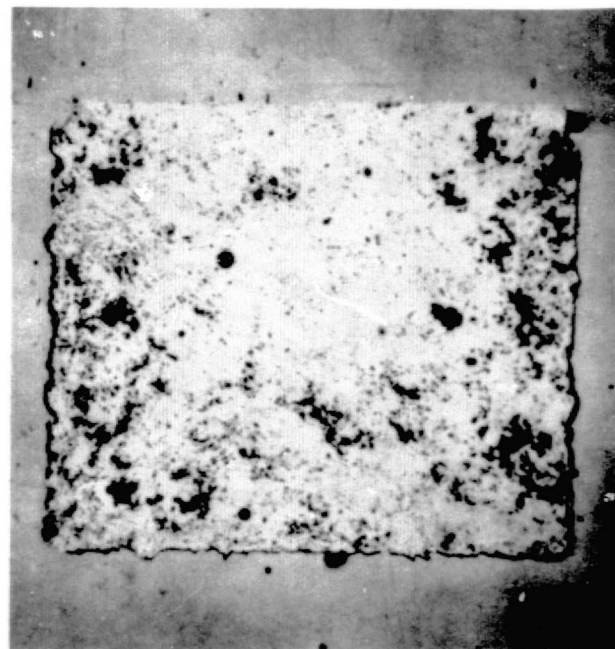
Mag: 83X Unetched

Mag: 88X Etched

Figure 9. Typical Appearance of Aluminum Filler

FD 78491A

25
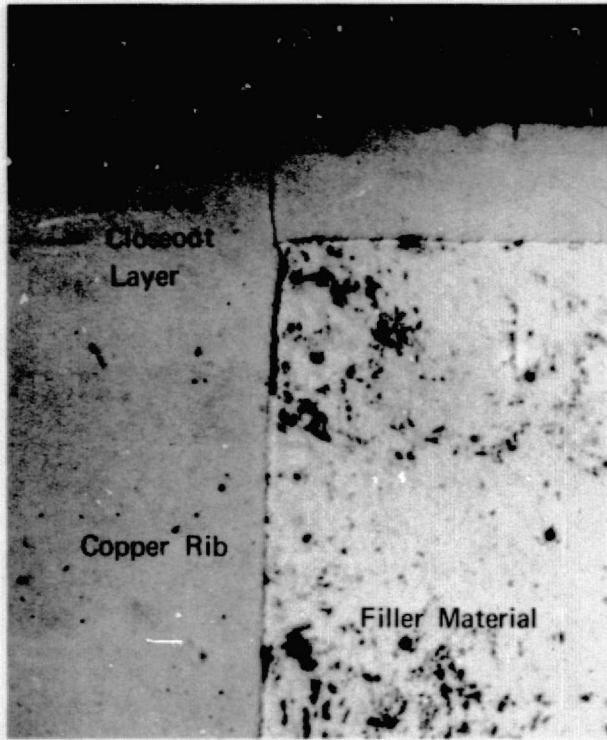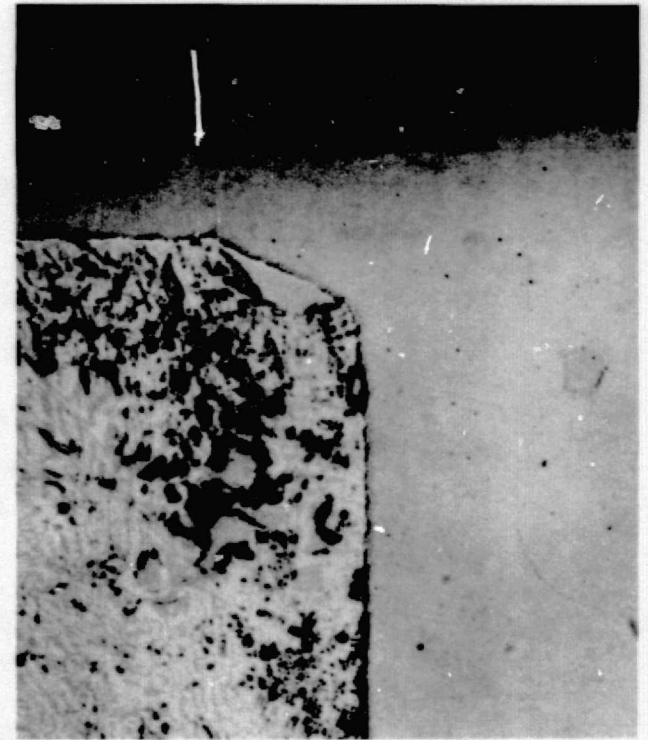
Mag: 100X Unetched   Mag: 100X Unetched

Figure 10.   Burring and Closeout Layer Cracking Resulting from Normal Lathe Machining, Run I-7   FD 78485A
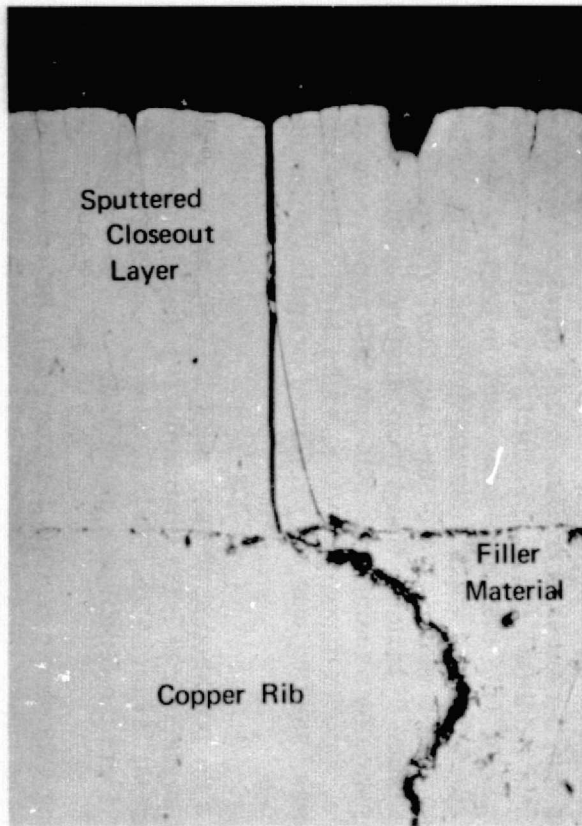
Mag: 100X Unetched

Mag: 100X Etched

Figure 11. Burring and Closeout Layer   FD 78486A   Figure 12. Appearance of Closeout Layer   FD 78487A
Cracking Resulting from   on Dry Machined and Sanded
Lengthwise Milling, Run I-16   Substrate, Run I-20

Concurrent with the variations in machining, surface deformation techniques such as glass bead peening and shot peening were also tried as a means of further sealing the incipient cracks at the rib walls and, in the case of the flame-sprayed aluminum filler, densifying the surface layer to decrease outgassing and seal the surface porosity. Though these techniques resulted in further decreasing the cracking frequency and severity, the problem was not totally eliminated. (See figures 13 and 14.) Other techniques, such as vacuum baking prior to installation in the sputtering chamber (runs I-16 and I-24), radiation heating of the sample at high vacuum in the sputtering chamber for 54 ks (15 hr) (runs I-17 and I-18), and multiple sputter clean-pumpdown cycles (runs I-13, I-14, and I-16), were used to reduce filler outgassing and crack formation. Though these techniques were successful in reducing the filler outgassing, the cracking problem persisted.

The effects of the different surface treatments on the presence of defects in the closeout layer were initially deduced from the comparison of the structures of the closeout layers on the filled copper substrates from several runs. However, the effect of surface finish was usually overshadowed by other effects, attributable to the filler material, deposition parameters, etc. The glass bead peening operation seemed to contribute most to the interfacial contamination on the copper substrates (figure 15) and promote defect formation. To further confirm this, a separate deposition similar to I-14 was performed on an aluminum substrate prepared with three different surface finishes (glass bead peened, vapor blasted, and sanded with 600-grit SiC paper) on different areas of the cylindrical substrate. It was again observed that the glass bead peening operation promoted the formation of defects in the coating. (See figure 16.) The defects were normal to the surface and traced back to the centers of the concave regions of the surface. The defects probably resulted because of the deposition rate difference between the concave regions and the convex regions. The concave regions exhibited a lower growth rate since these areas were exposed to a smaller segment of the cylindrical target (shadowing effect) than the convex regions. As the deposition continued, the difference in growth rate increased, resulting in deeper and deeper "valleys." The junction between the coating on adjacent "hills" eventually became a sharp cusp moving outward trailing a thin crack or open boundary. The vapor-blasted area exhibited the same effect, but with fewer resultant defects. (See figure 17.) This may have been due, in part, to the contamination at the interface, attributed to the vapor blasting process. It should be noted that vapor blasting usually resulted in a clean interface, (figure 18), so that the above result was not taken to indicate that vapor blasting should be discontinued. However, the preparation by sanding with 600-grit SiC paper resulted in a defect-free structure, smooth deposit surface, and a high quality interface. (See figure 19.) Hence, sanding was the preferred preparation technique for the latter runs.

Deposition on a 6μ polished surface (runs I-5, I-6, and I-15) and on a chemically polished surface (run I-17) invariably resulted in poorer adherence of the sputtered closeout layer. This, in both cases, was attributed to contamination resulting from the techniques employed.

Sputter cleaning was shown in runs I-1 and I-2 to be essential in obtaining a good bond between the substrate and the coating. Variations in sputter cleaning procedure were tried with each filler material examined. (See table II.) The determination of the optimum sputter cleaning procedure was for the most part empirical, being based on the relative difficulty of mechanically removing the sputtered layer.
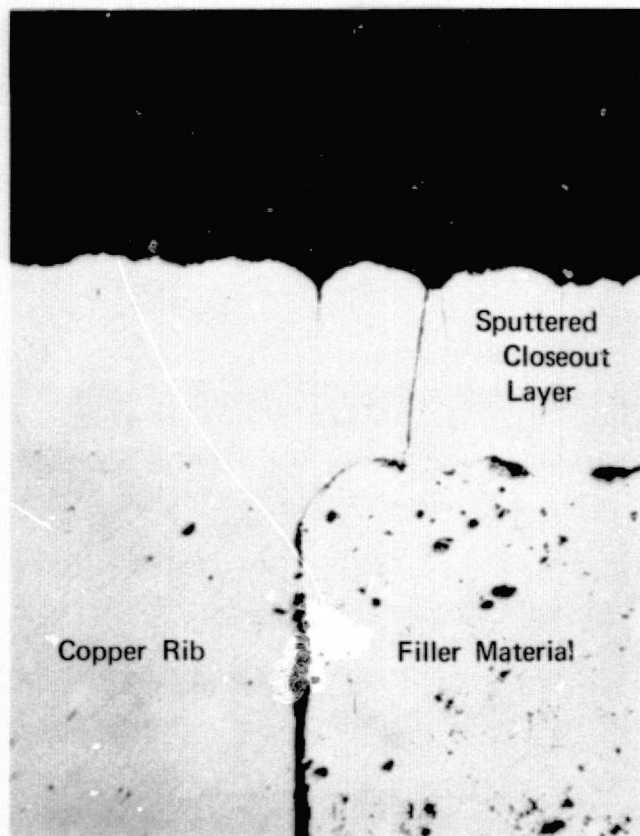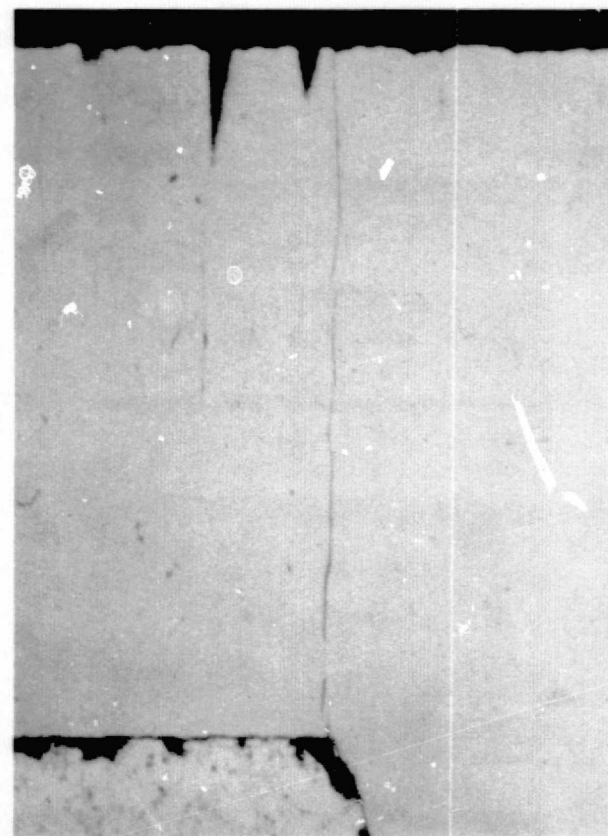
Mag: 100X Unetched

Figure 13. Cracking of Closeout Layer on
Glass-Bead-Peened Surface,
Run I-13

FD 78488A

Mag: 250X Unetched

Figure 14. Cracking of Closeout Layer on
Shot-Peened and Dry Milled
Surface, Run I-19

FD 78489A
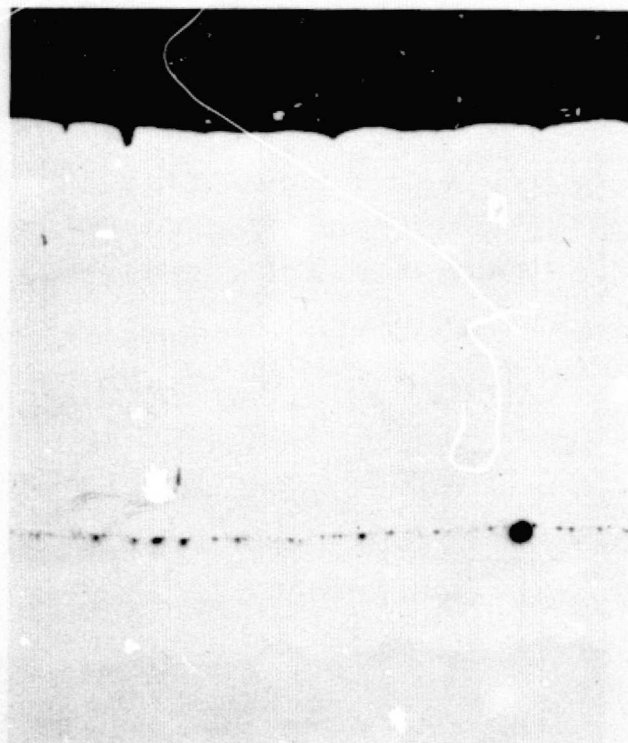
Mag: 250X Unetched   Mag: 250X Etched

Figure 15. Interfacial Contamination Resulting from Glass Bead Peening, Run I-16   FD 78492A
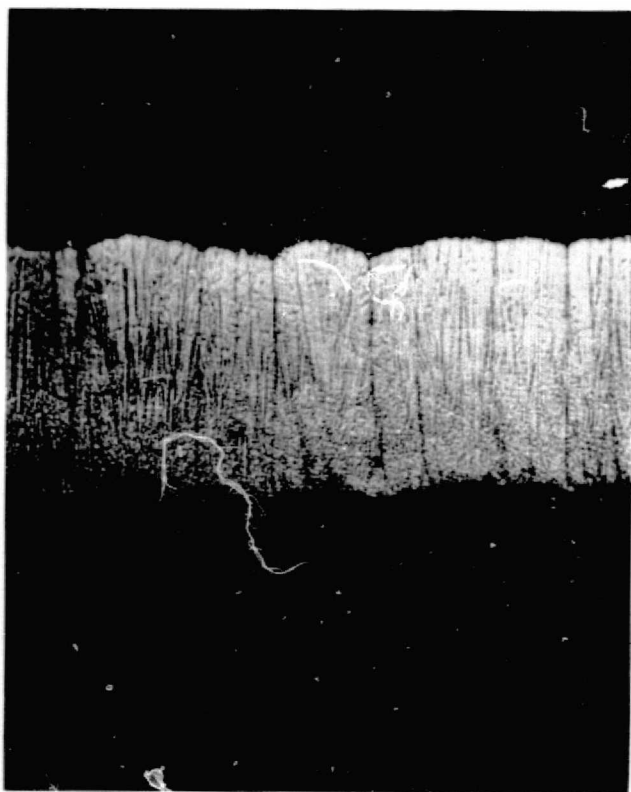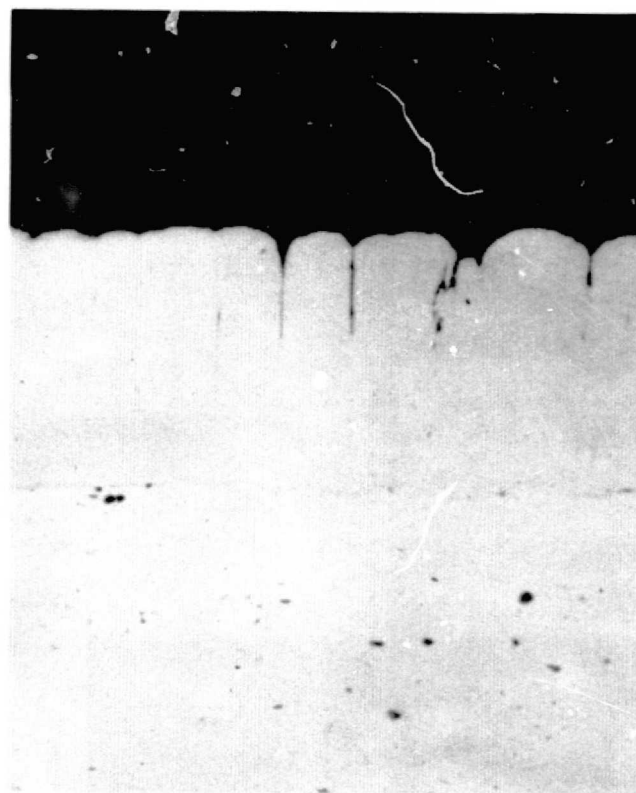
Mag: 250X Substrate Removed, Etched   Mag: 250X Unetched

Figure 16. Microstructure of Sputtered OFHC Copper on Glass-Bead-Peened Region of Type 6061 Aluminum Alloy Substrate   FD 78494A
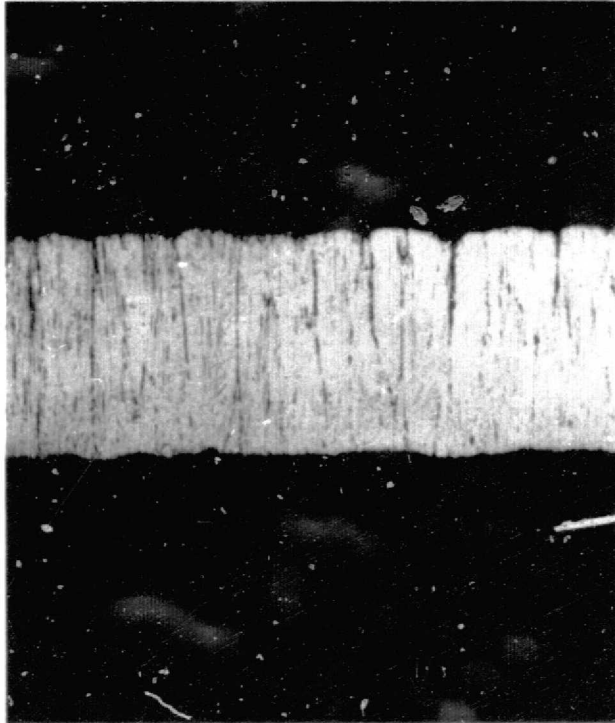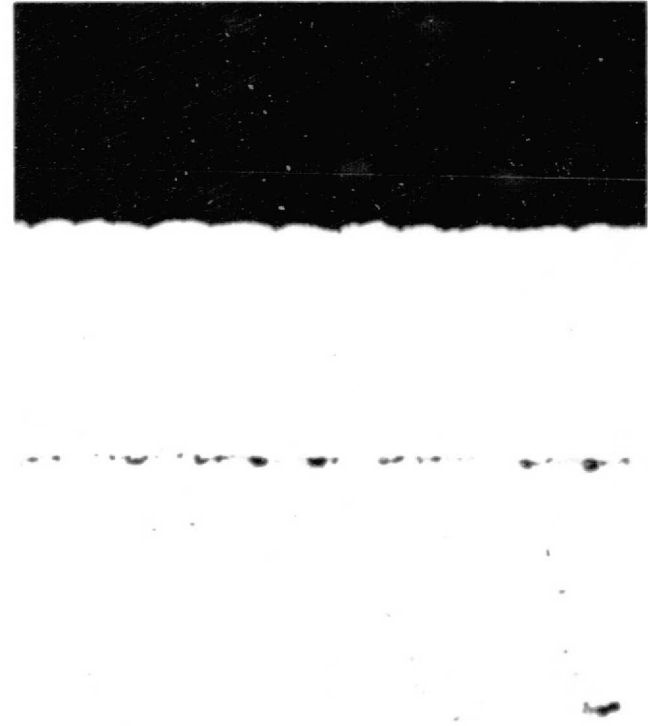
Mag: 250X Substrate Removed, Etched   Mag: 250X Unetched

Figure 17.   Microstructure of Sputtered OFHC Copper on Vapor-Blasted Region of Type 6061 Aluminum   FD 78496A
            Alloy Substrate
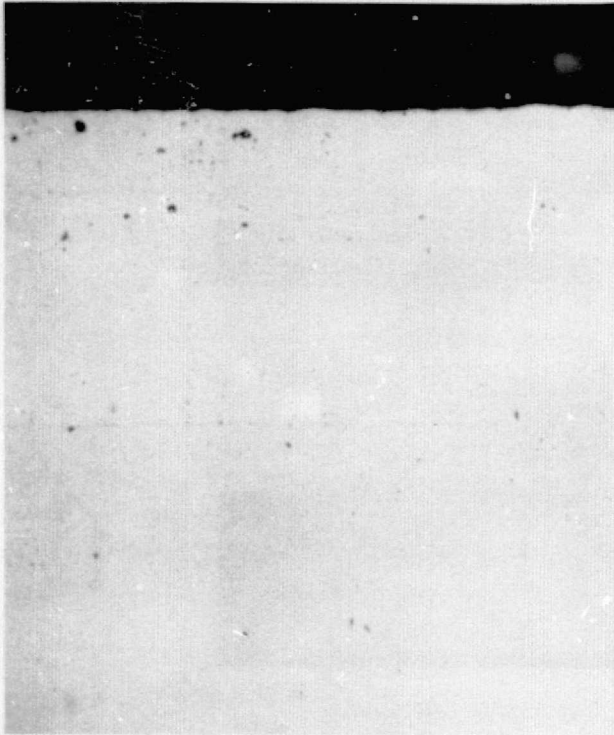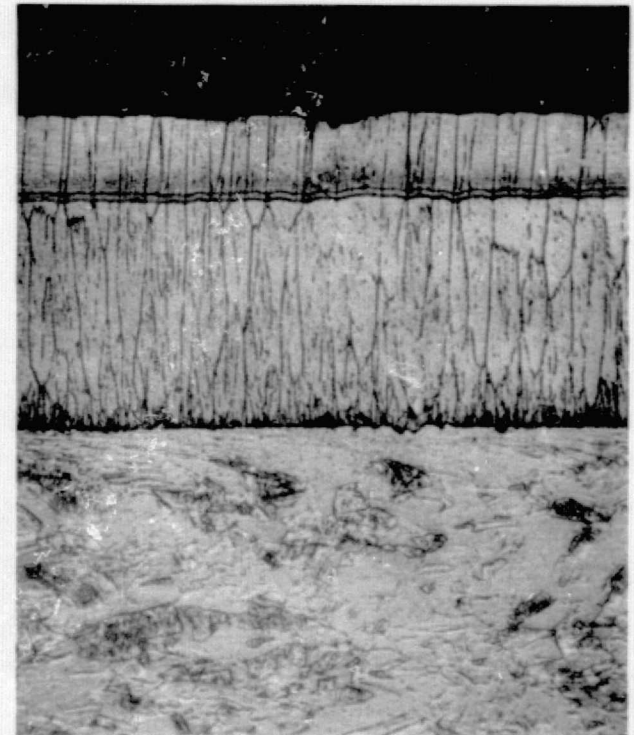
Mag: 250X Unetched   Mag: 250X Etched

Figure 18. Typical Clean Interface Between Closeout Layer and Substrate Obtained Using Vapor Blasting as Well as Final Surface Preparation, Run I-7   FD 78493A
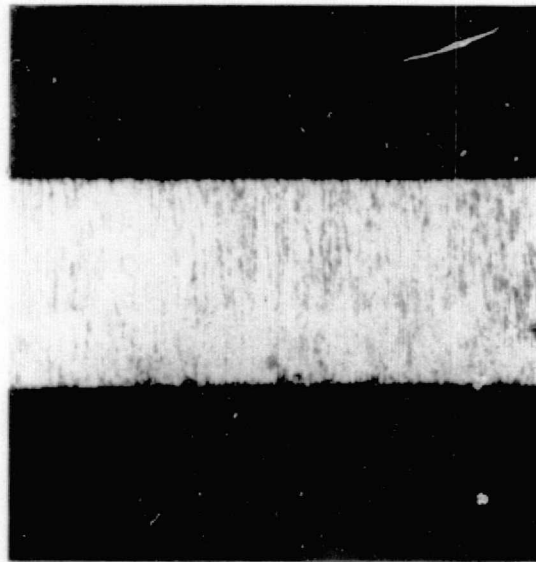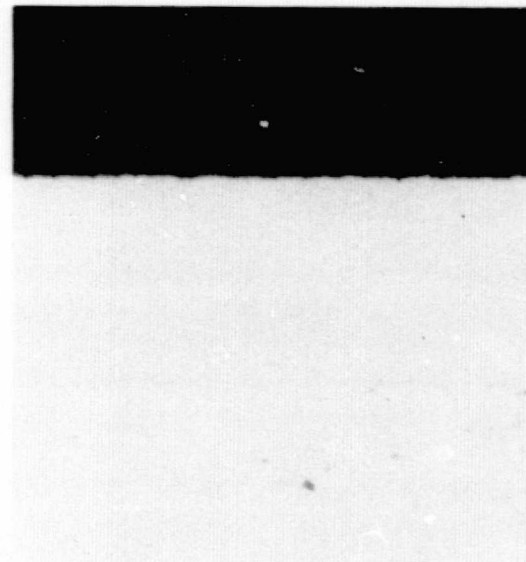
MAG: 250X SUBSTRATE REMOVED, ETCHED MAG: 250X UNETCHED

Figure 19. Microstructure of Sputtered OFHC Copper on 600-Grit-Sanded Region of Type 6061 FD 78495
     Aluminum Alloy Substrate

In tensile testing the closeout layers on cylinders C-15 and C-18 (aluminum filler), failure stresses of 63.6 and 72.3 MN/m^2 (9,230 and 10,500 psi) were attained. (See table IV.) Yielding of the rib would be expected to occur at about 45,000 psi. The above failures occurred by pulling closeout layer material from between the ribs. (See figure 20.) The closeout layer was not removed from the rib surfaces. This type of fracture was attributed to the presence of cracks in the closeout layer that resulted during deposition. Since material was not removed from the rib areas, a bond strength could not be determined. A similar failure also occurred at 67.6 MN/m^2 (9,800 psi) with the sample tested from cylinder C-19 (CERROTRU filler). The sample from cylinder C-21 (CERROTRU filler) exhibited a 0.69 MN/m^2 (100 psi) bond strength, and all of the closeout layer was removed. This extremely low bond strength was attributed to overheating in the initial sputter cleaning, which resulted in substantial interface contamination. A similar failure, however, at a higher stress, 10.6 MN/m^2 (1540 psi) was exhibited by the sample from cylinder C-20 (CERROTRU filler). (See figure 21.) With this sample, the low bond strength was probably due to inadequate sputter cleaning, since a 240-second cleaning cycle was employed as compared to an 840-second cycle for cylinder C-19.

On the closeout layer removed from the rib lands in tensile testing of the three CERROTRU filled samples (C-19, C-20, and C-21) a visual discoloration was observed on the underside of the deposit. Quantitative chemical analysis of the closeout layer from cylinders C-19 and C-21 showed minimal quantities of filler elements. (See table V.) The surface contamination resulting with CERROTRU may represent a contamination level beyond the detectable limits of normal chemical analysis. The results of the chemical analysis on the deposit removed from aluminum filled cylinder C-18 showed minimal aluminum contamination. Apparently, if aluminum is present at the interface, its presence results in less degradation of bond strength than does the presence of the CERROTRU material.

Effects of Deposition Parameters

The initial depositions performed in this program were directed at the use of high-rate sputter deposition at 21.1 to 35.3 nm/s (3.0 to 5.0 mils/hr) to form the closeout layer. The structure that resulted was filled with defects (cones, open boundaries, cracks). A typical cone is shown in figure 22. When the rate was decreased to 7.1 to 14.1 nm/s (1.0 to 2.0 mils/hr), the defects were generally reduced in number and severity. Variations in substrate bias and deposition temperature were employed along with variations in filler material, machining, and cleaning techniques in an attempt to eliminate the structural defects of the sputtered closeout layer.

It was not anticipated to perform a comprehensive parametric study of deposition parameters on deposit structure and properties. However, as the work progressed, it was apparent that certain deposition parameters were influential to the deposit integrity and were studied in further detail.

Table IV. Results of Room Temperature Tensile Testing

Run	Cylinder	Filler	Tensile Load,		Area,		Tensile Stress,		Remarks
			N	lb	m^2 x 10^{-4}	in^2	MN/m^2	psi	
I-19	C-15	Aluminum	21,350	4,800	3.35	0.520	63.6	9,230	Failure in coating between ribs; no material removed from rib area.
I-20	C-18	Aluminum	21,306	4,790	2.93	0.455	72.3	10,500	Failure in coating between ribs; no material removed from rib area.
I-18	C-19	CERROTRU®	22,685	5,100	3.35	0.520	67.6	9,800	54% of coating removed from rib area.
I-21	C-21	CERROTRU®	222	50	3.23	0.500	0.69	100	100% removed from rib area.
I-23	C-20	CERROTRU®	2,091	470	1.97	0.305	10.6	1,540	100% removed from rib area.

A. CYLINDER C-15 FROM RUN I-19   FAL 30486
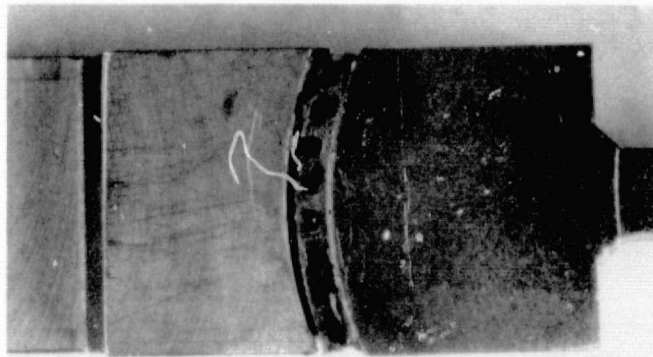
B. CYLINDER C-18 FROM RUN I-20   FAL 30537

Figure 20. Appearance of Closeout Layer Fracture   FD 78183
After Room Temperature Tensile Testing
of Segments from Aluminum-Filled
Cylinders C-15 and C-18
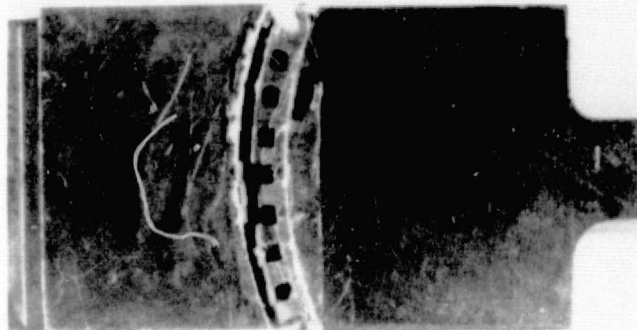
A. CYLINDER C-19 FROM RUN I-18   FAL 30488
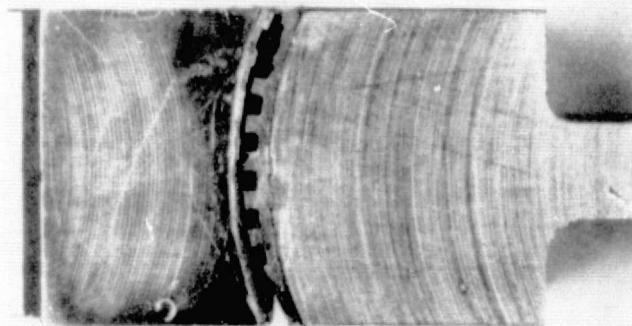
B. CYLINDER C-20 FROM RUN I-23

Figure 21. Appearance of Closeout Layer Fracture   FD 78191
After Room Temperature Tensile Testing
of Segments from CERROTRU®-Filled
Cylinders C-19 and C-20

Table V. Chemical Analysis of Sputtered Closeout Layer

Run	Cylinder	Filler	Bi	Sn	Kr(*)	Al
I-17	C-14	CERROTRU®	0.5 ppm	2 ppm	1040 ppm	0.2 ppm
I-20	C-18	Aluminum	<0.5 ppm	2 ppm	1800 ppm	2 ppm
I-18	C-19	CERROTRU®	0.5 ppm	2 ppm	2300 ppm	1 ppm
I-20	C-21	CERROTRU®	0.5 ppm	2 ppm	7300 ppm	0.2 ppm

*Krypton analysis performed by Pyrolysis Gas Chromatography; all others by Spark Source Mass Spectrography.
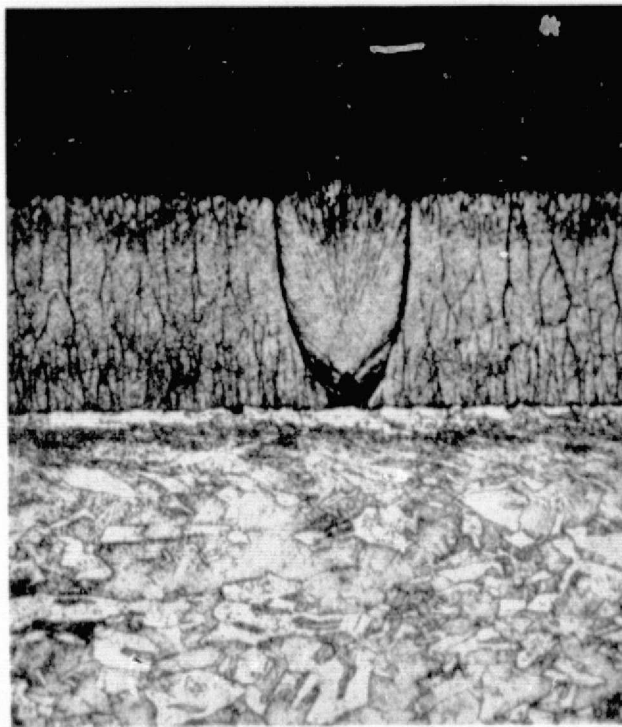
MAG: 250X   ETCHED

Figure 22.   Appearance of Cone in OFHC Copper   FD 78747
Closeout Layer – Run I-7

The effect of deposition temperature on coating structure generally correlated well with that observed by Thornton. [9] The depositions performed at $T/T_m = 0.2$ to 0.3 (271 to 406°K) exhibited columnar grains. (See figure 23.) The depositions performed at $T/T_m = 0.3$ to 0.5 (406 to 678°K) exhibited a more equiaxed structure and, for the highest temperatures in this T/T_m range, showed indications of concurrent recrystallization. (See figure 24.) As was expected, the temperature of deposition affected the hardness of both the closeout layer and the substrate, (figure 25 and table VI). The scatter in the closeout layer hardness at low temperatures was attributed to the openness of many of the low temperature deposits. (See figure 26.)

Since it was believed that outgassing of the filler material might be contributing to the formation of cracks in the closeout layer, low rate initial depositions were employed to minimize the filler material heating and subsequent outgassing. If the low rate deposition was followed by a high rate deposition not exceeding about 14.1 nm/s (2.0 mils/hr), the closeout layer was usually quite free of open defects. (See figures 27 and 28.)
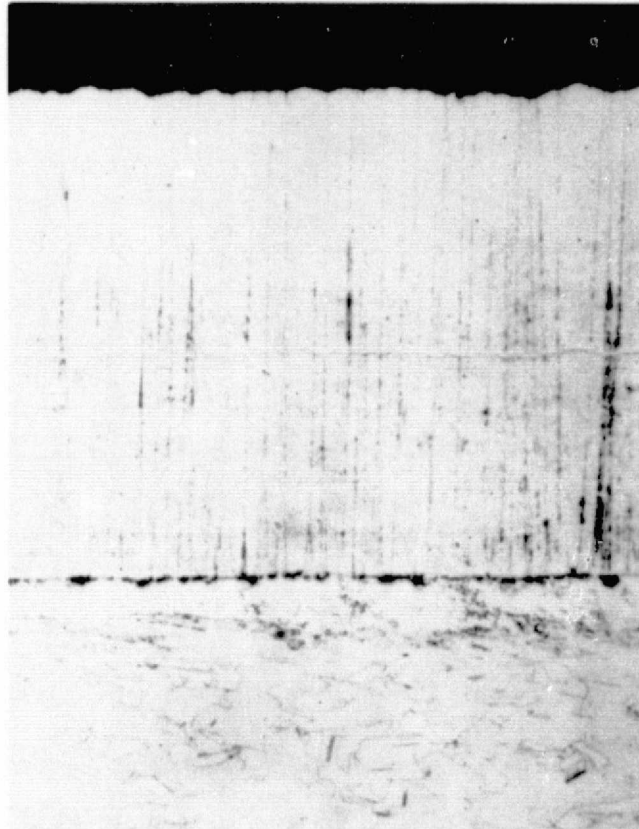
MAG: 250X

Figure 23.   Columnar Grain Structure of Sputtered   FD 78497
             OFHC Copper Applied at a Substrate
             Temperature of 355°K (82°C) – Run I-13
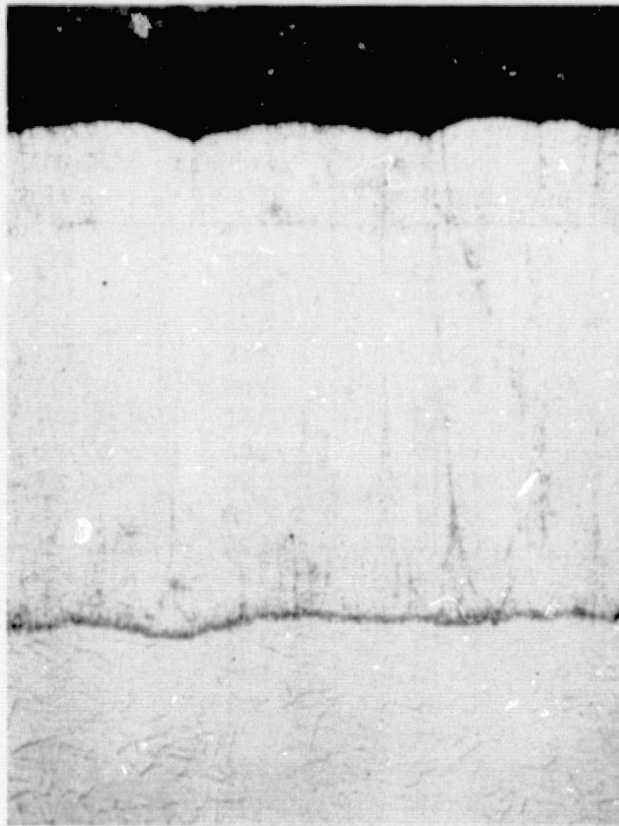
MAG: 250X   ETCHED

Figure 24. Microstructure of Sputtered OFHC   FD 78498
            Copper Applied at a Substrate Tempera-
            ture of 566°K (293°C), Run I-15
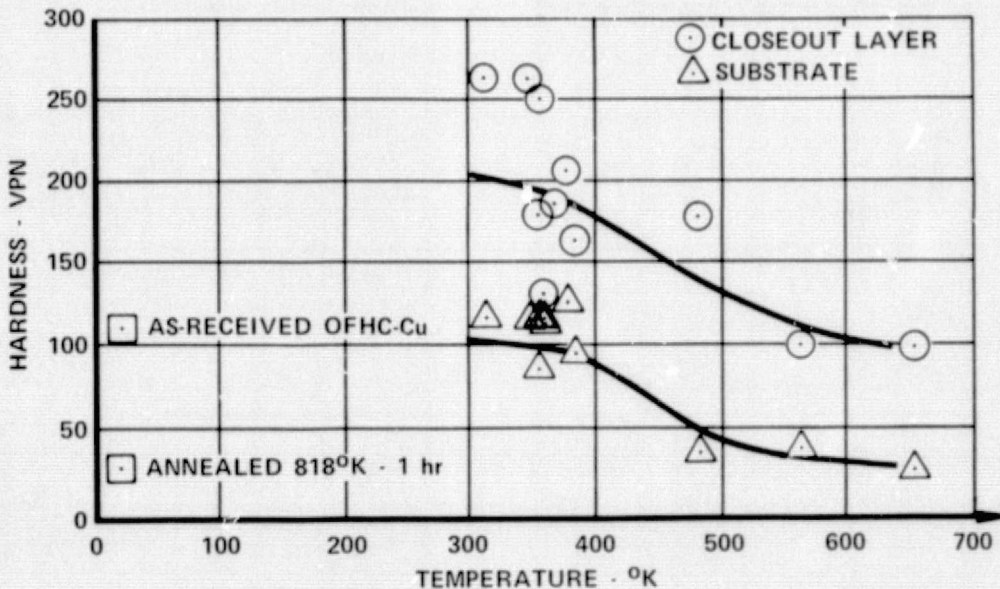
Figure 25. Effect of Substrate Temperature on   FD 78483
            Closeout Layer and Substrate Hardness

41

Table VI. Hardness of Sputtered OFHC Copper Coatings and Substrates
(0.2-kg Load, Diamond Pyramid Indenter)

Run Number	Cylinder Number	Coating Hardness (VPN)	Substrate Hardness (VPN)	Deposition Temperature (°K)
I-5	C-1	227	112	358
I-7	C-5	207	110	380
I-9	C-7	178	114	354
I-10	C-8	256	114	3?4
I-11	C-4	256	111	3-9
I-12	C-12	161	91	382
I-13	C-10	225	83	355
I-14	C-13	96	25	656
I-15	C-11	99	38	566
I-16	C-17	175	36	482
I-17	C-14	181	123	364
I-18	C-19	247	114	NM*
I-19	C-15	191	123	NM
I-20	C-18	247	129	NM
I-21	C-21	231	139	NM
I-22	C-22	79	123	NM
I-23	C-20	195	121	NM
I-24	C-16	183	127	NM

NM - Not measured
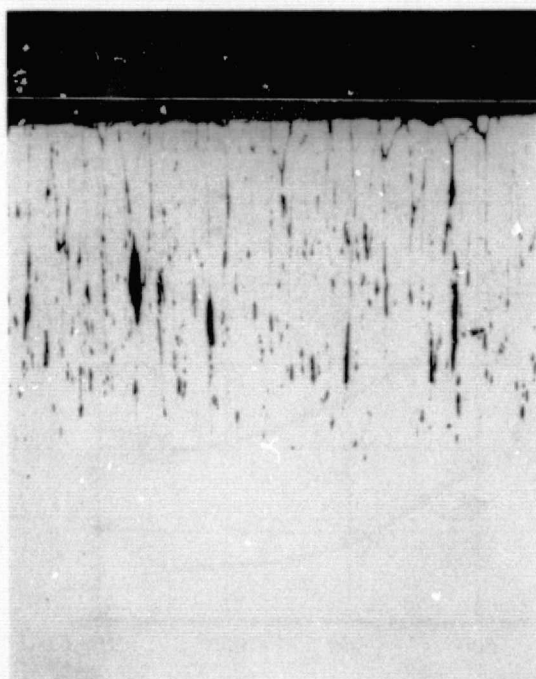
MAG: 100X UNETCHED
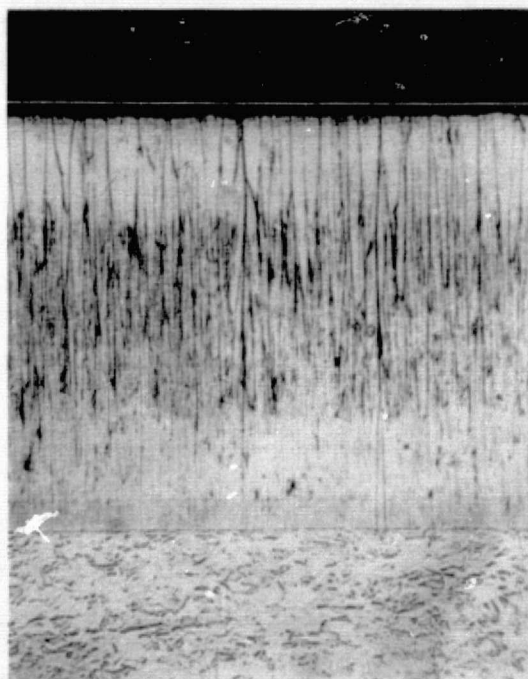
MAG: 100X ETCHED

Figure 26. Open Microstructure of Closeout Layer   FD 78499
Applied Using High Rate and Low Tem-
perature - Run I-17

42
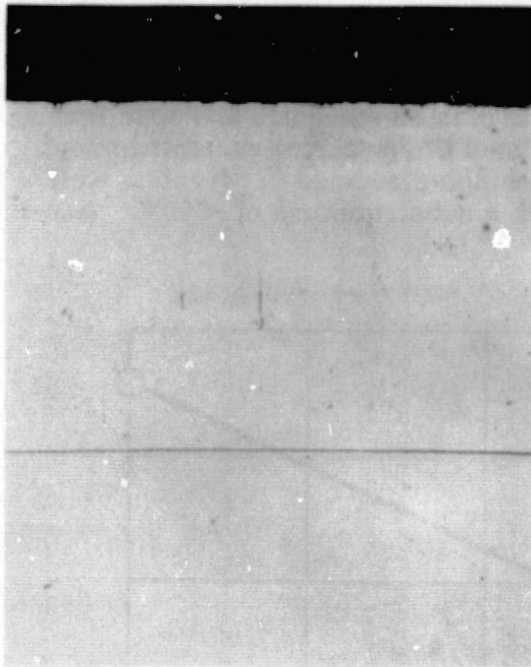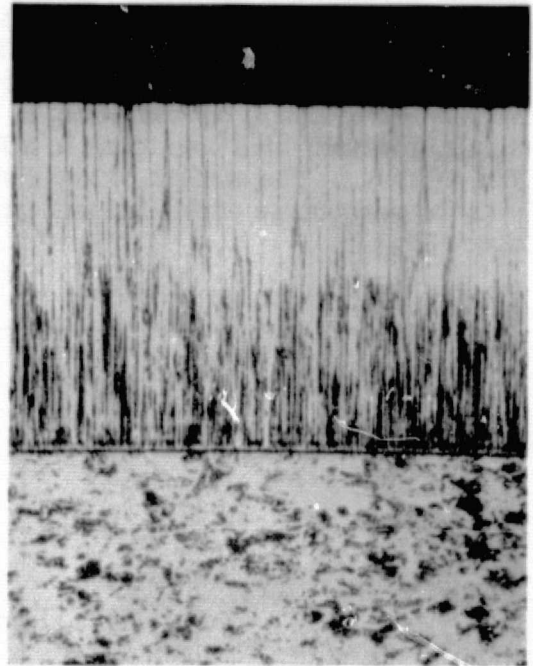
MAG: 100X UNETCHED

MAG: 100X ETCHED

Figure 27.   Microstructure of Closeout Layer Applied   FD 78500
            Using Low Rate Initial Deposition Followed
            By a High Rate Deposition at Less Than
            14.1 nm/s (2.0 mils/hr) – Run I-21
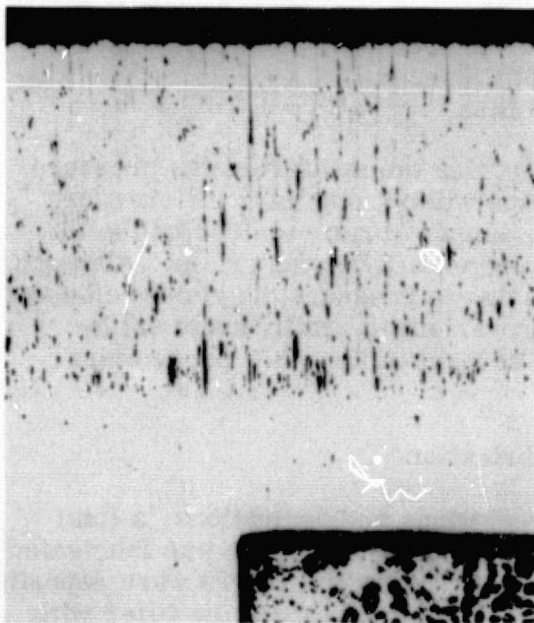
MAG: 100X UNETCHED
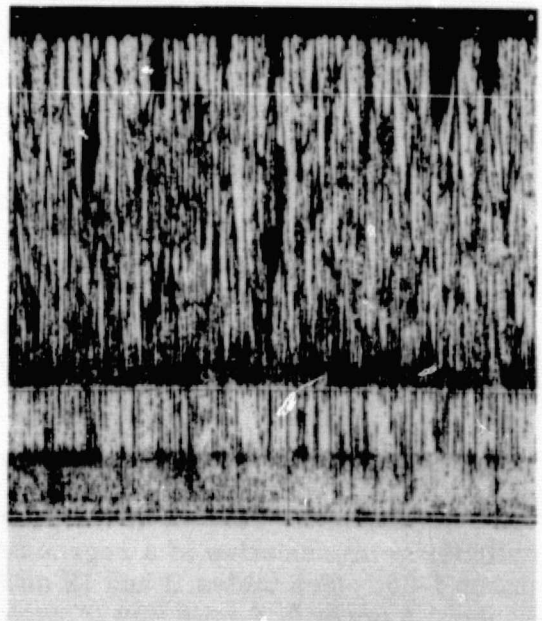
MAG: 100X ETCHED

Figure 28.   Microstructure of Closeout Layer Applied   FD 78743
            Using Low Rate Initial Deposition Followed
            by High Rate Depositions at More Than
            14.1 nm/s (2.0 mils/hr) – Run I-18

43

The bias on the substrate was varied to determine its effect on cone formation and closeout layer structure. The competing effects of substrate surface finish, filler material outgassing, deposition rate, and temperature made it impossible to single out the effect of substrate bias on structure and cone formation. However, bias was found to affect the level of sputtering gas entrapment. (See table V.) The amount of krypton in the samples seemed to correlate well with the percentage of the deposit applied with a substrate bias of -500V. (See figure 29.)
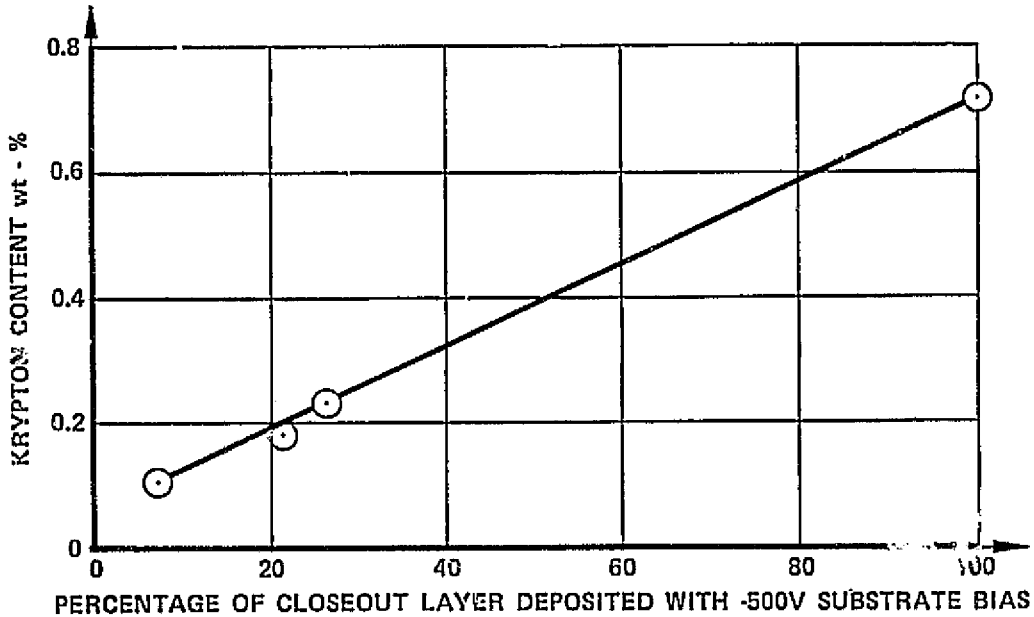
Figure 29. Variation of Closeout Layer Krypton   FD 78480
          Content With Percentage of Closeout
          Layer Applied With -500V Bias

Based on the results of Thornton, [9] lowering the sputtering gas pressure should permit the use of higher deposition rates without obtaining the characteristic open structures at the low deposition temperatures required by the OFHC copper substrates and/or the low melting point filler materials. Although the one run (I-24) performed with a lower discharge pressure did yield a closeout layer with fewer defects (figure 30), the improvement in quality could not be attributed solely to the lower pressure since several of the other parameters were also changed.

Final Cylinder Fabrication

Based on the results of the previous depositions and evaluations, a final cylinder representative of a regeneratively cooled thrust chamber was fabricated in run I-25. (See tables II and III and figure 31.) The initial layers were deposited at about 4 nm/s (0.6 mils/hr) to avoid filler heatup and to bridge the filler with a heat conductive layer. The remaining deposition was performed at a slightly higher rate, approximately 14.1 nm/s (2.0 mil/hr). The applied closeout layer thickness was approximately 0.102 cm in the center and 0.051 cm on the ends.
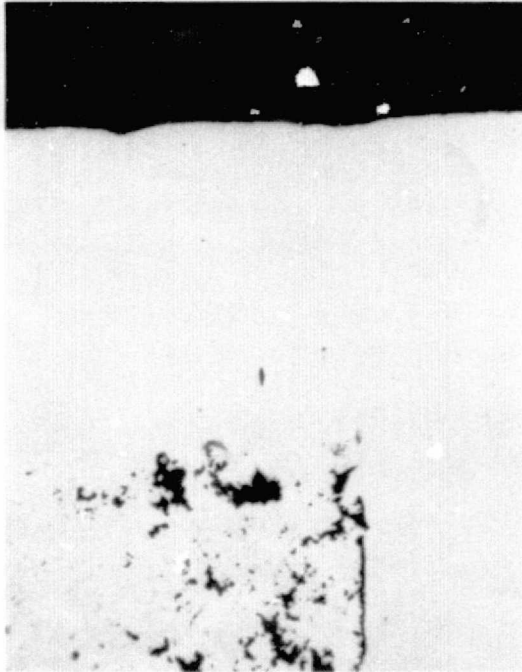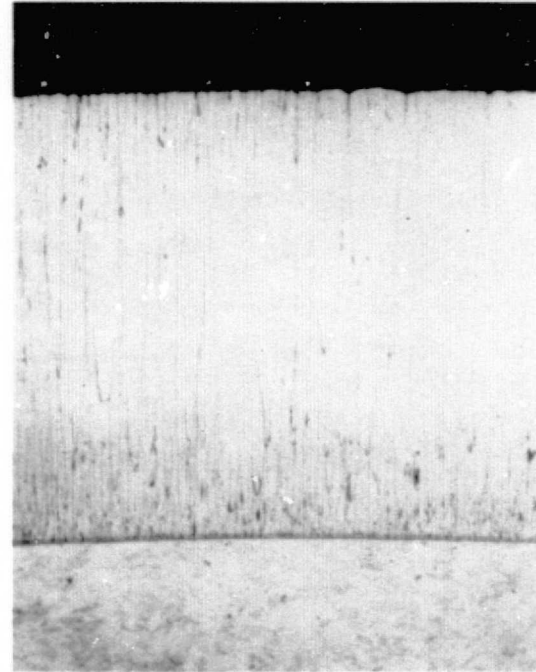
MAG: 200X UNETCHED   MAG: 200X ETCHED

Figure 30.   Microstructure of Closeout Layer Applied Using Lower Discharge Pressure – Run I-24   FD 78745
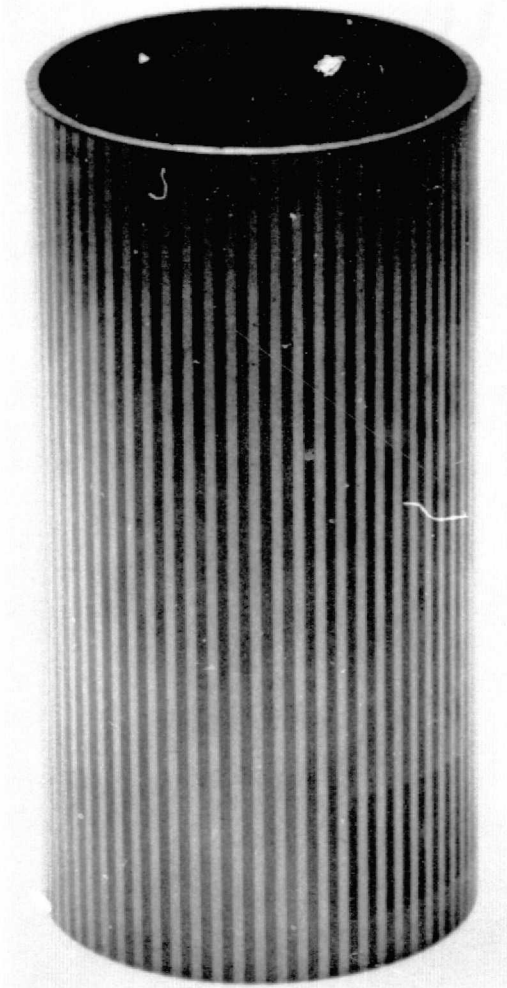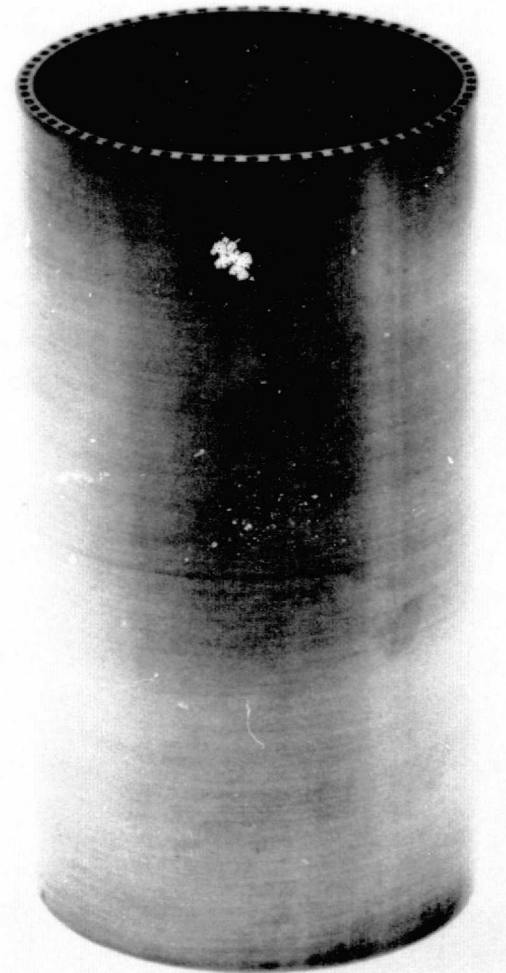
MAG: 1X   FE 136193   MAG: 1X   FE 136194

Figure 31. Appearance of CERROTRU®-Filled Ribbed Wall Cylinder and Final Finished Cylinder   FD 78484

The closeout layer was dry lathe machined and finish sanded to a 0.051 ±0.013 cm thickness over the cylinder length. After machining, the CERROTRU filler was removed by the techniques described earlier. Approximately 300s were required to remove, or to melt out, the filler material. The appearance of the as-machined filler cylinder and the final finished cylinder is shown in figure 31. Three small surface defects were present on the cylinder after finishing. These were attributed to arc discharges in the sputtering chamber during deposition. Since the finished cylinder was sent to NASA-LeRC for evaluation, a destructive metallographic analysis was not performed.

TASK I
CONCLUSIONS

Five materials were evaluated in this program with respect to their use as fillers in the sputter fabrication of regeneratively cooled thrust chambers. From this evaluation the following conclusions were drawn:

1. The closeout layers on substrates with the flame sprayed aluminum filler exhibited the highest bond strengths achieved in this program (in excess of 72.3 MN/m^2 (10,500 psi). The porosity resulting from the flame spraying technique was found to be the source of extensive system contamination leading to open closeout layer structures. Fully dense aluminum, although not evaluated in this program, would probably be the most advantageous filler material for the fabrication of thrust chambers.

2. An upward casting technique, developed for filling the grooved cylinders with the low melting alloys, resulted in complete filling of the grooves with CERROBEND and CERROTRU fillers. The high shrinkage of CERROCAST prevented complete filling by the technique employed and hence was eliminated from consideration.

3. CERROBEND was found to be incompatible with the high vacuum environment and excessive bond contamination invariably resulted when this material was used.

4. Of the filler materials evaluated, CERROTRU was the most suitable with respect to filling the grooves and vacuum system compatibility. However, the bond strength of the closeout layer was found to be sensitive to the length and severity of the sputter cleaning operation.

    Removal of CERROTRU was accomplished by placing one end of the filled cylinder in a pool of molten CERROTRU (453°K for 300S) withdrawing slowly. Removal of any last remnants of filler was accomplished by etching in a concentrated HCl solution.

5. The slurry-applied SERMETAL 481 was found to be incompatible with the high vacuum environment. Outgassing from the extensive porosity of this material prevented the normal vacuum levels from being obtained.

6. The machining technique used on the filled substrates was shown to influence the occurrence and severity of closeout layer cracks. Of the machining techniques investigated, dry bidirectional lathe machining contributed least to rib edge deformation and opening of the rib wall-filler interface and, therefore, resulted in reducing the occurrence of closeout layer cracking.

7. The final surface preparation technique was shown to influence the formation of defects in the closeout layer. Sanding with 600-grit SiC paper provided the cleanest interfaces and the fewest closeout layer defects. The use of glass peening or heavy vapor blasting introduced surface asperities that contributed to the formation of defects in the closeout layer.

8. The effects of variations in substrate bias on the elimination of structural defects in the sputtered closeout layer could not be ascertained due to concurrent variations in the filler material, machining, finishing, and cleaning techniques. However, Krypton entrapment was found to be the greatest in those closeout layers applied with the highest substrate bias levels.

9. The substrate temperature during deposition must be kept below approximately 400°K (127°C) if the properties of the OFHC copper substrate are to be retained after long term deposition cycles. At low substrate temperatures, typically less than 366°K (93°C), low rate depositions must be performed to eliminate open columnar or fibrous grain structures.

10. The use of a diode discharge in the deposition performed, showed that, with the sample and target configurations employed, a high integrity closeout was difficult to produce. Improvements in deposit integrity through the use of a triode discharge (higher energy plasma), may result and should be investigated in future work.

TASK II

SPUTTERED INNER WALL MATERIALS

The objective of Task II was to evaluate the properties of thick deposits of OFHC copper, 0.15 Zr-Cu (AMZIRC®), Al_2O_3-Cu and SiC-Cu. The structure, hardness, and tensile properties of each material were determined to delineate the property enhancement obtainable by sputter fabricating these materials.

Integral to this effort was a study of the effects of variations in sputtering parameters and post deposition processing on the structure and properties of the sputtered deposits.

EQUIPMENT AND PROCEDURES

In this task a hollow cathode coater and a flat plate coater were used for the depositions performed. The hollow cathode coater was similar in design to that used for Task I, except that the targets were extended from 14.5 cm to 24.8 cm for improved longitudinal thickness distribution. The extended coater configuration is shown schematically in figure 32. In the depositions performed, the coater was operated in either the diode or triode mode. In diode operation, the electron source (figure 32) was removed and an axial magnetic field applied. For triode operation the electron source was employed and the magnetic field removed.

The operation of the hollow cathode and the general procedures used in all depositions was described in Task I.

The hollow cathode coater was used for the deposition of OFHC and 0.15 Zr-Cu. The hollow (cylindrical) targets were machined from wrought Grade 101 OFHC copper tubing and wrought 0.15 Zr-Cu alloy billets. The water-cooled targets were 24.8 cm long with an internal diameter of 10.2 cm. Cylindrical substrates, 6.1 cm ID by 6.3 cm OD by 12.7 cm long, of either Grade 101 OFHC copper or Type 6061 aluminum alloy tubing were used for most depositions. However, a 1.9 cm OD solid Type 347 stainless steel substrate was employed to evaluate cathode-to-substrate spacing effects. The substrates for the low temperature depositions were water cooled, while in the depositions where higher temperatures were studied, the substrates were heated by plasma radiation and sputtered target material bombardment. All sputtering was performed using research grade krypton. In each run, target voltage and current were adjusted as necessary to establish the desired substrate temperature and deposition rate. Substrate temperature was measured with a chromel-alumel thermocouple located between the substrate and substrate holder.

The flat plate coater is shown schematically in figure 33. This coater was used in the deposition of 0.15 Zr-Cu, Al_2O_3-Cu and SiC-Cu alloys. All depositions were performed in a triode discharge. For most depositions, two targets were used with the anode filament arrangement as shown in figure 33. However, in some depositions four targets were employed. In this case, the two additional targets were placed where the anode and filaments are shown, and the filaments and anode placed respectively under and above the targets.

←Anode Cooling and Low Voltage Connection

Water Cooled Anode

←Vacuum Chamber

Cylindrical Substrate

Water Cooled Substrate Holder

Vacuum Pump
Port

Cylindrical Target

Water Cooled Target Holder

B
Magnetic Field Direction

Water Cooling Channel - Typical

Electron Source

Tungsten Filament

Target Cooling and High Voltage Connection
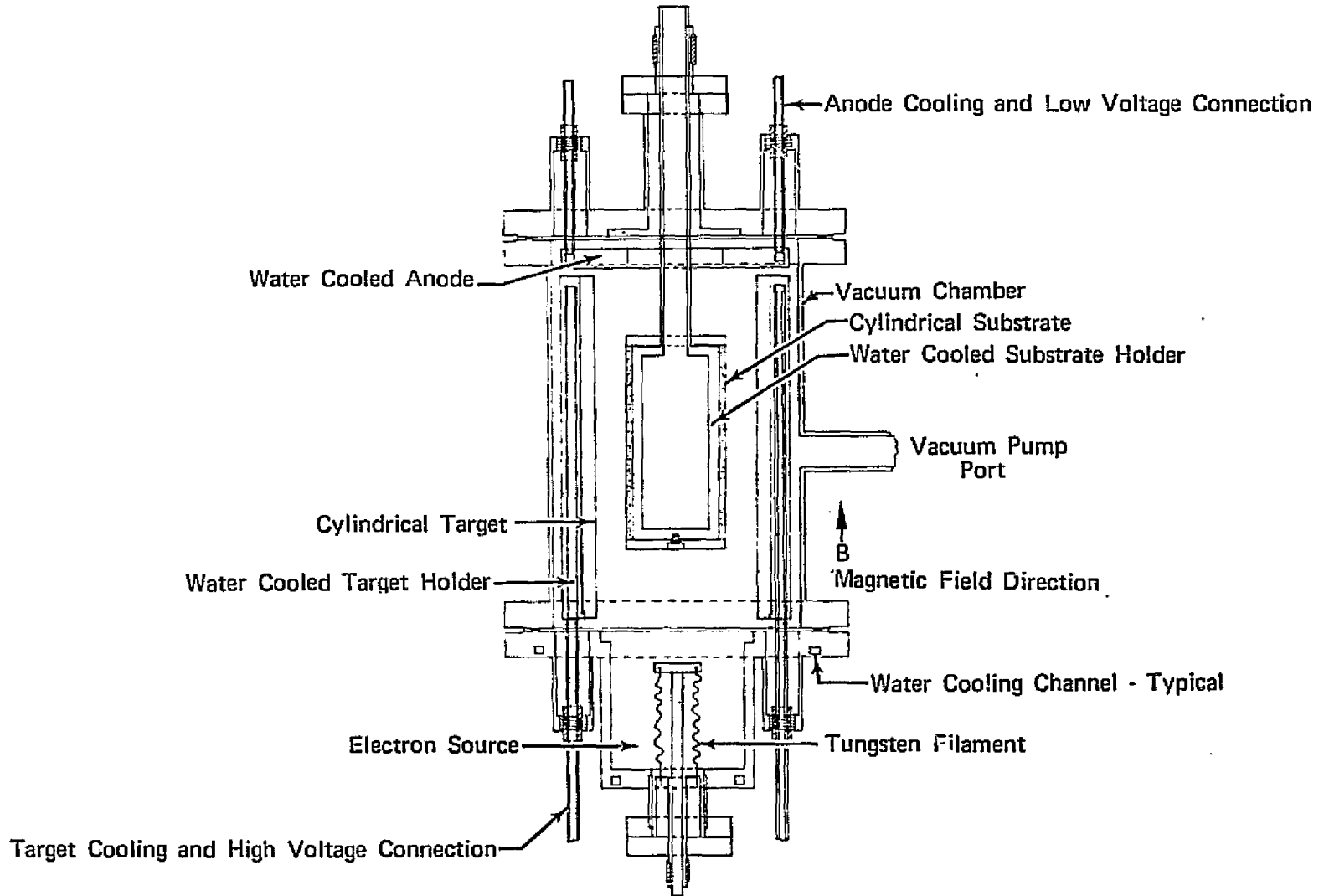
Figure 32.   Schematic of Hollow Cathode Coater

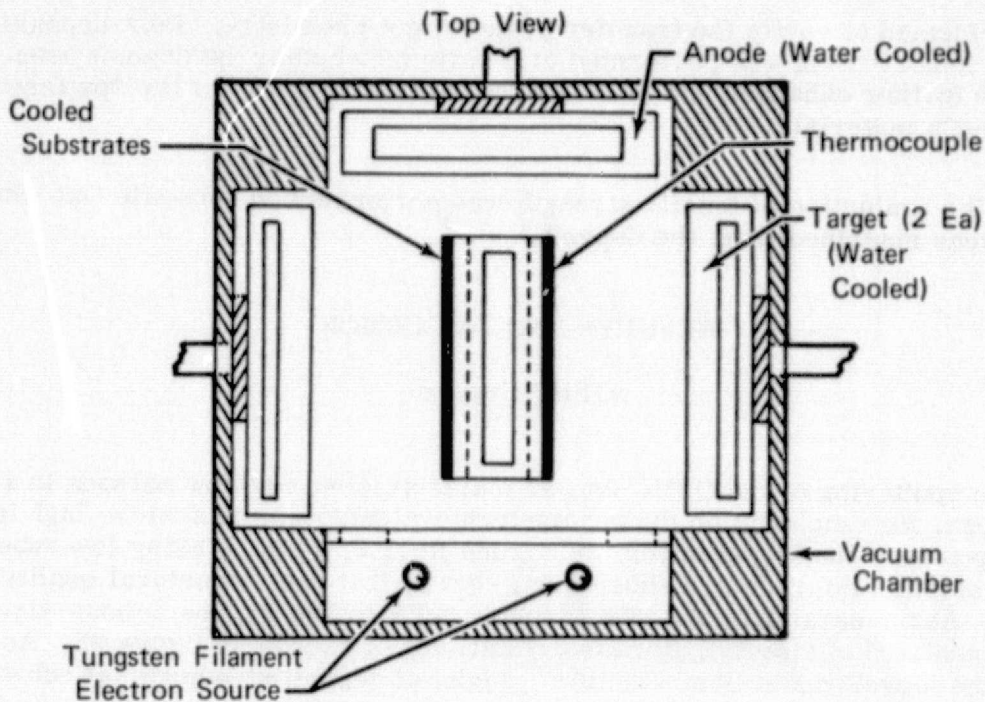FD 86716A

Figure 33.   Flat Target Coater (Some Ground   FD 87508
             Potential Shields Not Shown for Clarity)

The targets were 7.0 by 10.2 by 0.32 cm plates. The 0.15 Zr-Cu was machined from wrought billets. The Al_2O_3-Cu and SiC-Cu targets were composite targets consisting of ceramic plugs in OFHC plates, as shown in figure 34. The plugs were machined from Al_2O_3[12] and SiC[13] rods and pressed into the OFHC copper plates. The targets were water cooled during deposition.

The composite target configuration was selected, over powder metallurgy Cu-Al_2O_3 and Cu-SiC hot pressed targets, for ease and cost of fabrication. Since the ceramic plugs were surrounded with a metal matrix, deposition using a DC voltage target could be used.

The substrates used in the flat plate coater were either 0.32 cm OFHC copper or 1.3 cm Type 6061 aluminum alloy (5.1 cm by 7.6 cm) plates or 1.3 cm or 1.9 cm OD Type 347 stainless steel rods. As in the case where high substrate temperatures were evaluated, the substrates were not cooled, but heated by plasma radiation and material deposition.

In the initial part of this task substrate preparation was evaluated. The preparation procedures and sputter cleaning parameters used in each deposition are given in table VII. The detailed summary of deposition parameters is given in tables VIII and IX.

The depositions generated in this task were evaluated by standard metallographic techniques for structural integrity, thickness distribution, grain morphology, surface topography, interface contamination and interlayer bond quality. Microhardness and tensile properties were measured on the highest quality deposits. Chemical analysis of the 0.15 Zr-Cu targets and deposits

51

was performed to verify the transfer of the target chemistry. Post deposition vacuum heat treating was performed to determine whether the deposit properties could be further enhanced and to verify the thermal stability of the sputtered 0.15 Zr-Cu material.

The evaluation of tensile strength was performed on subscale flat tensile specimens machined from the deposit.

RESULTS AND DISCUSSION

OFHC Copper

In sputtering of the OFHC copper material from a hollow cathode in a diode discharge, the emphasis on the parameters evaluated was to achieve high integrity deposits. The initial depositions (runs II-1, 2, 4 and 5) using low substrate temperatures (water-cooled substrates) showed that poor structural quality resulted. At temperatures of 333°K to 389°K (80°F to 200°F), the deposit structures consisted of tapered, fibrous crystallites, as shown in figure 35. According to the Movchan and Demchishin[10] model of deposit structure, at substrate temperatures below approximately $T/Tm = 0.3$, the deposit structure should consist of open, unbonded, tapered grains with domed tops (Zone 1 type structure). In Zone 2, up to approximately $T/Tm = 0.45-0.5$, columnar grains with well defined boundary zones result, with the width of the crystallites increasing with T/Tm. At T/Tm over approximately 0.45-0.50, or Zone 3, the columnar grains gradually change to equiaxed grains. Thornton's work yields a revision of this model, showing that increased discharge pressure raises the transition temperature between Zones 2 and 3. In the deposits produced, II-1 to 5, the structures contained unbonded grain boundaries and were similar to the open, voided (Zone 1) structures described by Movchan and Demchishin[10] and Thornton[9]. These structures prevailed at all deposition rates investigated. These deposits generally exhibited a brittle behavior with a fibrous fracture surface. (See figure 36.) The higher rates resulted in an increase in the crystallite size and in the number of open or voided boundaries per unit area.

Biasing the substrate to promote ion bombardment of the substrate during deposition did somewhat reduce the openness of the structure for the conditions tested, figure 35. In the aggregate, biasing was ineffective in significantly altering structure morphology. With a diode discharge and the configurations used, an effective bombardment by ions from the plasma was not attained (as evidenced by low substrate current).

Increasing the substrate temperature eliminated the open structure, but only at the lower deposition rates. At 700°K (800°F) the structures were dense for deposition rates below about 14.1 nm/s (2.0 mils/hr), figure 37. At higher rates, the open structure prevailed, figure 38. At the lower rates, the structure exhibited a dense, equiaxed morphology, while at the higher rates, the structure was columnar with recrystallized grains within the poorly bonded columns. In run II-7, material deposited at 19.7 nm/s (2.8 mils/hr) exhibited low tensile strength, table X. No yielding occurred and the elongation was less than 0.5%. Although the overall fracture was brittle and exhibited a fibrous topography, the individual crystallites exhibited ductile deformation behavior, figure 39. However, at the lower deposition rates, the fracture was ductile as expected, figure 39.
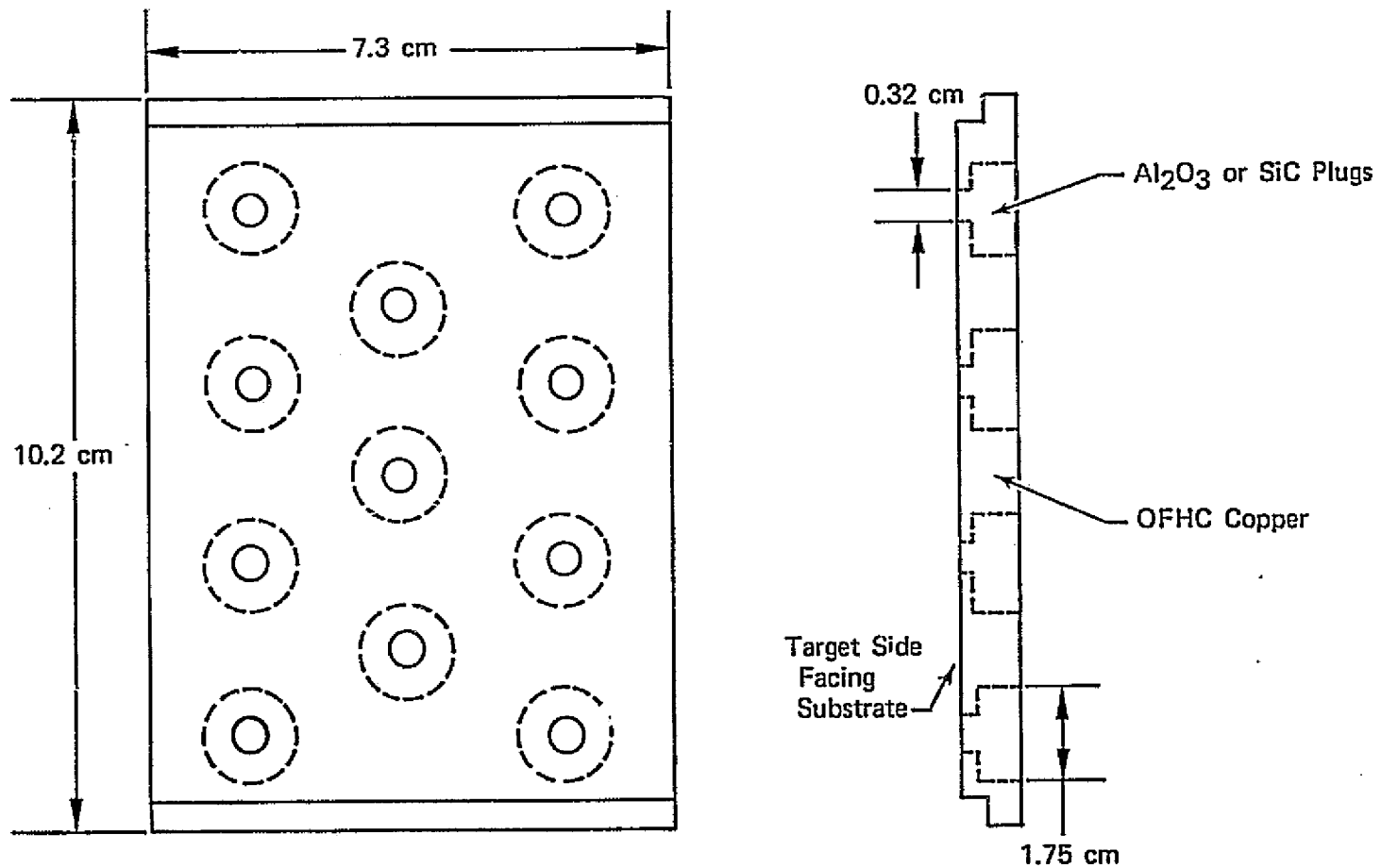
Figure 34. Composite Al_2O_3 – OFHC Copper and SiC – OFHC Copper Used in Flat Plate Coater

FD 91444

TABLE VII. SUMMARY OF SUBSTRATE PREPARATION AND SPUTTER CLEANING PARAMETERS FOR TASK II DEPOSITIONS

Run Number	Substrate Material	Finishing Treatment, Surface Preparation, and Primary Cleaning	Voltage, V	Sputter Cleaning[1] Current, mA	Duration, ks	Pressure, N/m²	μ
II-1	Type 6061 Aluminum alloy	Vapor blast and methanol rinse	-500	300	0.60	NM	NM
II-2	Type 6061 Aluminum alloy	Vapor blast and methanol rinse	-500	300	0.36	NM	NM
II-3	Type 6061 Aluminum alloy	25% polish to 600 grit, 25% vapor blast, 25% glass bead peen, 25% untreated	-350 to -500	300	1.08	1.13	8.5
II-4	Type 6061 Aluminum alloy	Sanded lengthwise with No. 600 paper, AJAX® scrub, methanol rinse, and methyl alcohol rub	-1000	400	1.42	2.3	17
II-5	Type 6061 Aluminum alloy	Sanded lengthwise with No. 600 paper, AJAX® scrub, methanol rinse and methanol alcohol rub	-1000	225	0.60	3.9	29
II-6	Type 6061 Aluminum alloy	Sanded lengthwise with No. 600 paper, AJAX® scrub, methanol rinse	-500 -1000	70 200	0.96 0.30	3.7 3.3	27 25
II-7	Type 6061 Aluminum alloy	Sanded lengthwise with No. 600 paper, AJAX® scrub, methanol rinse	-500 -1000	200 275	0.54 0.60	3.8 3.8	28 28
II-8	Type 6061 Aluminum alloy	Sanded lengthwise with No. 600 paper, AJAX® scrub, methanol rinse	-500 -1000	70 80	0.96 0.30	3.8 3.8	28 28
II-9	Type 6061 Aluminum alloy	Sanded lengthwise with No. 600 paper, AJAX® scrub, methanol rinse	-500	100	1.20	3.8	28
II-10	Type 6061 Aluminum alloy	Sanded lengthwise with No. 600 paper, AJAX® scrub, methanol rinse	-500	100	1.02	3.3	25
II-11	Type 6061 Aluminum alloy	Sanded lengthwise with No. 600 paper, AJAX® scrub, methanol rinse	-500	125	1.20	2.8	20
II-12	Type 6061 Aluminum alloy	Sanded lengthwise with No. 600 paper, AJAX® scrub, methanol rinse	-500	100	1.20	3.3	25
II-13	Type 6061 Aluminum alloy	Sanded lengthwise with No. 600 paper, AJAX® scrub, methanol rinse	-500	120	1.08	3.3	25
II-14	Type 6061 Aluminum alloy	Sanded lengthwise with No. 600 paper, AJAX® scrub, ethyl alcohol rinse	-500	150	0.96	3.2	24
II-15	Type 6061 Aluminum alloy	Sanded lengthwise with No. 600 paper, AJAX® scrub, ethyl alcohol rinse	-500	50	2.16	2.3	17
II-16	OFHC Copper	Sanded lengthwise with No. 600 paper, AJAX® scrub, ethyl alcohol rinse	-500	160	1.32	3.7	2.7

NOTES:

[1] Target and substrate cleaned simultaneously in triode discharge

[2] Substrate rotated during cleaning; all others stationary

[3] Cleaning and deposition performed simultaneously

NM - Not Measured

Run Number	Substrate Material	Finishing Treatment, Surface Preparation, and Primary Cleaning	Voltage, V	Sputter Cleaning[1] Current, mA	Duration, ks	Pressure, N/m²	Pressure, μ
II-17	OFHC Copper	Sanded lengthwise with No. 600 paper, AJAX® scrub, ethyl alcohol rinse	−500 −1000 −1000	85 280 300	0.78 3.60 1.80	3.7	22 22 27
II-18	OFHC Copper	Sanded lengthwise with No. 600 paper, AJAX® scrub, ethyl alcohol rinse	−500[3]	500	1.80	0.84	6.3
II-19	OFHC Copper	Sanded circumferentially on lathe with No. 600 paper, chemically polished (78F) for 10 min.	−250	50	0.06	5.2	39
II-20	347 Stainless Steel (1.9 cm dia)	Sanded lengthwise with No. 600 paper, AJAX® scrub, ethyl alcohol rinse	−750	30	0.90	0.90	6.8
II-21	347 Stainless Steel (1.9 cm dia)	Sanded lengthwise with No. 600 paper, AJAX® scrub, ethyl alcohol rinse	−500	30	0.06	3.3	25
II-22	347 Stainless Steel (1.9 cm dia)	Sanded lengthwise with No. 600 paper, AJAX® scrub, ethyl alcohol rinse	−500	40	0.30	3.5	26
II-23	347 Stainless Steel (1.9 cm dia)	Sanded circumferentially on lathe with No. 600 paper, AJAX® scrub, ethyl alcohol rinse	−500	55	0.30	3.1	23
II-24	347 Stainless Steel (1.9 cm dia)	Sanded circumferentially on lathe with No. 600 paper, AJAX® scrub, ethyl alcohol rinse	−25[1]	12	1.20	0.59	4.4
II-25	347 Stainless Steel (1.9 cm dia)	Sanded lengthwise with No. 600 paper, AJAX® scrub, ethyl alcohol rinse	0	0	0	0	0
II-26	OFHC Copper	Sanded lengthwise with No. 600 paper, AJAX® scrub, ethyl alcohol rinse	−25	650	0.30	0.73	5.5
II-27	Type 6061 Aluminum alloy	Sanded lengthwise with No. 600 paper, AJAX® scrub, ethyl alcohol rinse	−25	650	0.30	0.73	5.5
II-28	Type 6061 Aluminum alloy	ID sanded lengthwise with No. 600 paper, AJAX® scrub, ethyl alochol rinse	−25	1600	0.30	0.41	3.1
II-29	Type 6061 Aluminum alloy	ID Sanded lengthwise with No. 600 paper, AJAX® scrub, ethyl alcohol rinse	−25	2150	0.30	0.59	4.4
II-A-1	OFHC Copper (0.32 cm plate)	30 min. etch in bright dip solution, ethyl alcohol rinse	−500	40	0.30	3.5	26
II-A-2	OFHC Copper (0.32 cm plate)	Sanded lengthwise with No. 600 grit paper, ethyl alcohol rinse	−500	55	0.30	3.1	23

NOTES:

[1]Target and substrate cleaned simultaneously in triode discharge

[2]Substrate rotated during cleaning; all others stationary

[3]Cleaning and deposition performed simultaneously

NM – Not Measured

TABLE VII. SUMMARY OF SUBSTRATE PREPARATION AND SPUTTER CLEANING PARAMETERS FOR TASK II DEPOSITIONS (Continued)

Run Number	Substrate Material	Finishing Treatment, Surface Preparation, and Primary Cleaning	Voltage, V	Sputter Cleaning[1] Current, mA	Duration, ks	Pressure, N/m²	μ
II-A-3[2]	OFHC Copper (0.32 cm plate)	Sanded lengthwise with No. 600 grit paper, ethyl alcohol rinse	-25	12	1.20	0.59	4.4
II-A-4	OFHC Copper (1.9 cm dia bar)	3 min. etch in dilute HNO_3, ethyl alcohol rinse	-25	400	0.30	0.72	5.4
II-A-5[2]	OFHC Copper (1.9 cm dia bar)	3 min. etch in dilute HNO_3 ethyl alcohol rinse	-25	380	0.30	0.65	4.9
II-A-6	OFHC Copper and Type 6061 Aluminum alloy (0.32 cm plate)	Sanded lengthwise with No. 600 grit paper, AJAX® scrub, and ethyl alcohol rinse	-25	600	0.30	0.61	4.6
II-A-7	OFHC Copper and Type 6061 Aluminum alloy (0.32 cm plate)	Sanded lengthwise with No. 600 grit paper, AJAX® scrub, and ethyl alcohol rinse	-25	470	0.30	0.61	4.6
II-A-8	OFHC Copper and Type 6061 Aluminum alloy (0.32 cm plate)	Sanded lengthwise with No. 600 grit paper, AJAX® scrub, and ethyl alcohol rinse	-25	430	0.30	0.65	4.?
II-A-9	OFHC Copper and Type 6061 Aluminum alloy (0.32 cm plate)	Sanded lengthwise with No. 600 grit paper, AJAX® scrub, and ethyl alcohol rinse	-25	450	0.30	0.64	4.8
II-A-10	OFHC Copper and Type 6061 Aluminum alloy (0.32 cm plate)	Sanded lengthwise with No. 600 grit paper, AJAX® scrub, and ethyl alcohol rinse	-25	470	0.30	0.64	4.8
II-A-11	Type 304 Stainless Steel (1.3 cm dia)	Sanded lengthwise with No. 600 grit paper, AJAX® scrub, and ethyl alcohol rinse	-25	300	0.30	0.63	4.7
II-A-12	Type 304 Stainless Steel (1.3 cm dia)	Sanded lengthwise with No. 600 grit paper, AJAX® scrub, and ethyl alcohol rinse	-25	300	0.30	0.60	4.5
IV-A-13	OFHC Copper	Sanded lengthwise with No. 600 grit paper, AJAX® scrub, ethyl alcohol rinse	-25 -50 -100	500	0.30 0.60 0.30	0.40	3.0
IV-A-14	OFHC Copper	Sanded lengthwise with No. 600 grit paper, AJAX® scrub, ethyl alcohol rinse	-25 -50 -100	500	0.30 0.60 0.30	0.42	3.2
IV-A-15	OFHC Copper	Sanded lengthwise with No. 600 grit paper, AJAX® scrub, ethyl alcohol rinse.	-25 -50 -100	500	0.30 0.60 0.30	0.41	3.1

NOTES:

[1] Target and substrate cleaned simultaneously in triode discharge

[2] Substrate rotated during cleaning; all other stationary

[3] Cleaning and deposition performed simultaneously

NM - Not Measured

TABLE VIII. SUMMARY OF TASK II DEPOSITION PARAMETERS

Run Number	Target Material	Substrate Material	Substrate Voltage, V	Substrate Current, A	Target Voltage, V	Target Current, A	Magnetic Coils Current, A	Magnetic Coils Separation, cm	Time ks	Time hr	Substrate Temperature °K	Substrate Temperature °F	Maximum Deposit Thickness mm	Maximum Deposit Thickness mils	Average Deposition Rate nm/s	Average Deposition Rate mil/hr	Pressure N/m²	Pressure μ
II-1	OFHC Copper	Aluminum 6061	− 50	3	− 900	3.0	7.5	7.6	3.6	1.0	364	196	0.305	12.0	16.9	2.4	0.7	5.6
			− 50	3	− 775	3.0	7.5	7.6	5.4	1.5							0.7	5.6
			−100	110	− 770	2.0	5.0	7.6	3.6	1.0							3.6	27
			− 50	85	− 850	2.5	5.0	7.6	5.4	1.5							3.6	27
II-2	OFHC Copper	Type 6061 Aluminum alloy	−100	110	− 820	2.0	5.0	7.6	3.6	1.0	360	188	0.091	3.6	12.7	1.8	3.6	27
			−200	135	− 515	2.0	7.5	7.6	3.6	1.0							4.3	32
II-3	OFHC Copper	Type 6061 Aluminum alloy	−350	190	− 800	1.6	5.0	7.6	12.6	3.5	557	544	0.127	5.0	6.8	0.95	3.6	27
			−150	88	− 800	1.6	5.0	7.6	6.3	1.75								
II-4	OFHC Copper	Type 6061 Aluminum alloy	0	0	− 800	4.0	5.0	7.6	20.7	5.75	nm	0.444		17.5	21.1	3.0	1.9	14
II-5	OFHC Copper	Type 6061 Aluminum alloy	0	0	− 750	4.5	5.0	7.6	16.2	4.5	nm	nm	0.899	31.1	21.1	3.0	2.0	15
			0	0	− 900	3.0	5.0	7.6	10.8	3.0							0.27	2
			0	0	−1300	3.0	5.2	7.6	10.8	3.0[1]							0.27	2
II-6	OFHC Copper	Type 6061 Aluminum alloy	0	0	−1000	4.0	6.0	7.6	72.0	20.0	367	200	1.397	55.0	19.0	2.7	0.72	5.4
II-7	OFHC Copper	Type 6061 Aluminum alloy	0	0	−1000	4.2	6.0	7.6	70.2	19.5	700	800	1.524	60.0	21.8	3.1	0.62	3.5
II-8	OFHC Copper	Type 6061 Aluminum alloy	0	0	−1000	2.5	5.75	7.6	109.8	30.5	644	700	1.400	55.1	12.7	1.8	0.90	6.8
II-9[2]	Cu-0.15 Zr	Type 6061 Aluminum alloy	0	0	−1000	3.3	6.5	15.2	90.0	25.0	589	600	1.300	51.2	14.1	2.0	2.9	22
II-10	Cu-0.15 Zr	Type 6061 Aluminum alloy	0	0	−1000	3.7	4.0	10.2	92.7	25.75	644	700	1.270	50.0	13.4	1.9	2.7	20
II-11	Cu-0.15 Zr	Type 6061 Aluminum alloy	0	0	−1000	1.8	3.2	10.2	108.0	30.0	367	200	0.740	29.1	6.9	0.97	2.7	20
II-12	Cu-0.15 Zr	Type 6061 Aluminum alloy	0	0	−1000	3.5	5.5	10.2	55.8	15.5	589	600	0.686	27.0	12.7	1.8	0.93	7
II-13	Cu-0.15 Zr	Type 6061 Aluminum alloy	0	0	−1000	3.4	4.6	10.2	108.0	30.0	672	750	1.346	53.0	12.7	1.8	0.59	4.4
II-14	Cu-0.15 Zr	Type 6061 Aluminum alloy	0	0	− 700	5.0	5.0	10.2	3.6	1.0	644	700	0.528	20.8	12.7	1.8	3.9	29
			0	0	−1000	2.5	4.3	10.2	27.0	7.5	644	700					0.59	4.4
			0	0	−1000	2.5	4.3	10.2	25.2	7.0	644	700					0.45	3.4
II-15	Cu-0.15 Zr	Type 6061 Aluminum alloy	0	0	−1500	6.0	4.3	10.2	19.8	5.5	422	300	3.708	146.0	29.6	4.2	0.78	5.9
			0	0	−1500	5.0	4.3	10.2	104.4	29.0	422	300	3.708				0.47	3.6
II-16	Cu-0.15 Zr	OFHC Copper	−300	56	−1000	2.5	6.3	10.2	18.0	5.0	811	1000	1.189	46.9	10.6	1.5	1.9	14
			−250	47	−1000	2.5	5.5	10.2	25.2	7.0	811	1000					1.3	10
			0	0	−1000	2.5	6.2	10.2	48.6	13.5	811	1000					0.80	6.0
			0	0	−1000	2.5	4.8	10.2	21.6	6.0	811	1000					0.74	5.6
II-17	Cu-0.15 Zr	OFHC Copper	0	0	−1000	5.0	4.7	10.2	23.4	6.5	861	1090	1.466	57.7	20.4	2.9	1.0	7.6
			0	0	−1000	5.0	4.8	10.2	26.1	7.25	866	1100					0.68	5.1
			0	0	−1000	5.0	4.75	10.2	22.5	6.25	922	1200					0.69	5.1

NOTES:

[1] Deposition performed in triode discharge.

TABLE VIII. SUMMARY OF TASK II DEPOSITION PARAMETERS (Continued)

58

ORIGINAL PAGE IS OF POOR QUALITY

Run Number	Target Material	Substrate Material	Substrate Voltage, V	Substrate Current, A	Target Voltage, V	Target Current, A	Magnetic Coils Current, A	Magnetic Coils Separation, cm	Time ks	Time hr	Substrate Temp. °K	Substrate Temp. °F	Max Deposit Thickness mm	Max Deposit Thickness mils	Avg Deposition Rate nm/s	Avg Deposition Rate mil/hr	Pressure N/m²	Pressure μ
II-18	Cu-0.15 Zr	OFHC Copper	0	0	-1000	0.5	2.6	10.2	11.7	3.25	580	585	1.318	51.9	9.2	1.3	0.72	5.4
			-300	44	-750	5.0	2.5	10.2	0.72	0.2	372	210					2.1	15
			0	0	-1000	2.5	2.5	10.2	23.4	6.5	855	1080					0.85	6.4
			-1000	40	0	0	5.5	10.2	1.8	0.5	314	285					1.4	11
			-200	95	-1000	2.5	2.8	10.2	109.8	30.5	1019	1375					0.47	3.8
II-19	Cu-0.15 Zr	OFHC Copper	0	0	-1000	2.5	4.1	10.2	26.1	7.25	866	1100	0.541	21.3	9.2	1.3	0.56	4.2
			0	0	-1000	2.5	4.3	10.2	30.6	8.5	866	1100					0.52	3.9
II-20	Cu-0.15 Zr	347 Stainless Steel	-200	28	-1000	2.5	4.1	10.2	113.4	31.5	700	800	1.826	71.9	16.9	2.4	0.45	3.4
II-21	Cu-0.15 Zr	347 Stainless Steel	-50	8	-525	5.0	6.4	10.2	36.0	10.0	694	790	0.439	17.3	12.0	1.7	1.3	10
II-22	Cu-0.15 Zr	347 Stainless Steel	0	0	-2000	0.5	0.7	10.2	49.5	13.75	950	1250	0.419	16.5	2.7	0.38	0.49	3.7
			0	0	-2000	0.5	0.8	10.21	27.0	7.5	944	1240					0.33	2.5
			0	0	-2000	0.5	1.1	10.2	27.0	7.5	939	1230					0.16	1.2
			0	0	-2000	0.5	1.1	10.2	27.0	7.5	933	1220					0.19	1.4
			0	0	-2000	0.5	1.1	10.2	27.0	7.5							0.20	1.5
II-23	Cu-0.15 Zr	347 Stainless Steel	0	0	-2000	0.5	0.75	10.2	24.3	6.75	939	1230	0.193	7.6	2.6	0.37	1.13	8.5
			0	0	-2100	0.5	1.0	10.2	25.2	7.0	1077	1480					0.20	1.5
			0	0	-2000	0.5	1.0	10.2	23.4	6.5	1116	1550					0.20	1.5
II-24	Cu-0.15 Zr	347 Stainless Steel	-25	12	-1500	2.0	2.0	10.2	1.2	0.33	566	560	0.457	18.0	9.5	1.35	0.59	4.4
			-25	12	-1500	2.0	2.5	10.2	21.6	6.0	902	1165					0.32	2.4
			-25	12	-1500	2.2	2.2	10.2	3.6	1.0	877	1120					0.31	2.3
			0	0	-1500	2.0	2.7	10.2	3.6	1.0	900	1160					0.25	1.8
			+25	2	-1500	2.0	2.8	10.2	18.0	5.0	955	1260					0.26	1.9
II-25	Cu-0.15 Zr	347 Stainless Steel	+25	2.2	-1500	2.2	1.5	10.2	27.0	7.5	1093	1490	0.254	10.0	9.4	1.33	0.59	4.4
II-26[1]	Cu-0.15 Zr	OFHC Copper	-25	0.85	-25	2.3	Coils not Used		0.29	0.08	722	840	0.203	8.0	5.1	0.72	0.67	5.0
			-25	0.85	-25	2.5			1.8	0.50	755	900					0.41	3.1
			-25	0.85	-25	2.4			7.2	2.0	822	1020					0.41	3.1
			-25	0.85	-500	2.85			4.5	1.25	1122	1380					0.67	5.0
			-25	1.04	-25	3.2			0.29	0.08	772	930					0.35	2.6
			-25	0.91	-500	3.1			15.3	4.25	1186	1675					0.25	1.8
			-1.5	0.71	-500	2.85			10.8	3.00	1186	1675					0.35	2.6
II-27[1]	Cu-0.15 Zr	Type 6061 Aluminum alloy	-25	0.65	-25	1.6			0.29	0.08	294	70	0.249	9.8	5.1	0.72	0.73	5.5
			-25	1.10	-500	3.4			21.6	6.0	344	160					0.40	2.9
			-25	1.20	-500	3.3			27.0	7.5	350	170					0.49	3.7
II-28[1]	Cu-0.15 Zr	Type 6061 Aluminum alloy	-25	1.8	-500	3.5			3.6	1.0	419	295	0.594	23.4	10.0	1.42	0.45	3.4
			-25	2.3	-500	5.5			7.2	2.0	416	290					0.33	2.5
			-25	2.2	-500	5.4			6.3	1.75	427	310					0.33	2.5
			-25	2.2	-500	5.4			3.6	1.0	444	340					0.32	2.4
			-25	2.2	-500	5.4			13.5	3.75	464	375					0.29	2.3
			-25	2.15	-500	5.2			25.2	7.0	475	395					0.25	1.8
II-29[1]	Cu-0.15 Zr	Type 6061 Aluminum alloy	-25	2.3	-500	5.3			9.0	2.5	422	300	0.950	37.4	12.7	1.80	0.37	2.7
			-25	2.3	-500	5.3			3.6	1.0	450	350					0.41	3.1
			-25	2.24	-500	5.0			25.2	7.0	400	260					0.68	5.1
			-25	2.3	-500	5.0			22.5	6.25	400	260					0.63	4.7
			-25	2.25	-500	5.0			7.2	2.0	400	260					0.52	3.9
			-25	2.3	-500	5.0			7.2	2.0	411	280					0.49	3.7

NOTES:

[1] Deposition performed in triode discharge.

TABLE IX. SUMMARY OF TASK II DEPOSITION PARAMETERS FLAT PLATE COATER [1]

Run Number	Target Material	Substrate Material	Substrate Voltage, V	Substrate Current, A	Target Voltage, V	Target Current, A	Time ks	Time hr	Substrate Temperature °K	Substrate Temperature °F	Maximum Deposit Thickness mm	Maximum Deposit Thickness mils	Average Deposition Rate nm/s	Average Deposition Rate mil/hr	Pressure N/m^2	Pressure μ
II-A-1	Cu-0.15 Zr	OFHC Copper (0.38 cm plate)	-25	0.40	- 25	0.52	0.29	0.08	672	750	0.084	3.3	3.5	0.49	0.72	5.4
			-25	0.40	- 25	0.58	0.9	0.25	844	1060					0.72	5.4
			-25	0.38	-800	0.58	12.6	3.5	1111	1540					0.68	5.1
			0	0	-800	0.58	12.6	3.5	1122	1560					0.65	4.9
II-A-2	Cu-0.15 Zr	OFHC Copper (0.38 cm plate)	-25	0.38	- 25	0.56	0.29	0.08	822	1020	0.140	5.5	2.6	0.37	0.65	4.9
			-25	0.38	-800	0.57	52.2	14.75	1127	1570					0.64	4.8
II-A-3	Cu-0.15Zr [2]	OFHC Copper (0.38 cm plate)	-25	0.37	- 25	0.53	0.29	0.08	nm	nm	0.249	9.8	3.2	0.45	0.68	5.1
			-25	0.38	-800	0.58	25.2	7.0 [3]	(1116)	(1550)					0.65	4.9
			-25	0.38	- 25	0.52	0.29	0.08							0.71	5.3
			-25	0.38	-800	0.57	52.2	14.75							0.64	4.8
II-A-4	Cu-0.15 Zr	OFHC Copper (1.9 cm dia. bar)	-25	0.36	- 25	0.53	0.29	0.08	nm	nm	0.147	5.8	2.8	0.39	0.71	5.3
			-25	0.35	-800	0.57	51.3	14.5	(1116)	(1550)					0.64	4.8
II-A-5	Cu-0.15 Zr [2]	OFHC Copper (1.9 cm dia. bar)	-25	0.37	- 25	0.55	0.29	0.08	nm	nm	0.142	5.6	2.6	0.37	0.72	5.4
			-25	0.36	-800	0.55	53.1	15.0	(1116)	(1550)					0.61	4.6
II-A-6	Cu-0.15 Zr	OFHC Copper and Type 6061 aluminum alloy (0.38 cm plate)	-25	0.60	- 25	0.50	0.29	0.08	339	150	0.076	3.0	2.6	0.37	0.61	4.6
			-25	0.88	-800	0.77	28.8	8.00	351	190					0.31	2.3
II-A-7	Cu-0.15 Zr	OFHC Copper and Type 6061 aluminum alloy (0.38 cm plate)	-25	0.47	- 25	0.52	0.29	0.08	327	130	0.160	6.3	3.0	0.43	0.61	4.6
			-25	0.66	-800	0.76	52.2	14.75	350	170					0.57	4.3
II-A-8	Cu-0.15 Zr	OFHC Copper and Type 6061 aluminum alloy (0.38 cm plate)	-25	0.43	- 25	0.51	0.29	0.08	391	245	0.279	11.0	3.6	0.51	0.65	4.9
			0	0	-800	0.75	26.1	7.25	411	280					0.56	4.2
			-25	0.45	- 25	0.52	0.29	0.08	377	220					0.65	4.9
			0	0	-800	0.75	52.2	14.75	394	250					0.56	4.2
II-A-9	Cu-0.15 Zr	OFHC Copper and Type 6061 aluminum alloy (0.38 cm plate)	-25	0.45	- 25	0.51	0.29	0.08	377	220	0.152	6.0	2.9	0.41	0.64	4.8
			-10	0	-800	0.72	51.3	14.50	383	230					0.56	4.2
II-A-10	Cu-0.15 Zr	OFHC Copper and Type 6061 aluminum alloy (0.38 cm plate)	-25	0.47	- 25	0.49	0.29	0.08	377	220	0.051	2.0	1.2	0.17	0.63	4.7
			-50	0.65	-800	0.75	43.2	12.00	394	250					0.56	4.2
II-A-11	Cu-0.15 Zr	Type 304 Stainless Steel (1.3 cm dia.)	-25	0.30	- 25	0.50	0.29	0.08	339	150	0.191	7.5	3.6	0.52	0.63	4.7
			-25	0.50	-800	0.92	50.4	14.25	339	150					0.56	4.2
II-A-12	Cu-0.15 Zr	Type 304 Stainless Steel (1.3 cm dia.)	-25	0.30	- 25	0.48	0.29	0.08	339	150	0.254	10.0	5.6	0.80	0.60	4.5
			0	0	-800	0.88	45.0	12.50	339	150					0.56	4.2
IV-A-13	OFHC Copper and Al_2O_3	OFHC Copper	-25	0.48	-1500	0.50	252.0	70.0	389	240	-	-	-	-	0.40	3.0
IV-A-14	OFHC Copper and Al_2O_3	OFHC Copper	Ground	0	-1500	0.50	244.8	68.0	422	300	0.700	27.5	2.9	0.40	0.43	3.2
IV-A-15	OFHC Copper and SiC	OFHC Copper	-25	0.48	-1500	0.50	253.8	70.5	439	330	1.780	70.0	7.1	1.0	0.41	3.1

NOTES:

[1] All II-A depositions performed with triode discharge.

[2] Substrate rotated during entire run.

[3] System vented, filaments replaced.
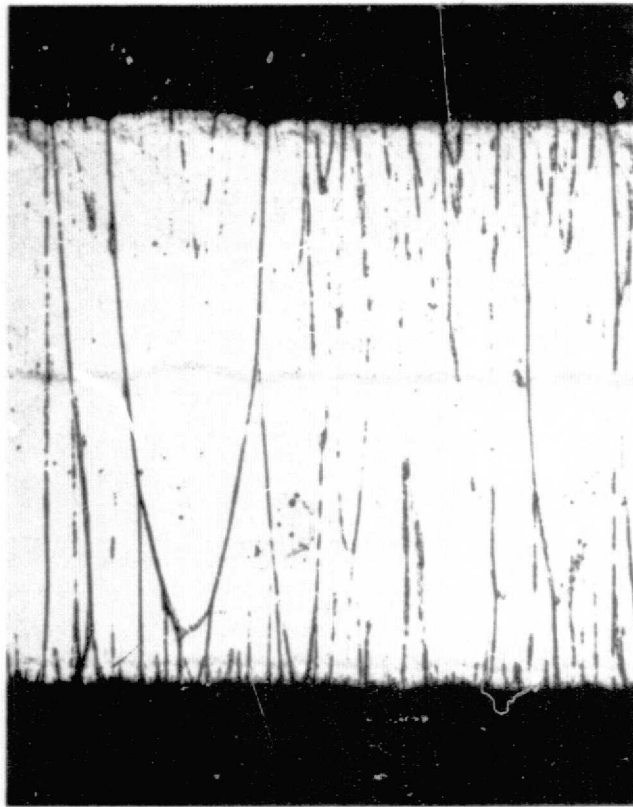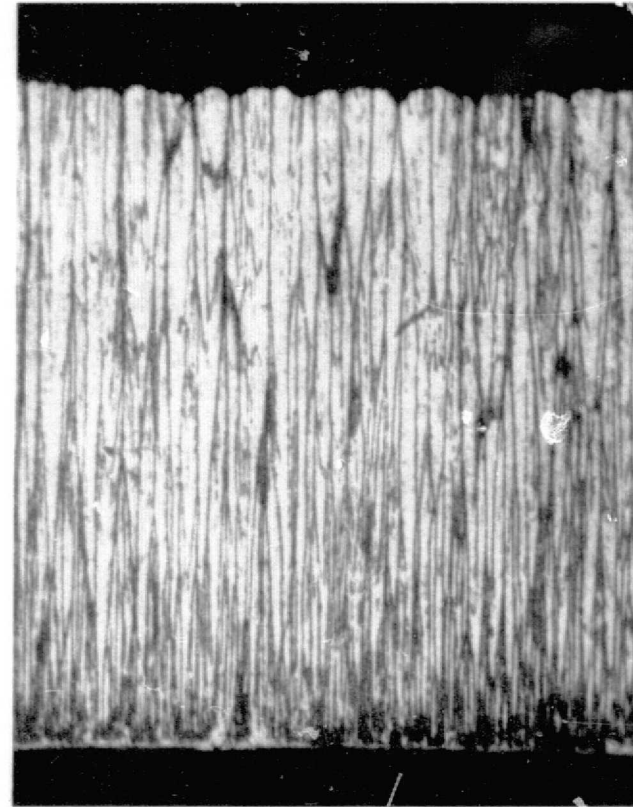
Biased
Run II-1

Biased
Run II-4

Mag: 250X

Figure 35. Open Fibrous Structure of OFHC Copper Sputtered at Low Substrate Temperatures
(333 to 389°K)

FD 91397

Mag: 65X

Figure 36. Typical Fracture Topography of OFHC   FD 91398
          Copper Deposited at Low Substrate
          Temperatures
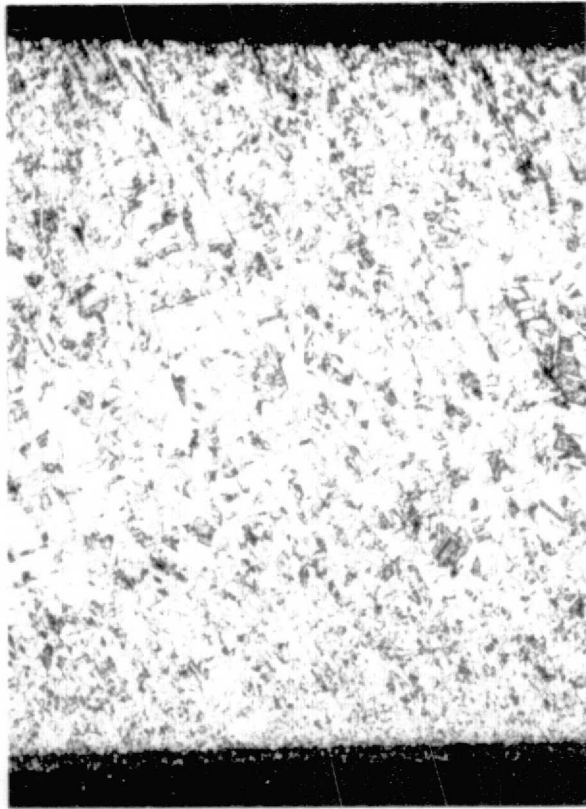
13.3 nm/s   30X

10.5 nm/s   250X

Figure 37. Microstructure of OFHC Copper Sputtered at 700°K (800°F) With Low Deposition Rates,   FD 91399
Run II-7

100X

250X

100 μ

Figure 38. Microstructure of Sputtered OFHC
Copper Deposited at 700°K (800°F) and
19.7 nm/s (2.8 mils/hr), Run II-7

FD 91400

63

TABLE X. SUMMARY OF ROOM TEMPERATURE TENSILE PROPERTIES OF TASK II SPUTTERED MATERIALS

Material	Run Number	Average Substrate Temperature		Condition or Post Deposition Heat Treatment	Yield Strength		Ultimate Tensile Strength		Elongation Percent
		°K	°F		MN/m^2	psi	MN/m^2	psi	
OFHC Copper	II-6	367	200	As sputtered	–	–	110.6	16,050	–
	II-6	367	200	As sputtered	–	–	115.1	16,700	–
	II-7	700	800	As sputtered	–	–	23.8	3,450	–
	II-7	700	800	As sputtered	–	–	25.9	3,760	–
	II-8	644	700	As sputtered	79.2	11,490	184.6	26,800	25
	II-8	644	700	As sputtered	110.9	16,080	189.5	27,500	23
	II-8	644	700	813°K-14.4ks-VAC	84.7	12,300	171.6	24,900	25
	II-8	644	700	813°K-14.4ks-VAC	80.1	11,630	175.0	25,400	26
0.15 Zr-Cu	II-9	589	600	As sputtered	–	–	20.9	3,040	–
	II-9	589	600	As sputtered	–	–	51.1	7,420	–
	II-16	813	1000	As sputtered	–	–	71.9	10,430	–
	II-16	813	1000	As sputtered	–	–	93.4	13,550	–
	II-29	423	300	1145°K-14.4ks-VAC	119.6	16,360	273.5	39,700	36
	II-29	423	300	1145°K-14.4ks-VAC	114.0	16,550	257.7	37,400	30
	II-29	423	300	1198°K-14.4ks-VAC	97.1	14,100	215.7	31,300	20
	II-29	423	300	1198°K-14.4ks-VAC	110.0	15,970	264.6	38,400	28
Al_2O_3-Cu	II-A-13	389	240	As sputtered	514.7	74,700	535.4	77,700	20
	II-A-13	389	240	As sputtered	598.1	86,800	636.0	92,300	8
	II-A-13[1]	389	240	As sputtered	155.7	22,600	226.7	32,900	40
	II-A-13[1]	389	240	As sputtered	159.2	23,100	221.9	32,200	20
	II-A-14	422	300	As sputtered	676.6	98,200	771.0	111,900	6
	II-A-14	422	300	As sputtered	497.5	72,200	749.6	108,800	6
	II-A-14[1]	422	300	As sputtered	458.2	66,500	739.3	107,300	12
	II-A-14[1]	422	300	As sputtered	578.8	84,000	702.8	102,000	8
SiC-Cu	II-A-15	439	330	As sputtered	426.5	61,900	585.0	84,900	12
	II-A-15	439	330	As sputtered	830.2	120,500	983.9	142,800	8
	II-A-15[1]	439	330	As sputtered	398.9	57,900	531.9	77,200	16

NOTES:

[1] Sample from substrate facing OFHC copper target.
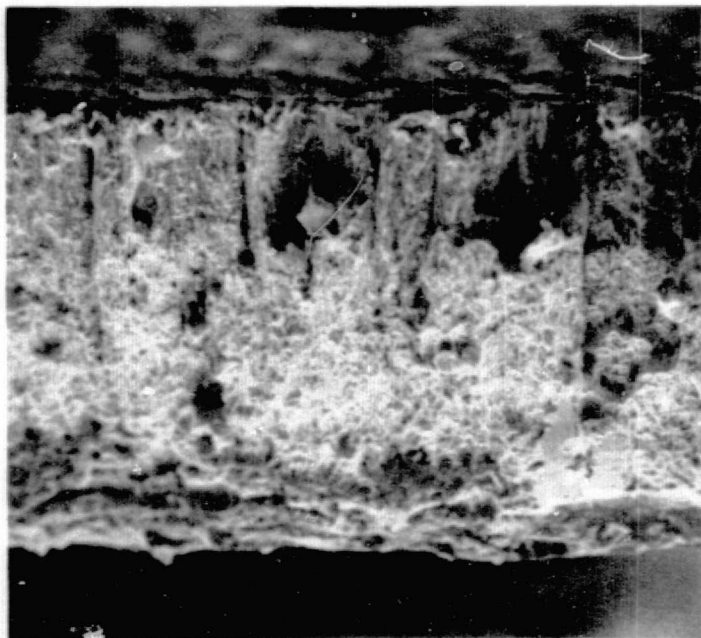
140X

Low Rate
(End of Substrate)
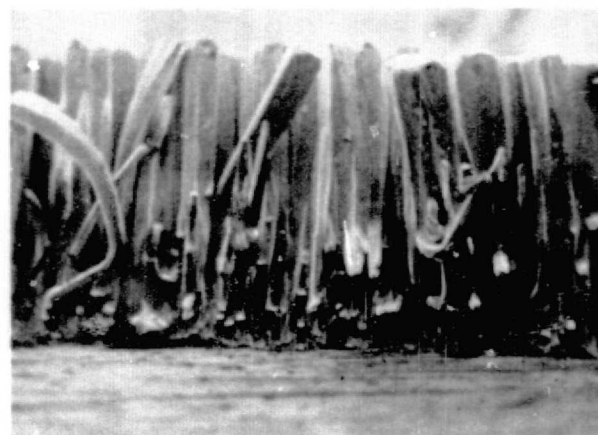
30X

High Rate
(Center of Substrate)

Figure 39. Fracture Topography of OFHC Copper Sputtered at Low Rate (7. 0 nm/s) and High Rate
(19. 7 nm/s) at 700°K (800°F) in Run II-7

FD 91401

At a substrate temperature of 644°K (700°F) and deposition rates between 3.5 and 12.7 nm/s (0.5 and 1.8 mils/hr) in run II-8 the structure was dense and appeared equiaxed, figure 40. The deposit made at 12.7 nm/s (1.8 mils/hr) exhibited a yield strength up to 110.9 MN/m² (16,090 psi) and an ultimate strength up to 189.5 MN/m² (27,500 psi), table X. The deposits were ductile, exhibiting high tensile elongations. However, the analysis of the fracture face of tensile specimens revealed evidence of a columnar macrostructure for the higher rate deposited material, figure 41. This structure did not prevent tensile elongations of 23 and 25% from being attained. Chemical analysis of the II-8 deposit for impurity gases showed that the deposit contained 10-20 ppm oxygen, 60 ppm hydrogen and less than 10 ppm nitrogen.

For the depositions where an open structure was obtained, a domed surface topography (figure 42) was noted. For equiaxed deposits, a domed surface topography was still present but the bonding between columns was apparent, figure 42. At low deposition rates (below about 14.1 nm/s) the structures of OFHC were similar to those predicted by the three zone models of Movchan and Demchishin[10] and Thornton[9]. At the higher deposition rates, the structures did not correlate with these models.

Other factors seemed to affect the deposit structure very little. The surface finish did affect structure, as discussed in Task I, with the rough vapor blasted surface promoting open type structures (run II-1, 2 and 3). The preparation by sanding (600 grit SiC) and Ajax® scrubbing was found to yield a suitable surface, so high quality deposits could be attained. In several runs (table VIII) discharge pressures up to 32 microns were investigated. With higher pressure, no significant effects in structure morphology were observed. This is in disagreement with the pressure-structure-temperature model described by Thornton[9]. This discrepancy is probably due to system configuration and deposition parameter variations between the two studies. In this work, the aggregate analysis is that temperature and deposition rate are the most influential in dictating OFHC copper deposit growth morphology.

0.15Zr-Cu (AMZIRC®)

The effect of deposition rate and substrate temperature on the structure of 0.15Zr-Cu was similarly observed in sputtering from the hollow cathode. At substrate temperatures from 360°K to 423°K (200°F to 300°F), the structures contained tapered columns with open or nonbonded boundaries. This structure (figure 43) was observed at deposition rates from 7.0 to 29.6 nm/s. As was found typical with low substrate temperatures, a domed surface topography resulted. With increasing rate, the column diameter increased, as did the openness of the structure. At substrate temperatures and deposition rates where OFHC copper exhibited a dense structure, the 0.15Zr-Cu deposits remained columnar and open. At 589°K (600°F) and 644°K (700°F) and deposition rates between 7.0 to 16.9 nm/s (1.0 and 2.4 mils/hr), the structure was similarly open with recrystallization occurring within the tapered columns, figure 44. At the higher deposition rates, 16.9 to 24.7 nm/s (2.4 and 3.5 mils/hr) at 698°K (800°F) the open columnar structure still resulted, figure 45. At higher substrate temperatures 898°K to 943°K (980°F to 1240°F) and for deposition rates between 2.6 and 20.4 nm/s (0.37 and 2.9 mils/hr) similar structures prevailed. Although the extent of intergrain bonding was increased with higher substrate temperatures total annihilation of voids between the grains was not achieved. The typical structures produced within these temperatures and deposition rates are shown in figure 46. Only at the low deposition rate of 2.6 nm/s (0.37 mil/hr) and a substrate temperature of 943°K (1240°F) did the structure of 0.15 Zr-Cu approach full density, figure 46.

100X

100X

200 μ
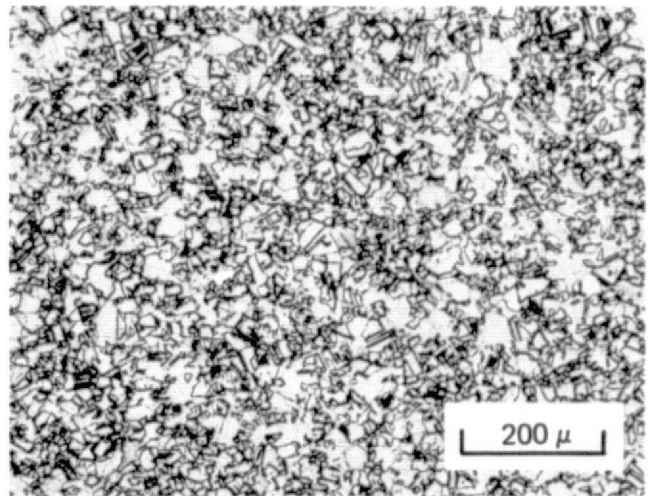
Figure 40. Microstructure of OFHC Copper   FD 91402
            Sputtered With a Substrate Tempera-
            ture of 644°K (700°F) and a Deposition
            Rate of 8.5 nm/s (1.2 mils/hr) in
            Run II-8

250X   65X
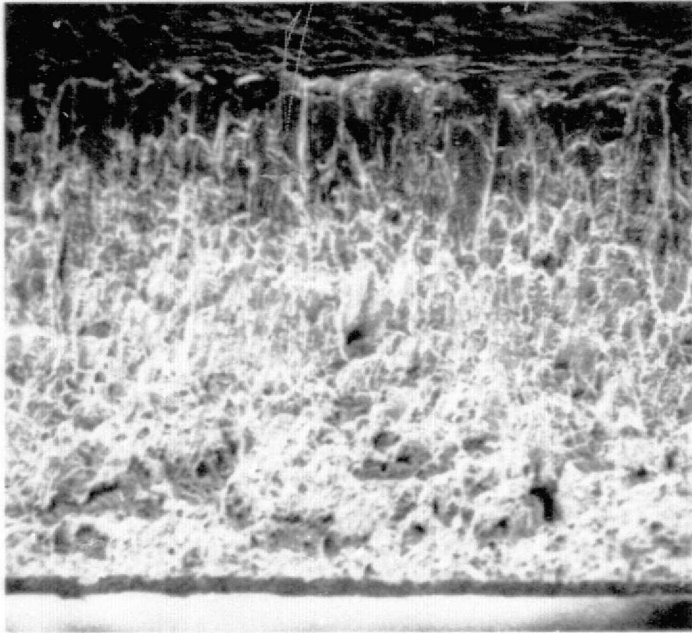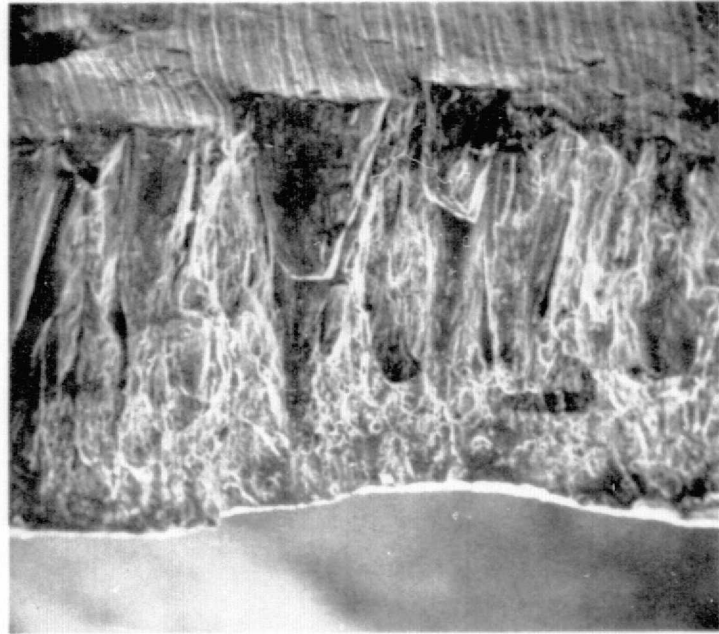
Low Rate, 7.0 nm/s   High Rate, 12.7 nm/s

Figure 41.   Fracture Topography of OFHC Copper, Run II-8

FD 91403

210X   220X
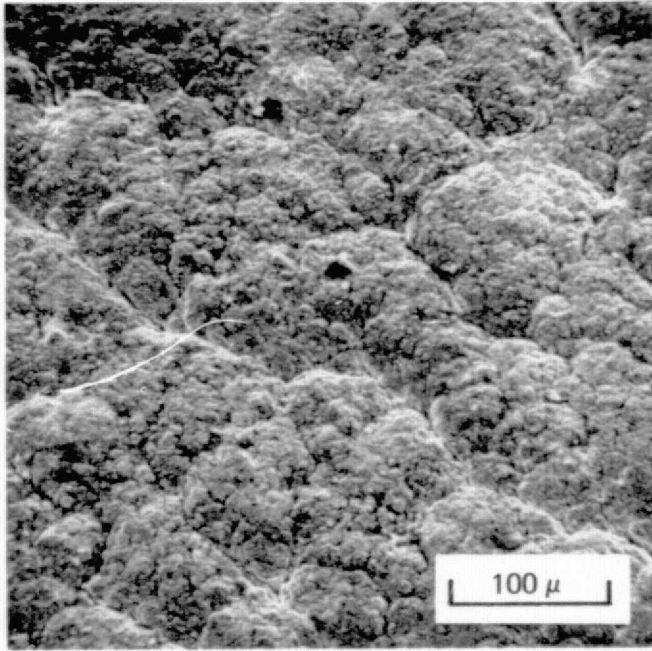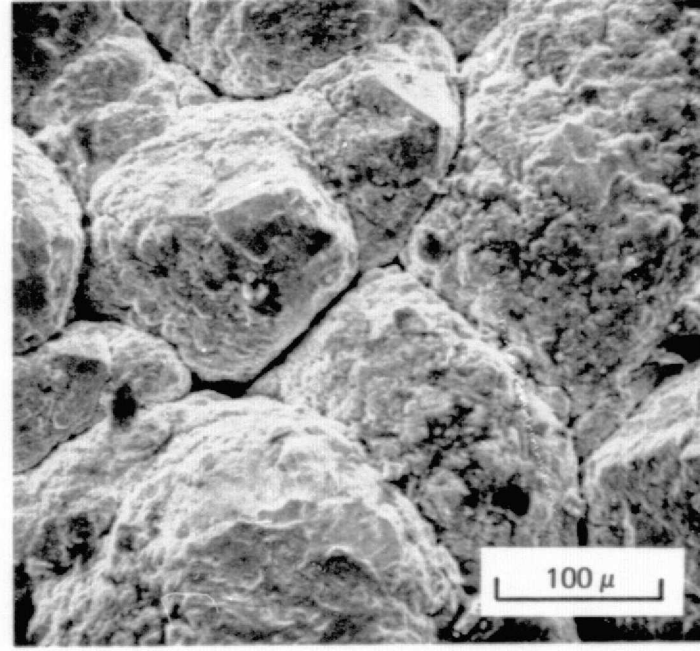
7.0 nm/s   14.1 nm/s

Figure 42. Surface Topography of High and Low Deposition Rate Deposits on Run II-7 Substrate   FD 91404

60X 125X

200 μ
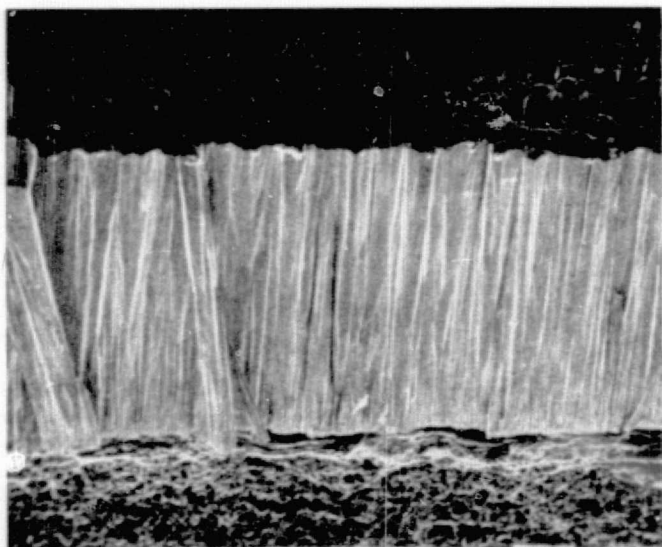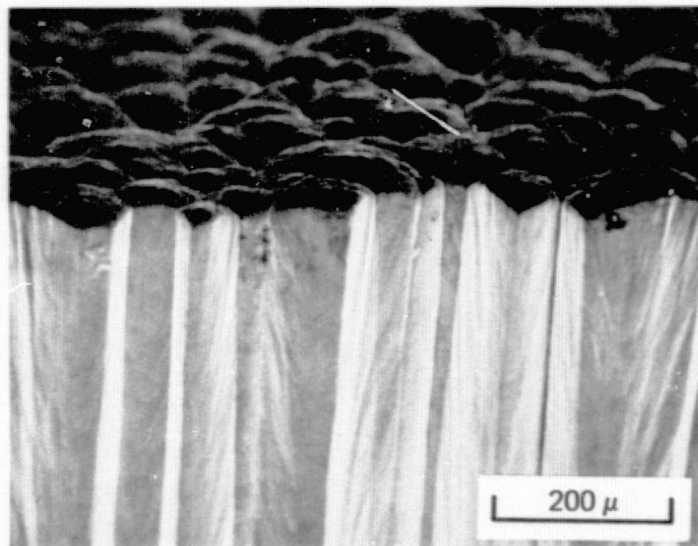
Figure 43. Typical Fibrous Morphology of Sputtered 0. 15 Zr-Cu Deposited at Low Substrate Temperatures   FD 91405

50X
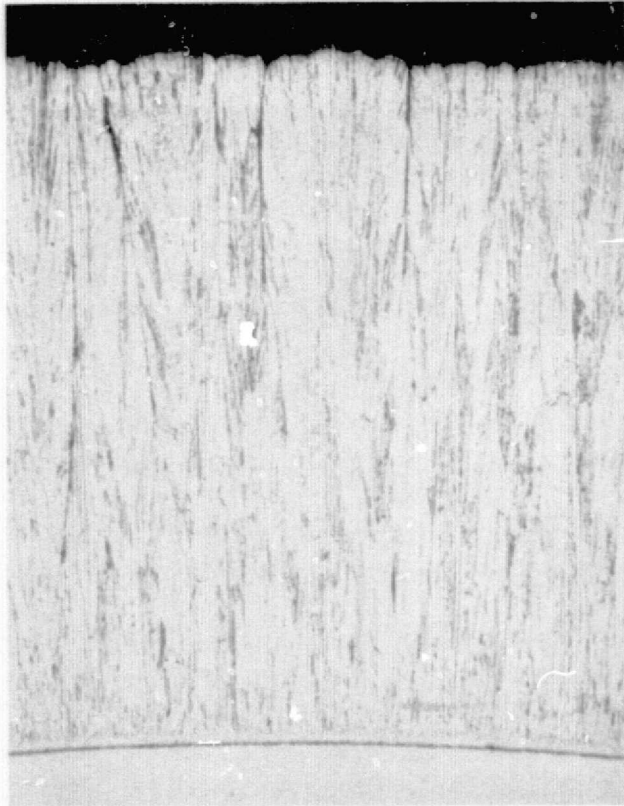
150X

Figure 44. Microstructure of Sputtered 0.15 Zr-Cu Deposited With a Substrate Temperature of 589°K (600°F) at a Deposition Rate of 16.9 nm/s (2.4 mils/hr)   FD 91406
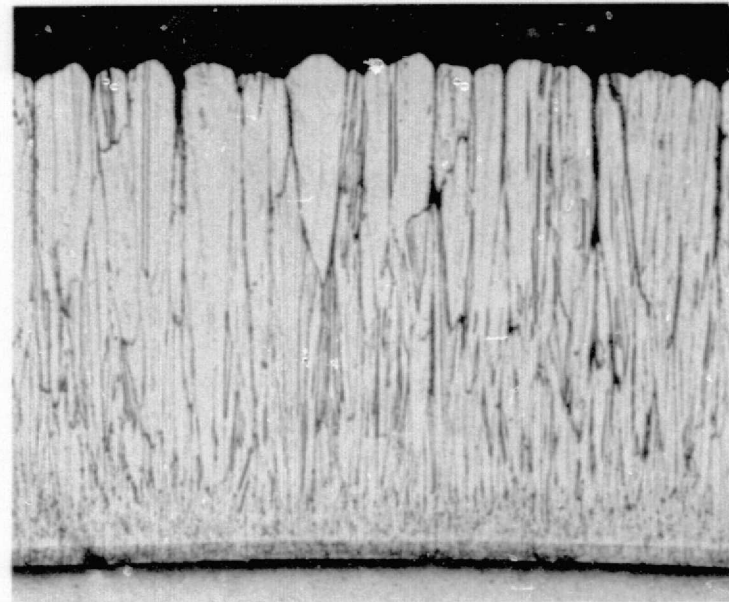
Figure 45. Microstructure of 0.15 Zr-Cu Deposited at 24.6 nm/s (3.5 mils/hr) and a Substrate Temperature of 698°K (800°F)   FD 91407

71
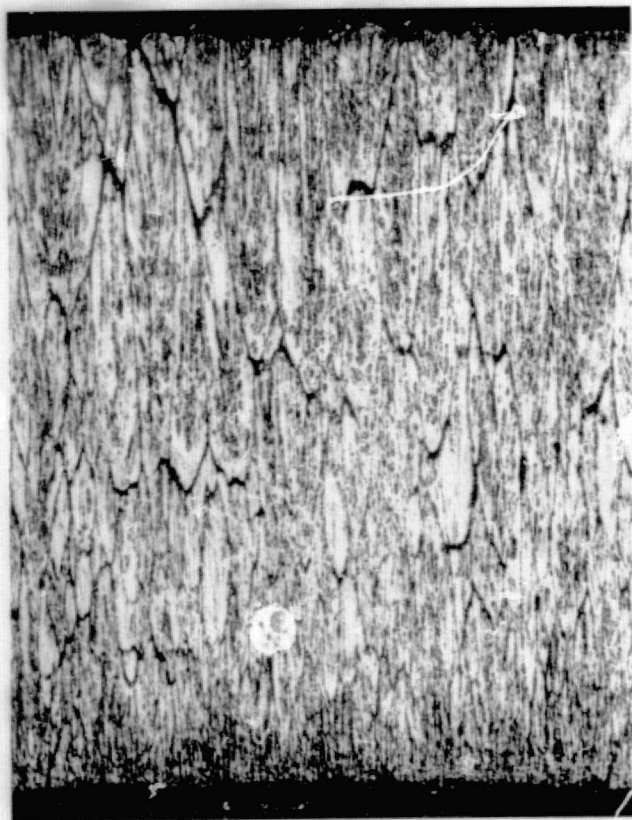
898K-9.2 nm/s   943K-2.6 nm/s

Figure 46. Microstructure of Sputtered 0.15 Zr-Cu Deposited With a Substrate Temperature
of 898°K (980°F) and 943°K (1240°F)

FD 91408

In sputtering the 0.15 Zr-Cu alloy, the zirconium content of all deposits was within ±0.02 wt% of the target zirconium level. On the sample from run II-13, a gas analysis showed that the deposit contained 10 ppm nitrogen, 90 ppm oxygen, and 24 ppm hydrogen. These levels are not excessively high, but are higher than those observed for the sputtered OFHC copper in run II-8. It is felt that some gas presence is attributed to the open structure of this deposit. The surface topography on all 0.15 Zr-Cu deposits exhibited the domed appearance similar to that shown in figure 47. In no deposition did a faceted or flat surface topography result. All structures exhibited brittle fracture, figure 48, and low tensile strength, table X. On the deposit sputtered at 14.1 nm/s (2.0 mil/hr) and a substrate temperature of 589°K (600°F) the tensile strength was 51.1 MN/m^2 (7420 psi). At 813°K (1000°F) and a 10.5 nm/s (1.5 mil/hr) deposition rate, a tensile strength of 93.4 MN/m^2 (13,500 psi) was obtained. No yielding was observed and elongation was less than 0.5% in each case.

The difficulty in generating a dense deposit of 0.15 Zr-Cu was attributed to a combination of cathode geometry (cylindrical targets) and decreased surface and bulk mobility due to the zirconium addition. In studies by Thornton[9] with a hollow cathode, a greater side flux of low energy (low angle) material impacts the substrate surface which increases intergrain shading and decreases surface mobility. The difference in diffusion behavior between 0.15 Zr-Cu and OFHC copper is indicated by the increased temperature (approximately 305°K (550°F) higher) required to anneal and recrystallize wrought 0.15 Zr-Cu as compared to that of wrought OFHC copper.

In several depositions (II-17, 18 and 19) post heat treatment was evaluated as a means of eliminating the open boundaries. Heat treatment for 3.6 ks (1 hr) in vacuum at 1033°K and 1145°K (1400°F and 1600°F) did not heal the open structure; the only observed effect was an increase in deposit recrystallization and decrease in deposit hardness, table XI and figure 49. These observations were c 'stent with post annealing studies performed by Spalvins and Brainard[11].

Several depositions were performed using a smaller substrate size, to determine if the larger cathode to substrate spacing would eliminate or minimize the susceptibility to open structure formation. In the runs performed, II-22 to II-25, no beneficial effects were observed.

To achieve a dense structure of 0.15 Zr-Cu, ion bombardment of the substrate during deposition was necessary. This was achieved by using a –25 V substrate bias and a triode discharge in the same hollow cathode configuration in runs II-26, 27, 28 and 29.

At substrate temperatures of 423°K and 453°K (300°F and 350°F) in depositions, run II-28 and II-29 respectively, the resultant structures were dense and had no evidence of open grain boundaries, figure 50. The grain structure was similar to that produced with a diode discharge at deposition rate of 9.2 nm/s (1.3 mils/hr) and a substrate temperature of 898°K (980°F) as discussed previously and shown in figure 46. Increasing the substrate temperature to 1183°K (1675°F) with a deposition rate of (0.72 mil/hr) resulted in a fully dense recrystallized, equiaxed structure, figure 51. The surface topography of the triode depositions exhibited a somewhat domed appearance with no visual evidence of open regions between the individual column surfaces, figure 52.
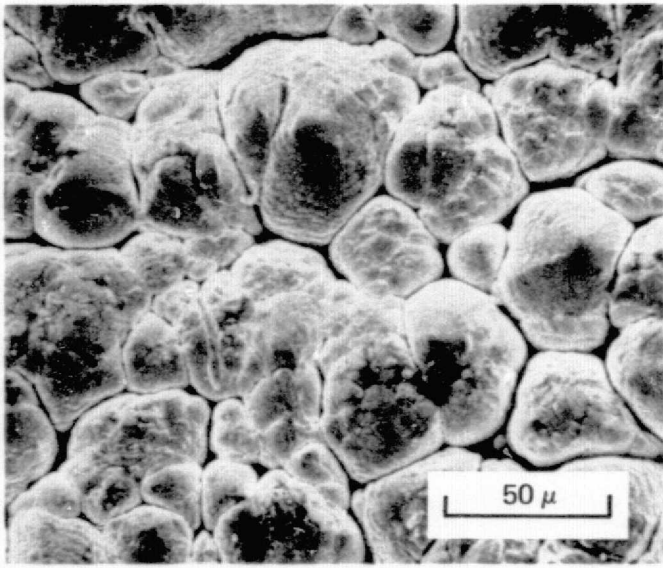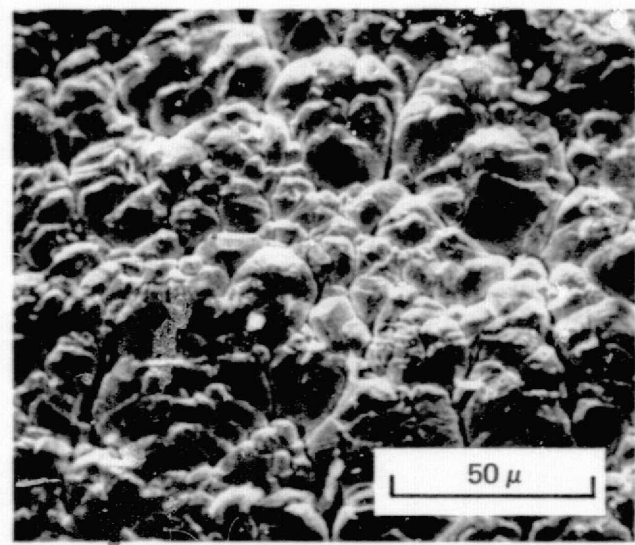
700K (800F)　　　　　　　　　866 (1100F)

Mag: 550X

Figure 47. Typical Surface Topography of Sputtered 0.15 Zr-Cu (Note Unbonded Grains)　　　　FD 91409

140X   110X
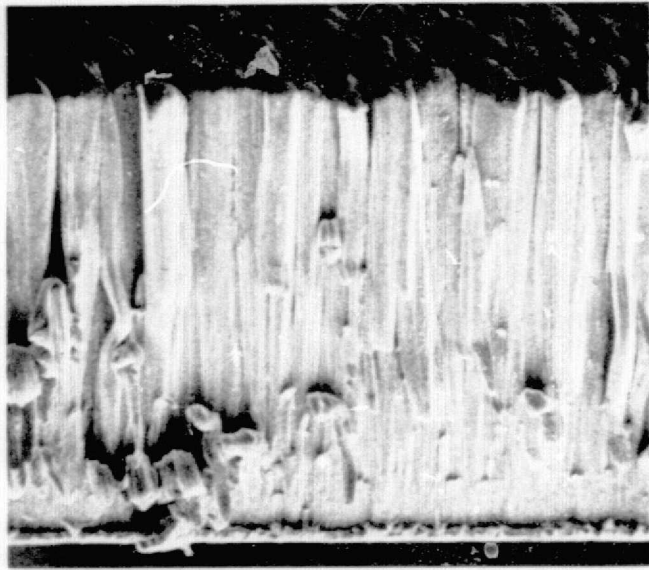
700K (800F)   866K (1100F)
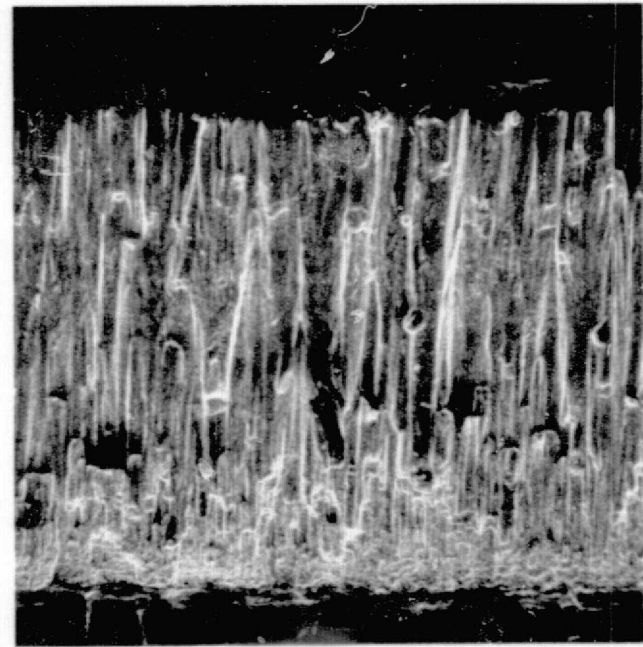
Figure 48. Typical Brittle Fracture Topography of 0.15 Zr-Cu Sputtered With High Substrate Temperatures   FD 91410

TABLE XI. EFFECT OF POST HEAT TREATMENT ON THE HARDNESS
OF SPUTTERED 0.15 Zr-Cu DEPOSITS

Run	Condition[2]	Maximum Substrate Temperature °K	°F	Hardness (VPN)[1] OFHC Copper Substrate	Cu-0.15 Zr Deposit
II-17	As deposited	923	1200	47, 49	55, 54
	1033°K (1400°F)			51, 51	53, 56
	1145°K (1600°F)			42, 41	58, 53
II-18	As deposited	1023	1375	44, 43	58, 55
	1033°K (1400°F)			46, 44	54, 57
	1145°K (1600°F)			44, 44	57, 51
II-19	As deposited	868	1100	56, 58	71, 67
	1033°K (1400°F)			49, 48	67, 61
	1145°K (1600°F)			39, 35	48, 47

NOTES:

[1] 0.5 Kg Load

[2] Post Heat Treatment, 3.6 ks in vacuum.

As Deposited

1033K-3.6ks-VAC
(1400F-1 HR-VAC)

1145K-3.6ks-VAC
(1600F-1 HR-VAC)
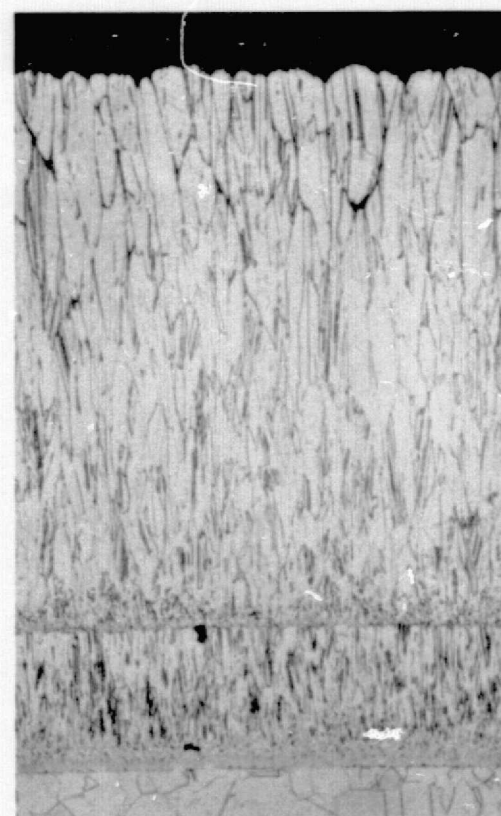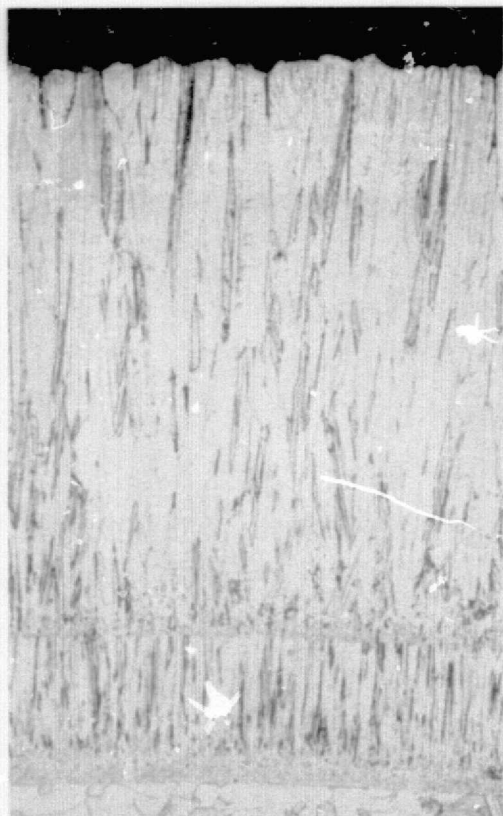
Mag: 70X

Figure 49. Microstructure of As Sputtered and Heat Treated 0.15 Zr-Cu Alloy Deposited in Run II-18. FD 91411
Substrate — OFHC Copper
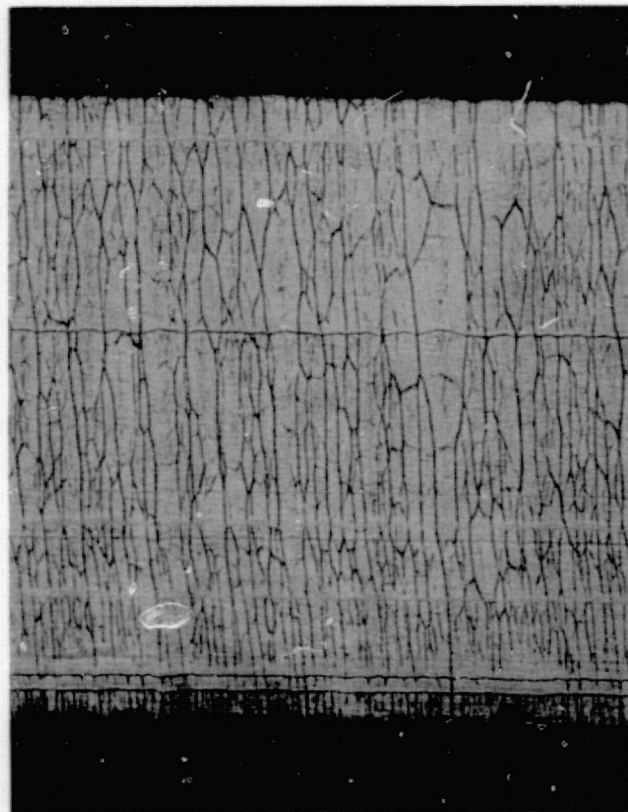
150X
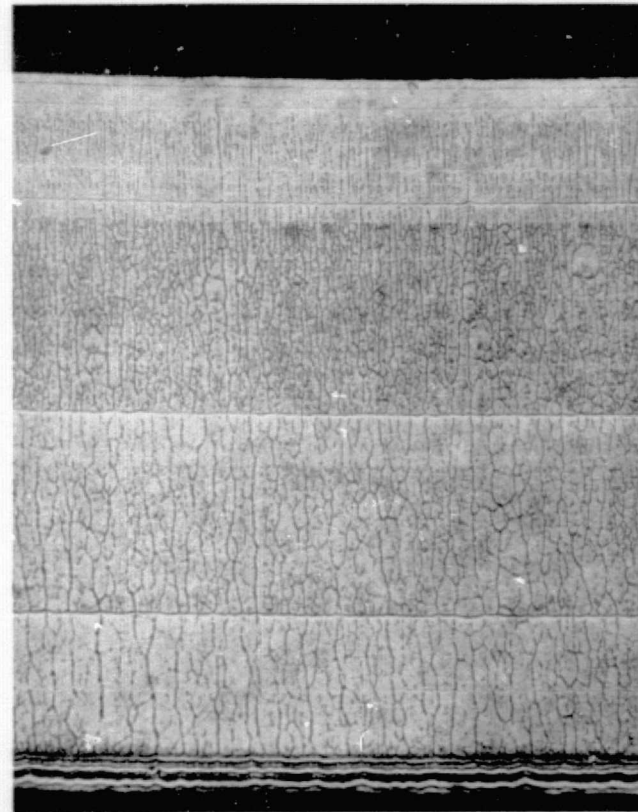
100X

Run II-28

Run II-29

Figure 50.   Dense Structure of 0.15 Zr-Cu Deposited from a Triode Discharge (Biased) in Runs II-28   FD 91412
         and II-29
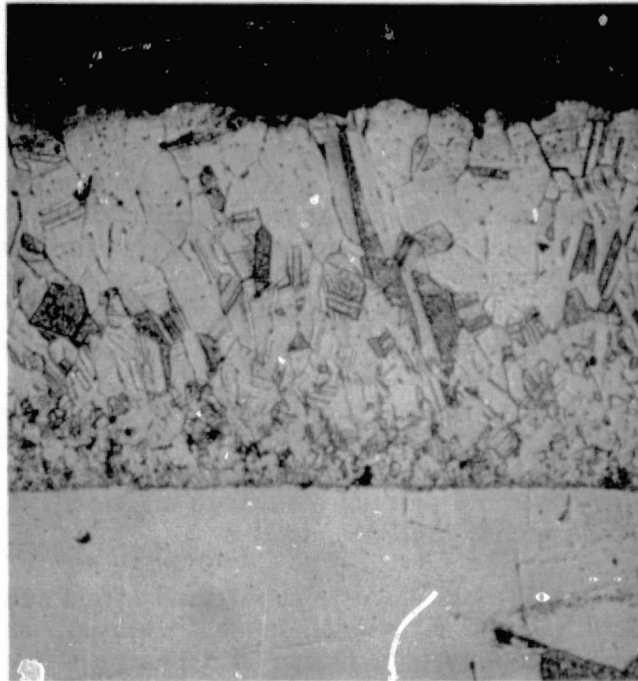
250X

Figure 51.   Microstructure of 0.15 Zr-Cu Deposited   FD 91413
             from a Triode Discharge With a Substrate
             Temperature of 1183°K (1675°F)
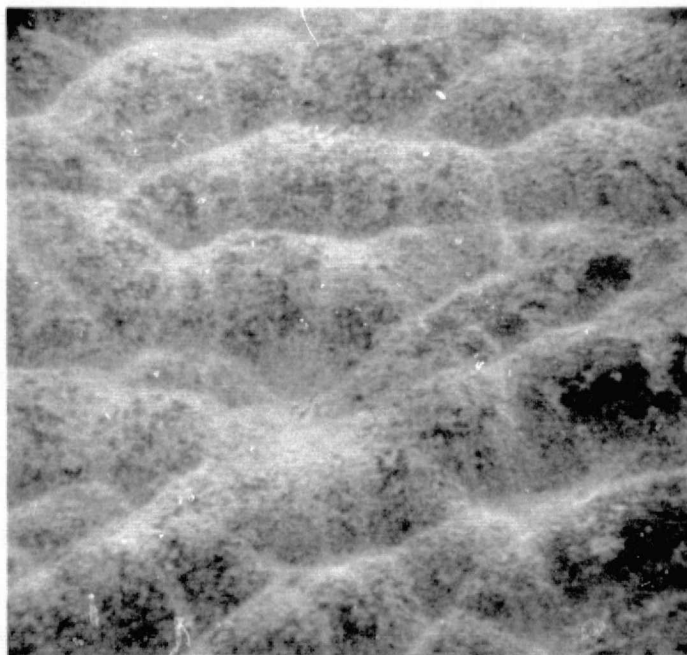
1000X

Figure 52.   Typical Surface Topography of 0.15 Zr-Cu   FD 91414
             Sputtered Using a Triode Discharge and
             Biased Substrate

With the low substrate temperature deposits, the as-sputtered material was brittle and exhibited a fibrous fracture morphology. With these deposits a post heat treatment was effective in increasing the deposit ductility. At post heat treatment temperatures of 813°K, 1145°K, and 1198°K for 14.4 ks (4 hours) a ductile equiaxed structure resulted, figure 53. The tensile ductility after the 1145°K and 1198°K exposure and resultant tensile strength is shown in table X. Although these conditions are over annealed, they represent the ability to transform the low temperature brittle type deposits to ductile equiaxed material. In the as-deposited condition, the brittle nature of the material was such that tensile samples could not be fabricated.

Concurrent to the deposition of 0.15 Zr-Cu from a hollow cathode, investigation of the structure of 0.15 Zr deposited from a flat plate target was performed. The targets (4 flat plates) were positioned to simulate a hollow cathode, see figure 33. In order to study the effects of discharge mode, all depositions were performed in the triode mode, table IX.

Depositions II-A-1 through II-A-5, performed with a substrate temperature of approximately 1115°K (1550°F), yielded dense, equiaxed, deposits which exhibited a faceted surface topography, figure 54. The rates of deposition studied were from 2.6 to 3.5 nm/s (0.37 to 0.49 mils/hr). Higher rates were not investigated since the substrates were not cooled and increased rates would have resulted in substrate melting.

The effects of substrate bias and geometry were studied in runs II-A-6 through II-A-12. In these runs 0.15 Zr-Cu was deposited on flat, water-cooled OFHC copper and Type 6061 aluminum plates in runs II-A-6 through II-A-10 using argon as the sputtering gas. All structures were dense and equiaxed although a columnar "superstructure" was apparent, figure 55. Deposition rates were varied from 1.2 to 5.6 nm/s (0.17 mils/hr to 0.80 mils/hr) but did not seem to affect either the interface or the deposit microstructure.

Runs II-A-11 and II-A-12 were deposited on 1.3 cm diameter Type 374 stainless steel tubing as a further variation of substrate geometry. Both structures were equiaxed and dense with a columnar "superstructure", figure 55.

From these results and those obtained in the flat plate coater and supported by the triode hollow cathode results, it was observed that substrate geometry has very little effect on deposit structure when a triode discharge is used. The results from the flat plate coater were identical to those obtained by McClanahan, Busch and Moss[1] in sputtering from a similar device.

Al_2O_3-Copper

In the depositions performed, the coater shown in figure 33, having two targets diametrically opposed, was used. One target was OFHC copper, while the other was of the composite type shown in figure 34. The substrates were water cooled as shown in figure 33. This approach was used to determine the difference in properties of OFHC copper and Al_2O_3 dispersion strengthened copper sputtered in the same deposition.
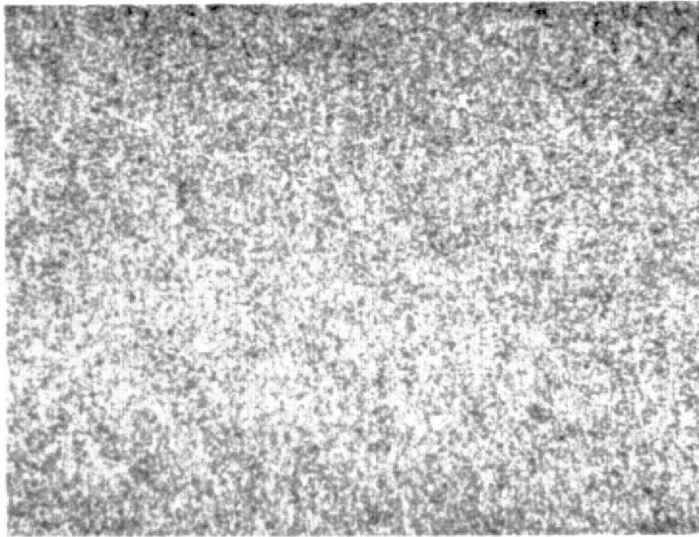
813K (1000F) for
14.4 ks (4 hrs)

1145K (1600F) for
14.4 ks (4 hrs)

Mag: 200X

Figure 53. Effect of Post Deposition Heat Treatment on the Structure of 0.15 Zr-Cu Deposited from a
Hollow Cathode Using a Triode Discharge and a -25V Bias, Run II-29

FD 91415

500X
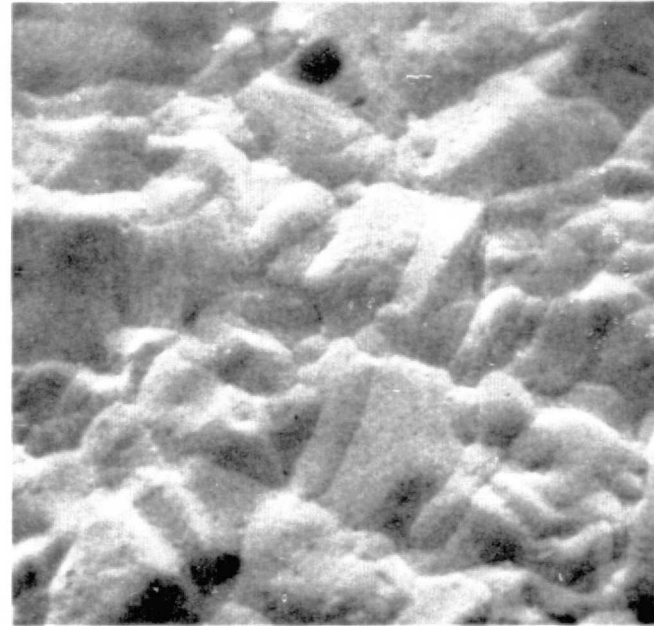
100X

Figure 54. Microstructure and Surface Topography of 0.15 Zr-Cu Sputtered in Run II-A-2. Substrate Temperatures 1115°K (1550°F)

FD 91416
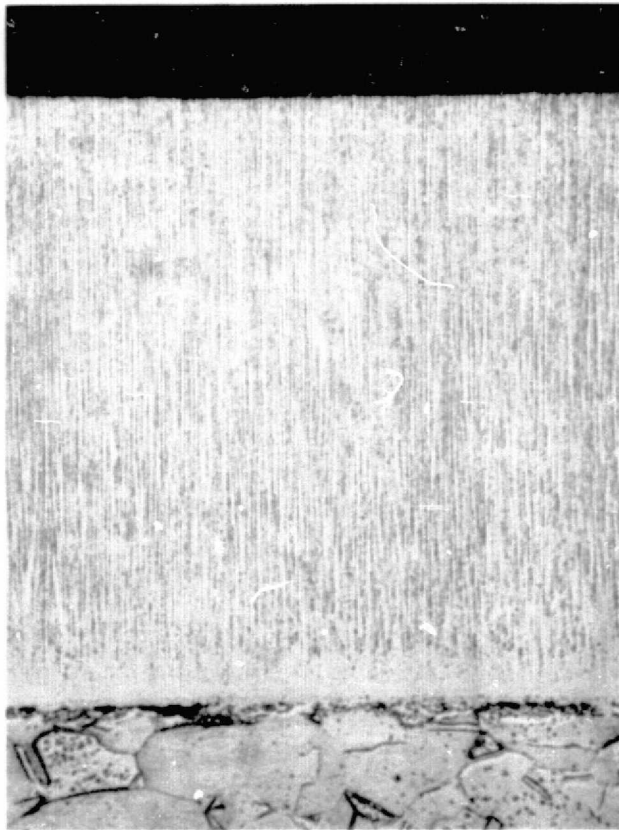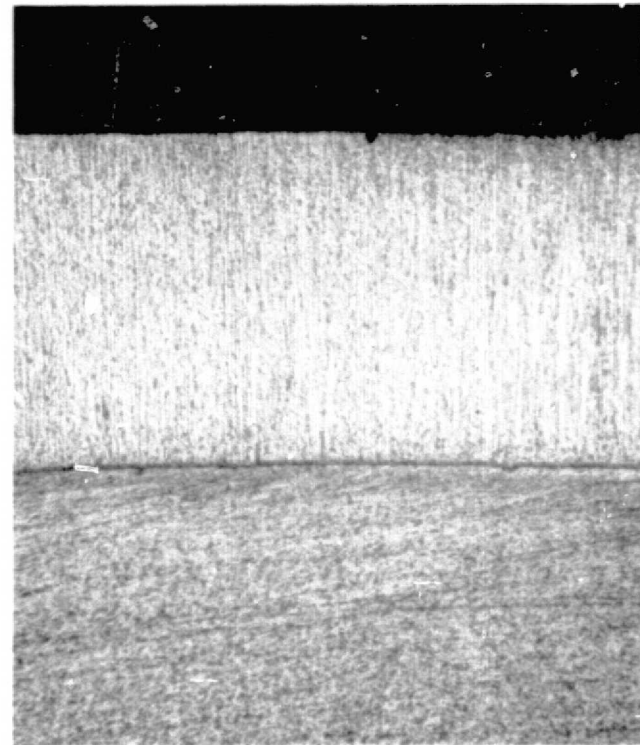
Run II-A-7   Run II-A-11

250X

Figure 5ɔ.   Microstructure of 0.15 Zr-Cu Deposited at Low Substrate Temperatures in Runs II-A-7 and   FD 91417
             II-A-11

The typical structure of the deposits obtained in runs II-A-13 and II-A-14 is shown in figure 56. The deposits were uniform, dense and of higher hardness than the OFHC copper substrate. A grain structure was not evident in optical microscopic analysis. In transmission electron microscopy, the deposits were fine grain, (~1 micron diameter), figure 57. No evidence of a secondary Al_2O_3 precipitate was found either by microscopy or electron diffraction.

However, based on the results of tensile tests, the cosputtering of Al_2O_3 and copper from the composite target resulted in increased deposit strength, table X. In the deposit facing the composite target tensile strengths up to 636.0 MN/m^2 (92,300 psi) and 771.0 MN/m^2 (111,900 psi) were obtained for run II-A-13 and run II-A-14. Elongations of 8% and 6% respectively were obtained. The deposits made that faced the OFHC copper targets exhibited tensile strength up to 221.9 MN/m^2 (32,200 psi) and 739.3 MN/m^2 (107,300 psi) for run II-A-13 and run II-A-14, respectively. Elongations of 40 and 12%, respectively, resulted. The difference in properties is possibly due to the bias conditions employed during deposition. That is to say, the bias (-25V) used in run II-A-13 may have reduced the Al_2O_3 (or Al and O_2) in the deposit through selective back sputtering. While with the grounded substrate in II-A-14, this did not result.

<div align="center">SiC-Cu</div>

In the deposition of SiC-Cu (run II-A-15), the same target-substrate arrangement as described for Al_2O_3-Cu was used. Extensive sputtering of the SiC resulted with the DC target voltage, such that the plugs and surrounding OFHC copper were sputtered back to the 1.3 cm diameter portion of the plug, reference figure 34. The resulting deposition rate was 7.0 nm/s (1.0 mil/hr).

The deposit structure from this run is shown in figure 58. While completely dense, the deposit was obviously nonuniform in grain size, probably as a result of increasing SiC incorporation resulting from target depletion, and increased area of SiC on the target. This is further supported by the higher hardness of the outer layer (applied during 1.3 cm diameter SiC exposure). It is postulated that small amounts of Si and C in solution promote grain growth, while large amounts retard growth; hence the reason for the duplex grain structure. In the outer layer of the deposit, no evidence of a SiC precipitate was observed, figure 59. This further supports the fact that Si and C may be in solution not as SiC. The deposit grain size in the top layer was 0.5 to 1.0 microns.

In the deposit facing the SiC plugged target, a tensile strength up to 983.9 MN/m^2 (142,800 psi) and 8% elongation was obtained. In the deposit facing the OFHC copper target tensile strength of 531.9 MN/m^2 (77,200 psi) and 16% elongation was obtained. Since the substrates were grounded during depositions, the results tend to support the observation made in the analysis of the Al_2O_3-Cu depositions that biasing reduces ceramic transfer to the deposit.

84

200 Gram Knoop
Microhardness

225

230

108
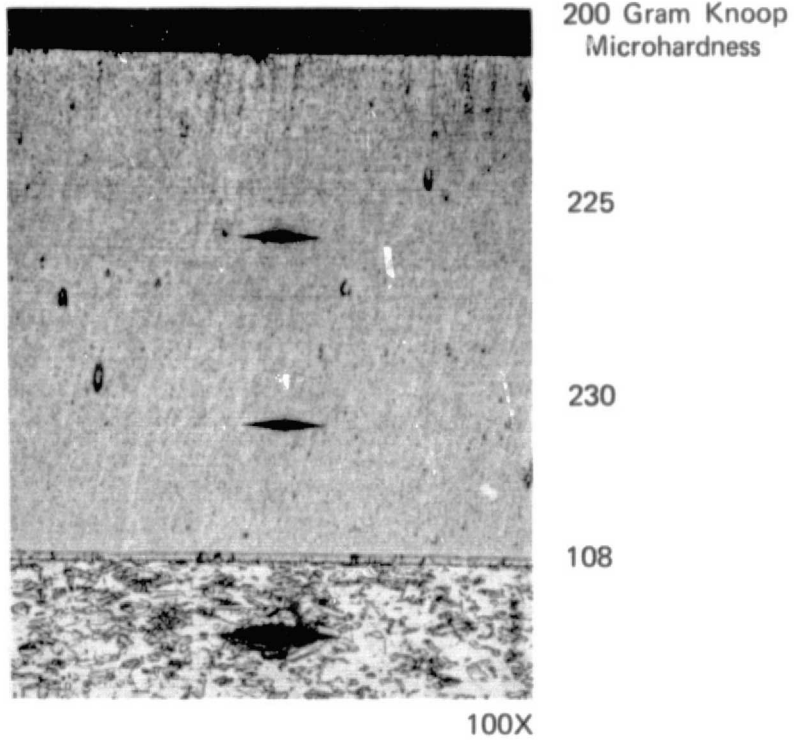
100X

Figure 56. Structure and Microhardness of as De-   FD 91418
posited Cu + Al_2O_3 in Run II-A-14

70,000X
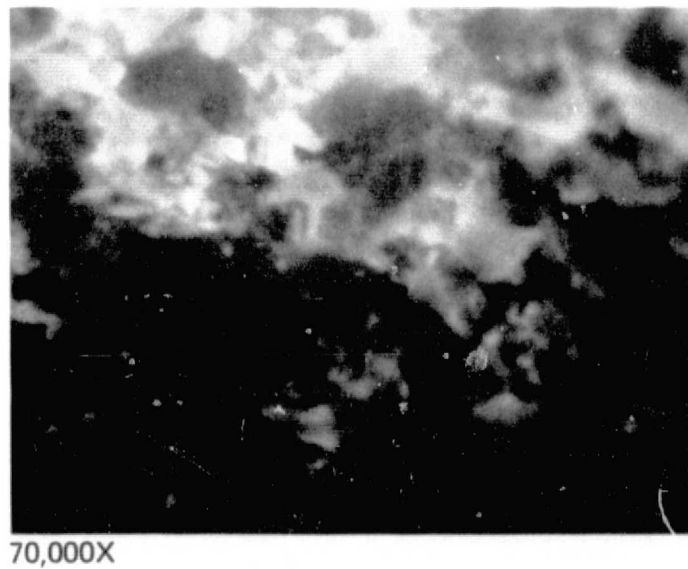
Figure 57. Transmission Electron Microstructure   FD 91419
of Run II-A-14, Cu + Al_2O_3

85
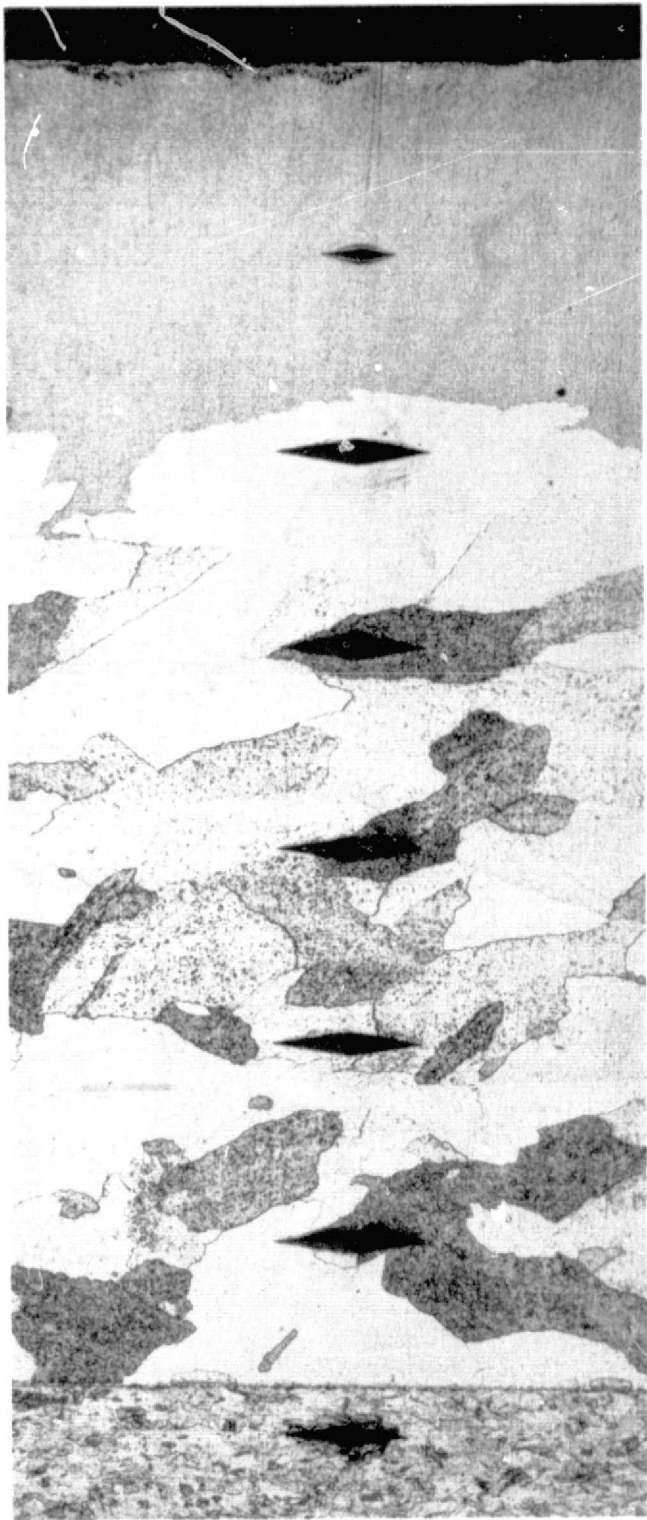
200 Gram Knoop
Microhardness Number

305

70

82

80

76

78

109

100X

Figure 58.   Structure and Microhardness of as Deposited Cu + SiC in Deposition II-A-15   FD 91424
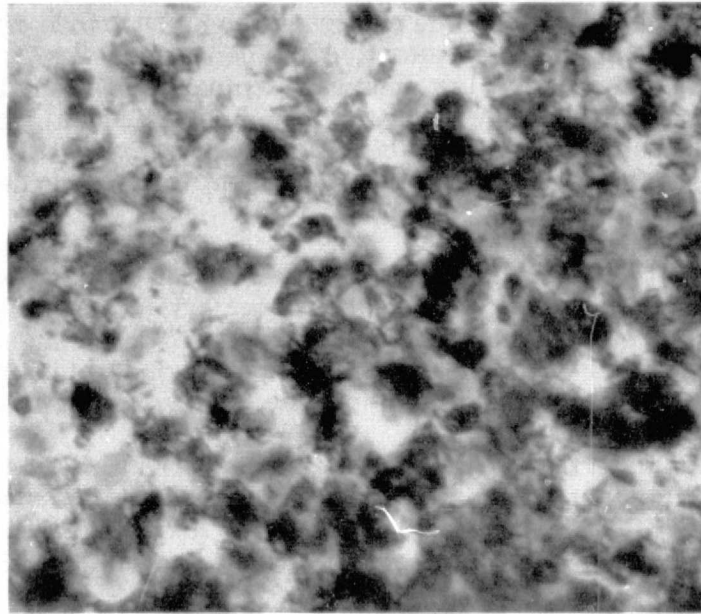
70,000X

Figure 59.   Transmission Electron Microstructure of   FD 91425
             the Surface Layer of Deposit II-A-15
             (SiC-Cu)

TASK II

CONCLUSIONS

From the depositions and observations made in this task, the following conclusions were drawn:

1.   With the hollow (cylindrical) cathode configuration and techniques used in this evaluation, this target geometry, operated in a diode discharge, was unacceptable for generating dense deposits of OFHC copper or 0.15 Zr-Cu at low substrate temperatures and practical deposition rates.

2.   Dense ductile deposits of OFHC copper could be attained in the hollow cathode-diode discharge if low deposition rates and high substrate temperatures were used. However, at the higher substrate temperatures, the structures were annealed and ductile, but of lower strength. In deposition of 0.15 Zr-Cu from this geometry and discharge open brittle deposits prevailed at almost all substrate temperatures investigated. Only by going to 1183°K in substrate temperature could dense deposits be produced.

3. Using the hollow cathode configuration and a triode discharge, substrate biasing was effective and dense 0.15 Zr-Cu deposits could be attained at low substrate temperatures (423°K-453°K) and moderately high deposition rates (10-13 nm/s). However, the deposits produced at these conditions were brittle and required post deposition heat treatment to improve deposit ductility.

4. It is not apparent that Al_2O_3-copper or SiC-copper co-sputter to form a dispersion strengthened material. From the observation made, it is suspected that the Al and O_2 or Si and C are in solution and strengthen the deposit through solid solution strengthening and not by dispersion strengthening mechanisms.

5. Of the materials sputtered, the co-sputtered Al_2O_3-Cu and SiC-Cu produced the highest tensile strengths. Tensile strengths up to 771.0 MN/m^2 and 983.9 MN/m^2 for Al_2O_3-Cu and SiC-Cu respectively were obtained with 6% or greater ductility.

TASK III

INNER WALL GRADATION AND LAMINATION

The objective of this task was to evaluate layered or graded structures for the fabrication of thrust chamber inner walls. Layered structures made using OFHC copper and 0.15 Zr-Cu were evaluated for bond integrity, layer hardness and fatigue properties.

EQUIPMENT AND PROCEDURES

A post cathode coater, figure 60, was used to sputter layered deposits of OFHC copper and 0.15 Zr-Cu. The deposition parameters were selected so as to produce the required hardness variation from the inner to outer layer of each deposit. The substrate preparation and sputter cleaning parameters used for each run are given in table XII, while the deposition parameters are summarized in table XIII.

The post targets used were machined from wrought OFHC copper rods and wrought 0.15 Zr-Cu (AMZIRC®) billets. The substrates were 2.54 cm high OFHC copper rings (6.6 cm ID). The OFHC copper was sputtered using DC target voltage in a triode discharge, while both DC and RF target voltage was used to apply 0.15 Zr-Cu. The DC portion of the deposition was performed in a triode discharge, while the RF portion was performed using a diode discharge.

All deposits were evaluated by low cycle fatigue testing and standard metallographic analysis. In fatigue testing a 2.54 cm long ring, 6.6 cm ID, was cycled through a total strain of 2% (-0.8% to +1.2%). The test was strain controlled. A strain gauge cemented to the OD of the sample, at the point of maximum strain, was used to control the strain range.

RESULTS AND DISCUSSION

The depositions parameters in run III-1 and III-2 were adjusted to yield a different hardness in each layer, and successively graded in hardness such that the outer layer was the hardest. In the deposition of OFHC copper, run III-1, hardness variations between layers were accomplished by varying the substrate bias. In run III-2, bias and deposition techniques were varied to change hardness.

The four layer deposit microstructure and layer hardness of run III-1 is shown in figure 61. The first layer was deposited with a -50V bias, while the successive layers were applied with a -25V, OV and +11V bias. The deposition rate was approximately equivalent for each layer; 2.4 to 2.8 nm/s (0.34-0.39 mils/hr). The substrate reached a temperature of 730°K during deposition of the first layer and decreased to 616°K during deposition of the third layer due to decreasing bias. With the positive 11V bias imposed in sputtering the last layer, the temperature increased to (661°K) due to electron bombardment heating. The resultant structure was completely dense with high quality interfaces, figure 61. In fact, it was not possible to differentiate between the first and second layers. The structure shown in figure 61 was overetched to show the finer grain structure of the outer layers and the outer layer thickness.
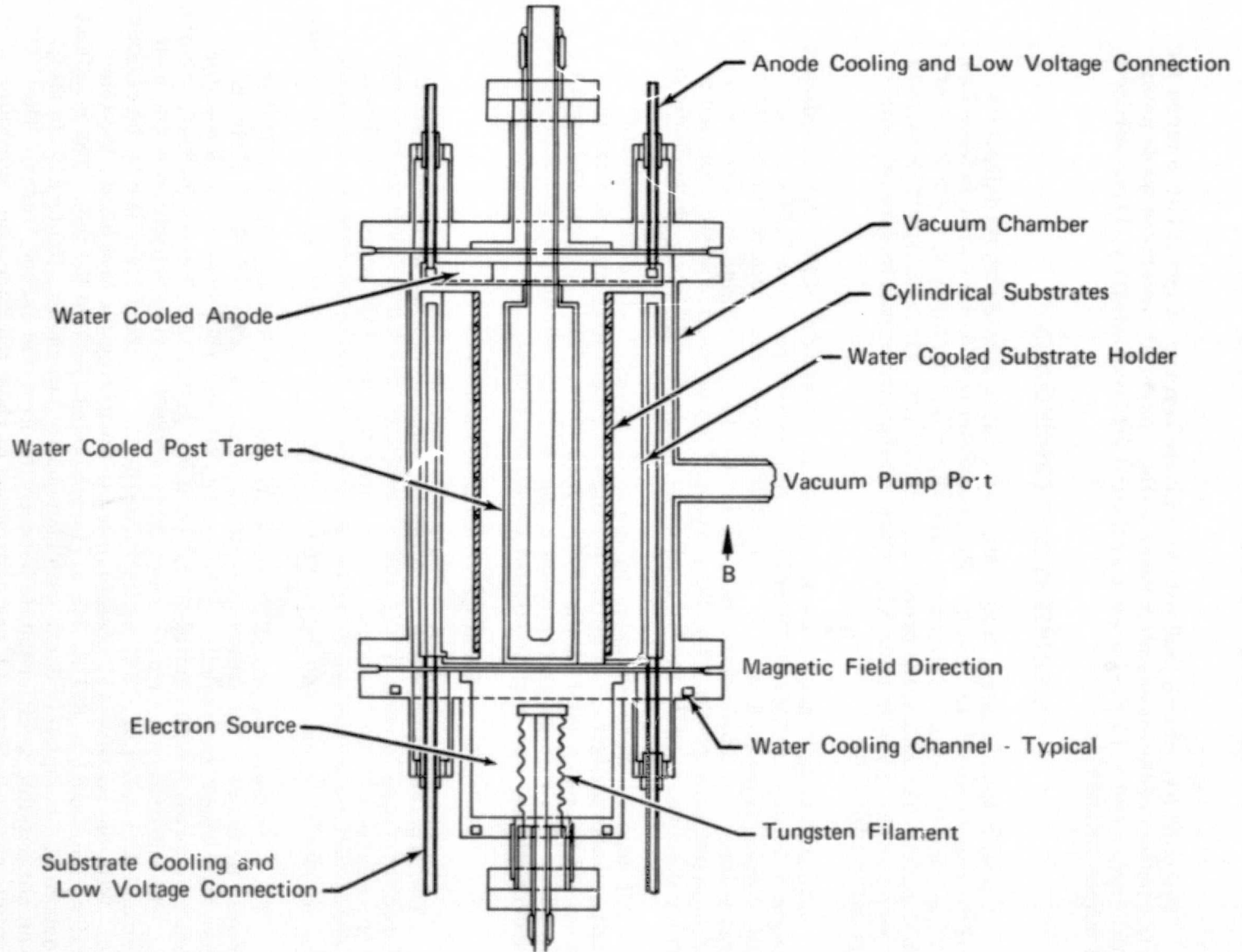
Figure 60. Schematic of Post Cathode Coater

FD 91426

TABLE XII. SUMMARY OF TASK III SUBSTRATE PREPARATION AND SPUTTER CLEANING PARAMETERS

| Run No. | Substrate Material | Finishing Treatment, Surface Preparation, and Primary Cleaning | Voltage, V | Sputter Cleaning | | Pressure | |
				Current, ma	Duration, s	N/m^2	μ
III-1	OFHC Copper	ID sanded circumferentially with No. 600 grit paper, buffed with jeweler's rough, Ajax® scrub, ethyl alcohol rinse.	-25	3000	300	0.81	6.1
III-2	OFHC Copper	ID machined, Ajax® scrub, ethyl alcohol rinse.	-25	3400	300	0.32	2.4
III-3	Aluminum	Ajax® scrub, ethyl alcohol rinse.	-25	1700	600	1.13	8.5
			-25	1500	2700	0.90	6.8

TABLE XIII. SUMMARY OF TASK III DEPOSITION PARAMETERS

Run No.	Target Material	Substrate Voltage, V	Substrate Current, A	Target Voltage, V	Target Current A	Time ks	Time hr	Substrate Temp °K	Substrate Temp °F	Max Deposit Thickness mm	Max Deposit Thickness mils	Max Deposit Rate nm/s	Max Deposit Rate mil/hr	Pressure N/m²	Pressure μ
III-1[1]	OFHC Copper	−25	3.0	−25	1.00	0.29	0.08	602	625					0.82	6.1
		−25	3.3	−25	1.05	0.29	0.08	655	720					0.49	3.7
		−25	3.15	−25	1.05	0.29	0.08	672	750					0.49	3.7
		−50	3.7	−500	1.45	23.4	6.50	730	855	0.066 (first layer)	2.6 (first layer)	2.8	0.39	0.38	2.8
		−25	3.1	−25	1.00	0.29	0.08	569	565					0.53	4.0
		−25	3.1	−25	1.00	0.29	0.08	577	580					0.45	3.4
		−25	3.8	−500	1.40	24.3	6.75	661	730	0.066 (second layer)	2.6 (second layer)	2.7	0.38	0.32	2.4
		−25	3.0	−25	0.90	0.29	0.08	577	580					0.48	3.6
		−25	3.0	−25	1.00	0.29	0.08	616	650					0.45	3.4
		0	0	−500	1.40	25.2	7.00	616	650	0.066 (third layer)	2.6 (third layer)	2.6	0.36	0.33	2.5
		−25	2.8	−25	0.90	0.29	0.08	669	745					0.45	3.4
		−25	3.0	−25	0.90	0.29	0.08	672	750					0.39	2.9
		+11	2.85	−500	1.30	27.0	7.50	661	730	0.066 (fourth layer)	2.6 (fourth layer)	2.4	0.34	0.28	2.0
III-2[3]	0.15 Zr-Cu	−25	0.8	800W[3]	12W[4]	75.6	21.00	NM	NM	0.188	7.4	2.6	0.35	0.32	2.4
		−50	3.3	−500	1.40	36.0	10.00			0.112	4.4	3.1	0.44	0.32	2.4
		−25	3.0	−500	1.40	39.6	11.00			0.228	9.0	5.8	0.82	0.32	2.4
		−100 (RF Floating)	−	800W[3]	7.5W[4]	87.3	24.25			0.317	12.5	3.6	0.51	0.43	3.2
III-3[5]	0.15 Zr-Cu	Floating	−	800W[3]	6.0W[4]	65.7	18.25[6]	NM	NM	3.8 (total thickness)	150.0	4.9	0.70	0.34	2.6
		Floating	−	800W[3]	6.0W[4]	255.6	71.00[7]							0.53	4.0
		−20	2.4	−500	1.3	47.8	13.25							0.87	6.8
		−20	2.4	−500	1.3	50.4	14.00							0.95	7.3
		−20	3.3	−500	1.6	36.0	10.00							0.66	5.1
		−20	2.6	−500	1.4	43.2	12.00							0.53	4.1
		−20	3.0	−500	1.6	39.6	11.00							0.66	5.1
		−20	3.0	−500	1.5	36.0	10.00[7]							0.53	4.1
		−20	2.6	−500	1.4	23.4	6.50							0.40	3.1
		−20	3.0	−500	1.5	48.6	13.50							0.44	3.4
		−20	3.3	−500	1.6	53.2	14.75							0.48	3.6
		−20	3.4	−500	1.6	52.3	14.50							0.49	3.7
		−20	3.4	−500	1.6	26.1	7.25							0.49	3.7

NOTES:

[1] Deposition performed in triode discharge.

[2] Deposition of first and fourth layers deposited using RF and diode discharge; second and third layers deposited using DC and triode discharge.

[3] Forward RF power.

[4] Reflected RF power.

[5] Deposition of first and second layers deposited using RF and diode discharge; remaining layers deposited using DC and triode discharge.

[6] Between layer deposition target and substrate cleaned with −50V bias for 300 S.

[7] System vented to air to inspect target.

4th Layer: 183

3rd Layer: 183

2nd Layer: 123

1st Layer: 103

Substrate: 100

Mag: 300X
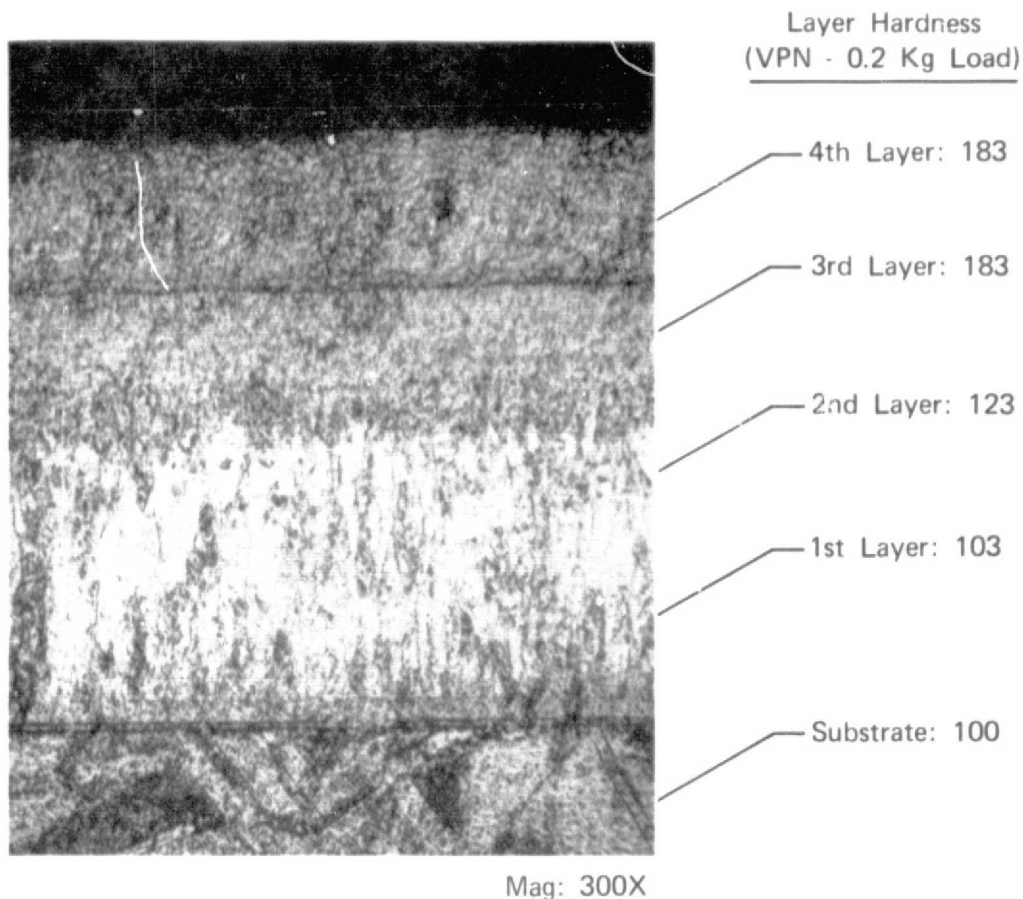
Figure 61.   Microstructure and Hardness of 4 Layer   FD 91427
OFHC Copper Deposit (Run III-1)

The hardness of the first layer was essentially the same as the substrate (VPN 100) and increased in the second layer to VPN 123. The last two layers were identical in hardness, VPN 183. The substrate hardness before deposition was VPN 100.

The structure of the four layer 0.15 Zr–Cu and layer hardness is shown in figure 62. The resultant structure was dense and of high integrity, both within the layers and at the interfaces. All layers were of higher hardness than those obtained with the OFHC copper deposit. The initial layer, applied with a −25V bias by RF discharge, exhibited an average hardness of VPN 270. The second layer hardness decreased to VPN 231 in the DC biased (−50V) application. The third layer applied at −25V bias potential with DC sputtering was the same hardness as the first layer VPN 270. The outer layer, applied by RF sputtering and a floating bias, was the hardest, VPN 320.

In LCF testing, the difference in performance of the two deposits was readily apparent, table XIV. The layered OFHC copper withstood 374 cycles until a surface crack resulted, and failed at 585 cycles. This life was comparable to the baseline OFHC copper fatigue life. A significant reduction in fatigue properties was observed with the first 0.15 Zr–Cu layer structure tested.

Layer Hardness
(VPN-0.2 Kg Load)

4th Layer: 320

3rd Layer: 270

2nd Layer: 231

1st Layer: 270

Substrate: 114

Mag: 250X
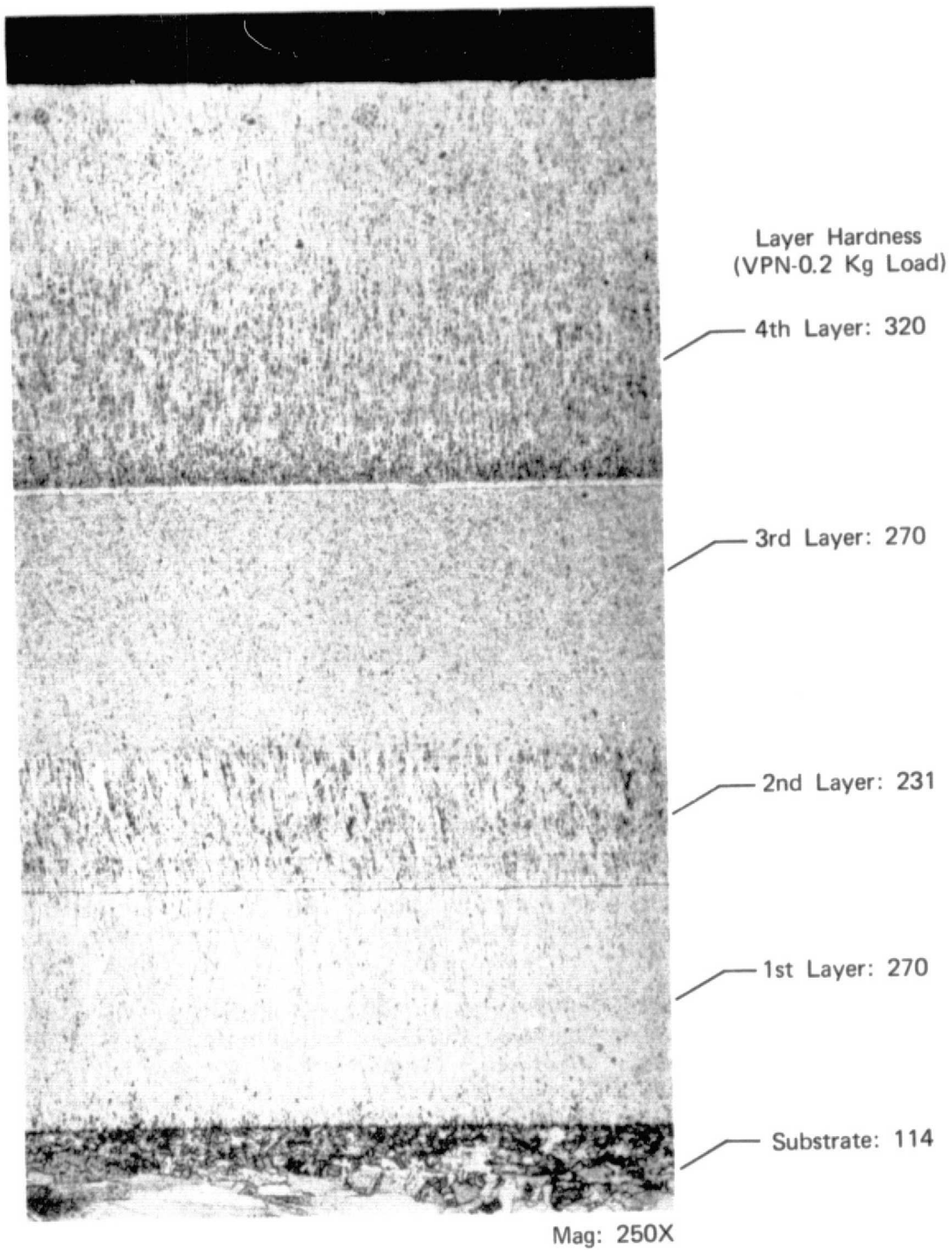
Figure 62.   Microstructure and Hardness of 4 Layer   FD 91428
0.15 Zr-Cu Deposit, Run III-2

TABLE XIV. LOW CYCLE FATIGUE TESTING OF SPUTTERED INNER WALL DEPOSITS

Sample	Strain Range	Cycles to Deposit Crack[1]	Cycles to Failure
III-1 (4 layer OFHC copper)	-0.8 to 1.2%	374	585
III-2A (4 layer 0.15 Zr-Cu)	-0.6 to 1.4%	62	267
III-2B (4 layer 0.15 Zr-Cu)	-0.8 to +1.2%	Did not crack[2]	Did not fail[2]
III-2B[3] (4 layer 0.15 Zr-Cu)	-0.3 to +0.85%	850	1003
III-3[4] (13 layer 0.15 Zr-Cu)	-0.8 to 1.2%	509	580
OFHC copper baseline	-1.0 to +1.2%	300	438
OFHC copper baseline	-0.8 to +1.2%	400	697

NOTES:

[1]Based on visual observation.

[2]Delaminated in first cycle, continued in test, substrate cracked at 384 cycles, and failed at 430 cycles. Deposit discontinued in test at 600 cycles with no failure.

[3]Failed substrate removed in gauge area, regauged, and continued in test.

[4]Sample 100% sputtered 0.15 Zr-Cu.

The cycles to crack initiation were 62, with failure resulting at 267 cycles. Although the strain range used was identical on each, the 0.15 Zr-Cu strain of -0.6 to +1.4% was slightly different than the OFHC copper strain, -0.8 to 1.2%. However, this difference in strain maxima is probably not the principal reason for the decreased life of the 0.15 Zr-Cu structure. Undoubtedly the high hardness of the outer layers contributed most to the poor fatigue properties. The fracture face morphology of the failed fatigue specimens, figure 63, illustrates the brittle nature of the 0.15 Zr-Cu deposit.

Based on this result a second ring segment from III-2 was tested. This sample was located at the top of the substrate stack during deposition. In LCF testing, the 4 layer deposit, delaminated in the first cycle, and was removed from test with no deposit failure after 600 cycles, figure 64. Since the strain range on the deposit probably decreased after delamination, the OFHC copper substrate was removed in the gauge area, the deposit strain gauged and continued in test. Due to deposit thickness, only a strain of -0.3 to +0.85% could be obtained. At this strain, approximately 850 cycles-to-crack and 1003 cycles-to-failure resulted. No delamination of the deposit layers was observed in the fracture, figure 64. Metallographic post-test analysis revealed that the delamination was due to insufficient sputter cleaning, caused by the substrate being at the top of the discharge.

Four Layer OFHC Copper
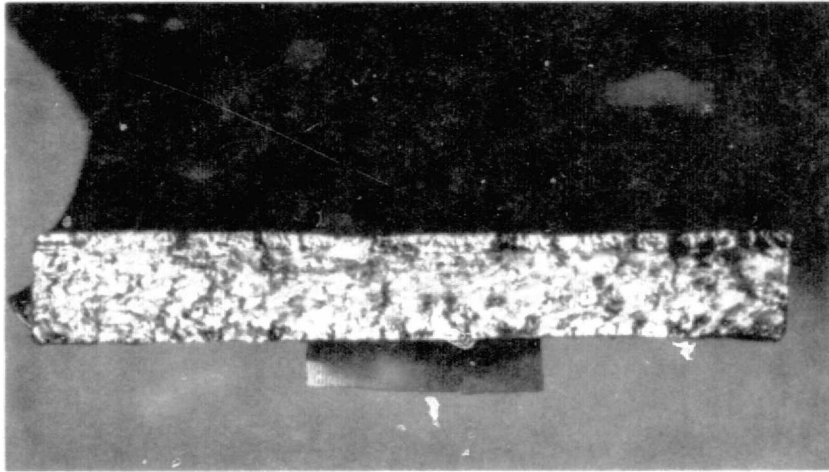
Four Layer 0.15Zr-Cu

62 Cycles to Crack
267 Cycles to Failure
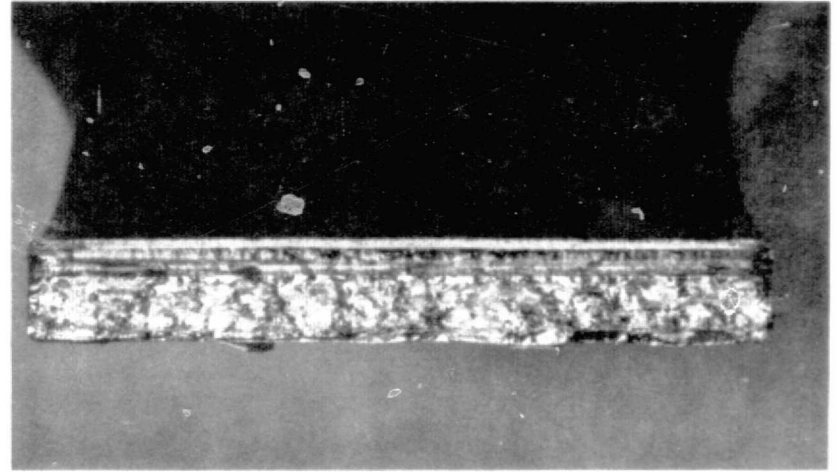
374 Cycles to Crack
585 Cycles to Failure

Mag: 6X

Figure 63. Appearance of Fracture Face of Low Cycle Fatigue Specimen. (Four Layer Deposits on Specimen ID. Note Brittle Appearance of Zr-Cu Deposit)

FD 91429

3X   6X

Delamination and Fracture of OFHC Copper
Substrate After 600 Cycles   Fracture Morphology of Four Layer Deposit After 1003 Cycles
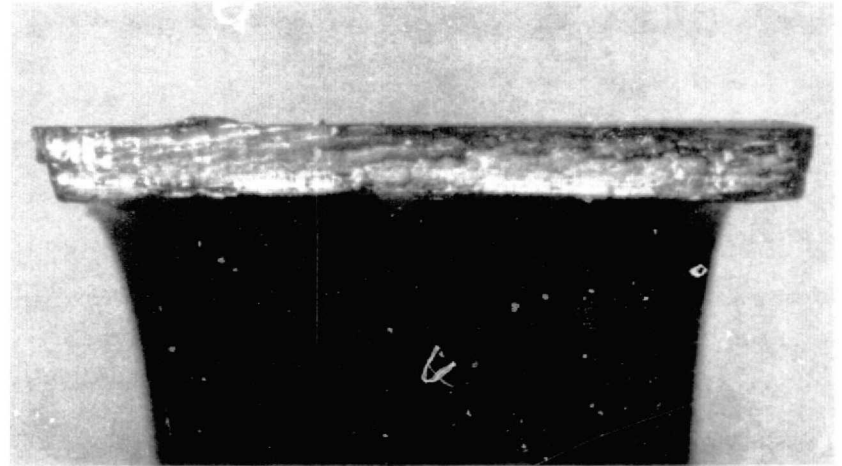
Figure 64.   Appearance of Delamination of LCF Sample III-2B, and Fracture Morphology of Four Layer   FD 91421
0.15 Zr-Cu Deposit of III-2B

97

Based on the LCF properties of the four layer 0.15 Zr-Cu deposits, a thick multilayer deposit of uniform hardness between layers was produced in run III-3. This was produced to evaluate a fully-sputtered deposit of approximately the same thickness as the OFHC copper baseline and layered LCF samples. The III-3 deposit was made in 13 layers, with no significant variation in hardness between the layers. As with the 0.15 Zr-Cu four layer deposit, two of the layers were deposited using RF diode, while the remaining layers were deposited with DC target voltage and a triode discharge, table XIII. The resultant deposit was 3.8 mm (150 mils) thick, with a hardness of 167 ±13 VPN (0.2 Kg load). The deposit structure is shown in figure 65.

The III-3 deposit was tested in LCF at 2% total strain, -0.8 to +1.2%. Cracking the deposit required 509 cycles, and failure 580 cycles, table XIV. The deposit fracture was ductile with no observable delamination, figure 65. The cycles-to-crack of this deposit exceeded that of the 4 layer OFHC copper deposit and the OFHC baseline. This result showed that layered 0.15 Zr-Cu sputtered deposit can provide good LCF properties. Based on the good performance of this deposit, the tensile properties of both as-sputtered and annealed samples were determined, table XV. The properties obtained exceeded those obtained for 0.15 Zr-Cu in Task II and were equivalent to the properties of sputtered 0.15 Zr-Cu evaluated by McClanahan, Bush and Moss. [1]
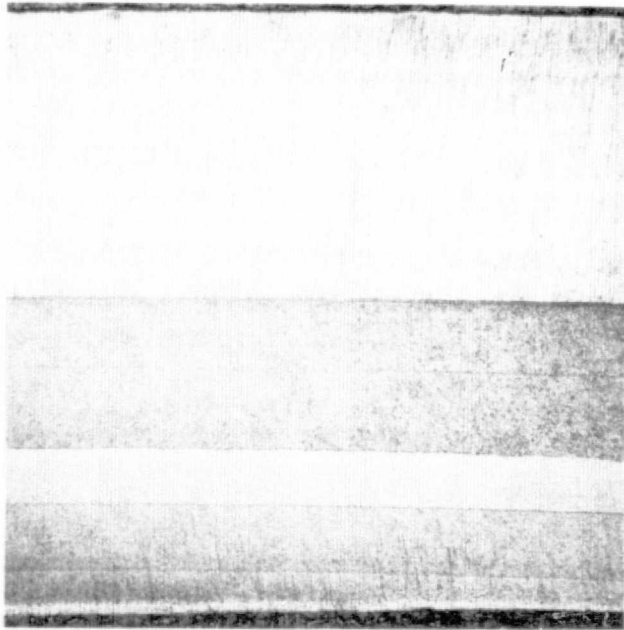
40X
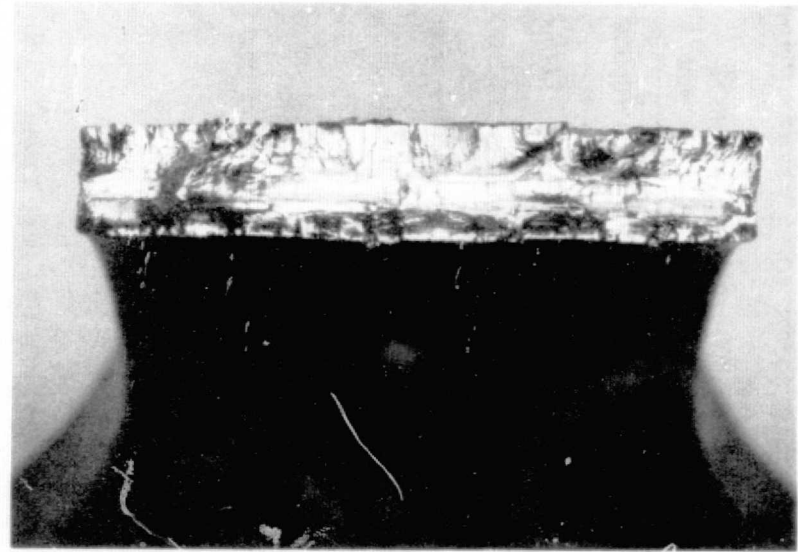
6X

Figure 65. Microstructure and Fracture Morphology of 100% Sputtered 0.15 Zr-Cu (Deposited in Run III-3) After LCF Testing for 580 Cycles

FD 91420

TABLE XV.   TENSILE PROPERTIES OF LAYERED 0.15 Zr-Cu
DEPOSITED IN RUN III-3

Condition	Yield Strength MN/m²	psi	Ultimate Tensile Strength MN/m²	psi	Elongation Percent
As sputtered	578.8	84,000	623.5	90,500	8.0
As sputtered	562.2	81,600	602.2	87,400	5.0
Annealed*	434.1	63,000	518.1	75,200	15.0
Annealed*	450.6	65,400	529.8	76,900	13.0

*Annealed at 863°K for 3.6 ks (1100°F for 1 hour) in argon.

TASK III

CONCLUSIONS

Based on the depositions and evaluations performed in this task the following conclusions were drawn:

1. Sputtering from a post cathode is a viable approach for fabricating a layered inner wall structure for thrust chambers. Graded or layered OFHC copper and 0.15 Zr-Cu deposits with hardness increasing from substrate to outer layer can be obtained by varying substrate bias and deposition parameters.

2. A four layer OFHC copper deposit on the ID of cylindrical OFHC copper sections, did not affect low cycle fatigue life of the wrought OFHC copper. However, a four layer 0.15 Zr-Cu deposit with higher layer hardness, resulted in a lower fatigue life.

3. A 100 percent sputtered 0.15 Zr-Cu deposit consisting of 13 layers of approximately constant hardness, exhibited a substantial improvement in fatigue life over the four layer 0.15 Zr-Cu structure with graded layer hardness. Based on the results obtained, grading from low hardness to high hardness at the surface layer may not be desirable.

4. Sputtered multilayer deposits offer potential for improving the LCF properties of chamber inner structures. Alternate techniques of grading, and post deposition heat treatment should be investigated.

TASK IV

SPUTTERED HIGH STRENGTH CYLINDERS

The objective of this task was to evaluate high strength materials for use as outer jacket structures of regeneratively cooled thrust chambers fabricated by sputtering. Three materials were chosen for evaluation from classes of alloys with high strength to weight ratios as conventionally processed. They were NASA IIb-11, [14] a nickel base superalloy; Ti-5Al-2.5Sn, [15] an alpha phase titanium alloy; aluminum; and Al_2O_3 dispersed aluminum. These alloys were evaluated on the basis of strength of the sputtered deposit and compatibility with the proposed copper alloy closeout layer.

EQUIPMENT AND PROCEDURES

For the depositions performed in this task, a hollow cathode and flat plate coater described in Task II (figures 32 and 33) were used. The targets were machined from wrought alloy billets. In the case of the Al_2O_3-Al, the target was of the composite type (figure 34), comprised of Al_2O_3 [12] slugs imbedded in a Grade 1100 aluminum plate. [16]

Substrate materials were OFHC copper, Type 6061 aluminum and Ti-5Al-2.5Sn. The copper was chosen to simulate sputtered thrust chamber material; the aluminum and titanium were used to evaluate alternate substrate materials. A summary of cleaning procedures for all experiments in this task is given in table XVI. Mechanically sanding with 600 grit SiC paper followed by an Ajax® scrub and ethyl alcohol rinse prior to sputter cleaning proved to be a satisfactory procedure and much superior to vapor blasting or chemical polishing in terms of interface cleanliness and coating adherence. Sputter cleaning was felt to be necessary and parameters were developed which gave excellent results for all coating and substrate materials as shown in table XVI for depositions IV-7 to IV-9 and IV-A-4 to IV-A-18.

The deposition parameters for experiments in this task are summarized in tables XVII and XVIII.

The initial effort was directed at producing sputtered cylinders in the hollow cathode coater. The first two runs were performed on aluminum substrates at low temperatures utilizing diode discharge with no substrate bias. When the structure of these deposits was found unsatisfactory, a shift to OFHC copper substrates was made. Higher substrate temperatures were employed and the effects of substrate bias were investigated. Based on the results of Task II triode depositions, diode sputtering was discontinued, and a triode discharge was employed.

Further experiments were carried out in the two target flat plate coater to establish the effects of substrate material, substrate geometry, cleaning procedures and target voltage.

Chemical analyses were obtained from eight Ti-5Al-2.5Sn deposits and two NASA IIb-11 deposits. The results which are given in tables XIX and XX confirm that there is little change in composition when a material is transferred from target to substrate by sputtering.

TABLE XVI. SUMMARY OF TASK IV SUBSTRATE PREPARATION AND SPUTTER CLEANING PARAMETERS

Run Number	Substrate Material	Finishing Treatment, Surface Preparation, and Primary Cleaning	Voltage, V	Sputter Cleaning[1] Current, mA	Duration, ks	Pressure, N/m^2	μ
IV-1[2]	Aluminum	Sanded lengthwise with No. 600 grit paper, AJAX® scrub, ethyl alcohol rinse	−500	110	1.20	2.9	22
IV-2	Aluminum	Sanded lengthwise with No. 600 grit paper, AJAX® scrub, ethyl alcohol rinse	−400	500	6.00	3.2	24
IV-3	OFHC Copper	Sanded lengthwise with No. 600 grit paper, AJAX® scrub, ethyl alcohol rinse	−500	85	0.30	3.7	27
IV-4	OFHC Copper	Sanded lengthwise with No. 600 grit paper, AJAX® scrub, ethyl alcohol rinse	−500	100	0.99	3.7	27
IV-5	OFHC Copper	Sanded lengthwise with No. 600 grit paper, chemically polished at (348K) 160F for 0.6 ks	−250	37	0.06	4.5	34
IV-6	OFHC Copper	Sanded lengthwise with No. 600 grit paper, AJAX® scrub, ethyl alcohol rinse	−25	1750	0.30	1.9	14
IV-7	OFHC Copper	Sanded circumferentially with No. 600 grit paper on lathe, AJAX® scrub, sanded lengthwise with No. 600 grit paper, ethyl alcohol rinse	−100	710	0.90	0.52	3.9
IV-8	OFHC Copper	Sanded circumferentially with No. 600 grit paper on lathe, AJAX® scrub, sanded lengthwise with No. 600 grit paper, ethyl alcohol rinse	−25	1750	1.80	0.70	5.2
IV-9	OFHC Copper	Sanded circumferentially with No. 600 grit paper on lathe, AJAX® scrub, sanded lengthwise with No. 600 grit paper, ethyl alcohol rinse	−25	1540	0.90	0.41	3.1
IV-A-1[3]	Ti-5Al-2.5Sn and Type 6061 Aluminum alloy	Vapor blast, AJAX® scrub, ethyl alcohol rinse	−25	550	0.30	0.28	2.1
IV-A-2[3]	Ti-5Al-2.5Sn and Type 6061 Aluminum alloy	Vapor blast, AJAX® scrub, ethyl alcohol rinse	−25	510	0.30	0.56	4.2
IV-A-3	Ti-5Al-2.5Sn and Type 6061 Aluminum alloy	Vapor blast, AJAX® scrub, ethyl alcohol rinse	−25	430	6.60	0.68	5.1

NOTES:

[1] Substrate and target cleaned simultaneously

[2] Cleaning in runs IV-1 to IV-6 performed using a diode discharge, in all others a triode discharge was employed

[3] Argon used as the sputtering gas, Krypton used in all others.

Run Number	Substrate Material	Finishing Treatment, Surface Preparation, and Primary Cleaning	Voltage, V	Sputter Cleaning[1] Current, mA	Duration, ks	Pressure N/m^2	μ
IV-A-4	Ti-5Al-2.5Sn and Type 6061 Aluminum alloy	Sanded lengthwise with No. 600 grit paper, AJAX® scrub, ethyl alcohol rinse	-25	400	0.60	0.55	4.1
IV-A-5	Ti-5Al-2.5Sn and Type 6061 Aluminum alloy	Sanded lengthwise with No. 600 grit paper, AJAX® scrub, ethyl alcohol rinse	-25	420	0.30	0.45	3.4
IV-A-6	Ti-5Al-2.5Sn and Type 6061 Aluminum alloy	Sanded lengthwise with No. 600 grit paper, AJAX® scrub, ethyl alcohol rinse	-25	400	0.30	0.45	3.4
IV-A-7	Ti-5Al-2.5Sn and Type 6061 Aluminum alloy	Sanded lengthwise with No. 600 grit paper, AJAX® scrub, ethyl alcohol rinse	-25	400	0.30	0.49	3.7
IV-A-8	Ti-5Al-2.5Sn and Type 6061 Aluminum alloy	Sanded lengthwise with No. 600 grit paper, AJAX® scrub, ethyl alcohol rinse	-25	400	0.30	0.47	3.5
IV-A-9	Ti-5Al-2.5Sn and Type 6061 Aluminum alloy	Sanded lengthwise with No. 600 grit paper, AJAX® scrub, ethyl alcohol rinse	-25 -50 -100	400 420 430	0.30 0.90 0.30	0.45 0.45 0.45	3.4 3.4 3.4
IV-A-11	OFHC Copper and Type 6061 Aluminum alloy	Sanded lengthwise with No. 600 grit paper, AJAX® scrub, ethyl alcohol rinse	-25 -50 -100	500 530 540	0.30 0.90 0.30	0.56 0.55 0.55	4.2 4.1 4.1
IV-A-12	OFHC Copper and Type 6061 Aluminum alloy	Sanded lengthwise with No. 600 grit paper, AJAX® scrub, ethyl alcohol rinse	-25 -50 -100	400 410 425	0.30 0.90 0.30	0.49 0.49 0.49	3.7 3.7 3.7
IV-A-13	OFHC Copper and Type 6061 Aluminum alloy	Sanded lengthwise with No. 600 grit paper, AJAX® scrub, ethyl alcohol rinse	-25 -50 -100	380 400 430	0.30 0.90 0.30	0.45 0.44 0.44	3.4 3.3 3.3
IV-A-14	OFHC Copper and Type 6061 Aluminum alloy	Sanded lengthwise with No. 600 grit paper, AJAX® scrub, ethyl alcohol rinse	-25 -50 -100	400 420 420	0.30 0.90 0.30	0.44 0.44 0.44	3.3 3.3 3.3
IV-A-15	OFHC Copper and Type 6061 Aluminum alloy	Sanded lengthwise with No. 600 grit paper, AJAX® scrub, ethyl alcohol rinse	-25 -50 -100	490 500 500	0.30 0.90 0.30	0.49 0.45 0.45	3.7 3.4 3.4

NOTES:

[1]Substrate and target cleaned simultaneously

[2]Cleaning in runs IV-1 to IV-6 performed using a diode discharge, in all others a triode discharge was employed

[3]Argon used as the sputtering gas, Krypton used in all others.

TABLE XVI. SUMMARY OF TASK IV SUBSTRATE PREPARATION AND SPUTTER CLEANING PARAMETERS (Continued)

Run Number	Substrate Material	Finishing Treatment, Surface Preparation, and Primary Cleaning	Voltage, V	Sputter Cleaning[1] Current, mA	Duration, ks	Pressure N/m²	μ
IV-A-16	OFHC Copper and Type 6061 Aluminum alloy	Sanded lengthwise with No. 600 grit paper, AJAX® scrub, ethyl alcohol rinse	-25 -50 -100	450 490 440	0.30 0.90 0.30	0.45 0.45 0.45	3.4 3.4 3.4
IV-A-17	OFHC Copper and Type 6061 Aluminum alloy	Sanded lengthwise with No. 600 grit paper, AJAX® scrub, ethyl alcohol rinse	-25 -50 -100	460 500 525	0.30 0.90 0.30	0.45 0.45 0.45	3.4 3.4 3.4
IV-A-18	OFHC Copper and Type 6061 Aluminum alloy	Sanded lengthwise with No. 600 grit paper, AJAX® scrub, ethyl alcohol rinse	-25 -50 -100	400 440 465	0.30 0.90 0.30	0.44 0.39 0.38	3.3 2.9 2.8

NOTES:

[1] Substrate and target cleaned simultaneously

[2] Cleaning in runs IV-1 to IV-6 performed using a diode discharge, in all others a triode discharge was employed

[3] Argon used as the sputtering gas, Krypton used in all others.

TABLE XVII. SUMMARY OF TASK IV DEPOSITION PARAMETERS

Run Number	Target Material	Substrate Material	Substrate Voltage, V	Substrate Current, mA	Target Voltage, V	Target Current, A	Magnetic Coils Current, A	Magnetic Coils Separation, cm	Time ks	Time hr	Substrate Temperature °K	Substrate Temperature °F	Maximum Deposit Thickness mm	Maximum Deposit Thickness mils	Average Deposition Rate nm/s	Average Deposition Rate mil/hr	Pressure N/m²	Pressure μ
IV-1[1]	Ti-5Al-2.5Sn	Aluminum	0	0	-600	5.0	4.0	10.2	25.2	7.0	366	200	0.899	35.4	0.6	0.94	1.73	13
			0	0	-1000	5.0	4.7	10.2	110.7	30.75	366	200					0.68	5.1
IV-2	Ti-5Al-2.5Sn	Aluminum	0	0	-1000	5.0	4.0	10.2	21.6	6.0	477	400	1.097	43.2	8.1	1.15	0.93	7.0
			0	0	-1000	5.0	3.6	10.2	113.4	31.5	477	400					0.90	6.8
IV-3	Ti-5Al-2.5Sn	OFHC Copper	-300	480	-400	0.6	3.3	10.2	3.6	1.0	741	875	0.711	28.0	6.3	0.90	3.33	25
			0	0	-1000	5.0	3.6	10.2	108.0	30.0	650	710					1.01	7.6
IV-4	Ti-5Al-2.5Sn	OFHC Copper	-100	126	-1000	5.0	2.6	10.2	79.2	22.0	694	790	0.737	29.0	6.8	0.97	1.9	14
			-100	215	-1500	5.0	2.3	10.2	20.7	5.75	741	875					1.9	14
			-100	130	-1000	5.0	2.5	10.2	6.3	1.75	741	875					1.9	14
IV-5	Ti-5Al-2.5Sn	OFHC Copper	-100	135	-1000	5.0	2.3	10.2	56.7	15.75	705	810	0.508	20.0	0.4	0.91	0.20	1.5
			-50	95	-1000	5.0	2.3	10.2	22.5	6.25	366	560					0.19	1.4
IV-6	Ti-5Al-2.5Sn	OFHC Copper	-25	1.75	-25	1.0	3.5	10.2	0.08	0.08	572	570	0.165	6.5	2.3	0.33	1.9	14
			-25	1.5	-800	2.0	2.4	10.2	1.5	0.41	686	780					0.43	3.2
			0	0	-800	3.0	2.4	10.2	21.6	6.0	755	900					0.49	3.7
			-100	1.0	-25	1.3	-	-	0.29	0.08	755	900					0.43	3.2
			0	0	-800	3.0	-	-	21.6	6.0	755	900					0.56	4.2
			-100	1.2	-25	2.95	-	-	0.9	0.25	694	790					0.52	3.9
			-25	1.0	-800	3.0	-	-	24.3	6.75	783	950					0.45	3.4
IV-7	Ti-5Al-2.5Sn	OFHC Copper	-100	0.71	-25	5.7	0	-	0.9	0.25	744	880	0.305	12.0	4.3	0.61	0.52	3.9
			-50	0.65	-1000	3.0	0	-	43.2	12.0	900	1160					0.26	1.9
			-100	0.74	-25	2.1	0	-	0.29	0.08	672	750					0.63	4.7
			-50	0.36	-1000	3.0	3.0	10.2	27.0	7.5	733	860					0.45	3.4
IV-8	Ti-5Al-2.5Sn	OFHC Copper	-25	1.75	-25	1.25	1.5	10.2	0.29	0.08	716	830	0.178	7.0	3.3	0.47	0.69	5.2
			-25	1.30	-1000	3.2	0	-	24.3	6.75	883	1130					0.53	4.0
			-25	1.35	-25	3.7	0	-	0.29	0.08	675	720					0.48	3.6
			-25	1.40	-1000	4.0	0	-	27.0	7.5	919	1195					0.25	1.9
IV-9	Ti-5Al-2.5Sn	OFHC Copper	-25	1.54	-25	3.9			0.9	0.25	732	840	0.279	11.0	5.1	0.73	0.41	3.1
			-25	1.45	-1000	4.3			24.3	6.75	927	1210					0.49	3.7
			-25	1.95	-1000	6.0			3.6	1.00	977	1300					0.51	3.8
			-25	1.80	-25	3.5			0.9	0.25	777	940					0.49	3.7
			-25	1.35	-1000	5.4			25.2	7.00	975	1295					0.35	2.6

NOTES:

[1] Runs VI-1 to IV-6 performed with diode discharge, triode discharge used in all others.

TABLE XVIII.   SUMMARY OF TASK IV DEPOSITION PARAMETERS
FLAT PLATE COATER

Run Number	Target Material	Substrate Material	Substrate Voltage, V	Substrate Current, A	Target Voltage, V	Target Current, A	Time ks	Time hr	Substrate Temperature °K	Substrate Temperature °F	Maximum Deposit Thickness mm	Maximum Deposit Thickness mils	Average Deposition Rate nm/s	Average Deposition Rate mil/hr	Pressure N/m²	Pressure μ
IV-A-1[1]	Ti-5Al-2.5Sn	Ti-5Al-2.5Sn and Type 6061 Aluminum	− 25	0.55	− 25	0.38	0.29	0.08	350	170	0.081	3.2	1.8	0.25	0.28	2.1
			− 25	0.73	−1000	0.54	17.1	4.75	377	220					0.24	1.8
			− 25	0.73	−1000	0.53	29.7	8.25	369	205					0.56	4.2
IV-A-2	Ti-5Al-2.5Sn	Ti-5Al-2.5Sn and Type 6061 Aluminum	− 25	0.51	− 25	0.33	0.29	0.08	333	140	0.061	2.4	2.4	0.34	0.56	4.2
			− 25	0.71	−1500	0.52	25.2	7.00	400	260					0.43	3.2
IV-A-3	Ti-5Al-2.5Sn	Ti-5Al-2.5Sn and Type 6061 Aluminum	− 25	0.43	− 25	0.31	0.6	0.16	333	140	0.135	5.3	2.7	0.38	0.68	5.1
			− 25	0.54	−1500	0.40	36.0	10.00	372	210					0.40	3.0
			− 25	0.55	−1500	0.39	13.5	3.75	351	190					0.45	3.4
IV-A-4	Ti-5Al-2.5Sn	Ti-5Al-2.5Sn and Type 6061 Aluminum	− 25	0.40	− 25	0.24	0.6	0.16	339	150	0.249	9.8	2.1	0.30	0.55	4.1
			− 25	0.58	−1500	0.42	27.0	7.50	389	240					0.45	3.4
			− 25	0.57	−1500	5.40	29.7	8.25	377	220					0.49	3.7
IV-A-5	Ti-5Al-2.5Sn	Ti-5Al-2.5Sn and Type 6061 Aluminum alloy	− 25	0.42	− 25	0.32	0.29	0.08	344	160	0.086	3.4	1.7	0.24	0.45	3.4
			− 25	0.44	− 25	0.33	0.9	0.25	352	175					0.48	3.6
			− 25	0.41	−1000	0.41	27.0	7.50	375	215					0.40	3.0
			− 25	0.31	− 25	0.31	0.29	0.08	350	170					0.49	3.7
			− 25	0.40	− 25	0.32	0.29	0.08	352	175					0.43	3.2
			− 25	0.38	−1000	0.41	23.4	6.50	372	210					0.39	2.9
IV-A-6	Ti-5Al-2.5Sn	Ti-5Al-2.5Sn and Type 6061 Aluminum alloy	− 25	0.40	− 25	0.37	0.29	0.08	350	170	0.137	5.4	1.7	0.24	0.45	3.4
			− 25	0.42	− 25	0.36	0.6	0.16	352	175					0.47	3.5
			− 50	0.50	− 25	0.36	0.29	0.08	355	180					0.47	3.5
			− 25	0.46	− 25	0.34	0.29	0.08	358	185					0.43	3.2
			− 50	0.47	− 25	0.35	0.6	0.16	366	200					0.43	3.2
			−100	0.47	− 25	0.35	0.29	0.08	372	210					0.43	3.2
			− 25	0.43	−1000	0.43	27.0	7.50	389	240					0.43	3.2
			− 25	0.43	− 25	0.33	0.29	0.08	351	190					0.45	3.4
			− 50	0.45	− 25	0.35	0.29	0.08	364	195					0.39	2.9
			− 25	0.44	−1000	0.44	54.0	15.00	389	240					0.37	2.7
IV-A-7	Ti-5Al-2.5Sn	Ti-5Al-2.5Sn and Type 6061 Aluminum alloy	− 25	0.40	− 25	0.31	0.29	0.08	497	435	0.081	3.2	1.5	0.21	0.49	3.7
			− 50	0.43	− 25	0.32	0.6	0.16	539	510					0.45	3.4
			−100	0.46	− 25	0.32	0.29	0.08	564	555					0.45	3.4
			0	0	−1000	0.40	26.1	7.25	566	560					0.44	3.3
			− 25	0.42	− 25	0.31	0.29	0.08	522	480					0.47	3.5
			− 50	0.42	− 25	0.33	0.29	0.08	547	525					0.47	3.5
			−100	0.47	− 25	0.32	0.6	0.16	577	580					0.47	3.5
			0	0	−1000	0.40	27.9	7.75	572	570					0.45	3.4

NOTES:

[1]All depositions performed with triode discharge.

TABLE XVIII. SUMMARY OF TASK IV DEPOSITION PARAMETERS FLAT PLATE COATER (Continued)

Run Number	Target Material	Substrate Material	Substrate Voltage, V	Current, A	Target Voltage, V	Current, A	Time ks	hr	Substrate Temperature, °K	°F	Maximum Deposit Thickness mm	mils	Average Deposition Rate nm/s	mil/hr	Pressure N/m²	μ
IV-A-8	Ti-5Al-2.5Sn	Ti-5Al-2.5Sn and Type 6061 Aluminum alloy	− 25	0.40	− 25	0.30	0.29	0.08	433	320	0.137	5.4	2.7	0.39	0.47	3.5
			− 50	0.42	− 25	0.31	0.6	0.16	444	340					0.43	3.2
			−100	0.43	− 25	0.31	0.29	0.08	466	380					0.43	3.2
			− 25	0.40	−1500	0.40	27.0	7.50	477	400					0.40	3.0
			− 25	0.41	− 25	0.32	0.29	0.08	433	320					0.41	3.1
			− 50	0.44	− 25	0.33	0.6	0.16	444	340					0.41	3.1
			−100	0.47	− 25	0.32	0.29	0.09	461	370					0.41	3.1
			− 25	0.41	−1500	0.39	23.4	6.50	494	430					0.37	2.7
IV-A-9	Ti-5Al-2.5Sn	Ti-5Al-2.5Sn and Type 6061 Aluminum alloy	− 25	0.39	−1500	0.40	20.6	5.72	544	520	0.361	14.2	2.4	0.34	0.41	3.1
			− 25	0.40	−1500	0.39	21.6	6.00	533	500					0.43	3.2
			− 25	0.40	−1500	0.40	27.9	7.75	516	470					0.43	3.2
			− 25	0.40	−1500	0.39	26.1	7.25	483	410					0.43	3.2
			− 25	0.41	−1500	0.40	26.1	7.25	500	440					0.41	3.1
			− 25	0.43	−1500	0.41	27.0	7.50	505	450					0.43	3.2
IV-A-11	Aluminum	OFHC Copper and Type 6061 Aluminum alloy	− 25	0.41	−1500	0.46	86.4	24.0	366	200	0.406	16.0	4.7	0.67	0.45	3.4
IV-A-12	Aluminum	OFHC Copper and Type 6061 Aluminum alloy	− 25	0.46	−1500	0.47	75.6	21.0	NM	NM	0.978	38.5	4.9	0.70	0.43	3.2
			− 25	0.42	−1500	0.46	106.2	29.5	400	260					0.39	2.9
			− 25	0.40	−1500	0.43	16.2	4.5	400	260					0.37	2.7
IV-A-13	Aluminum	OFHC Copper and Type 6061 Aluminum alloy	− 25	0.38	−1500	0.47	92.6	26	377	220	0.381	15.0	4.1	0.58	0.37	2.7
IV-A-14	Al-Al₂O₃	OFHC Copper and Type 6061 Aluminum alloy	− 25	0.40	−1500	0.49	97.2	27	350	170	0.221	8.7	1.3	0.19	0.37	2.7
			0	0	−1500	0.45	68.4	19	351	190					0.37	2.7
IV-A-15	Al-Al₂O₃	OFHC Copper and Type 6061 Aluminum alloy	− 25	0.47	−1500	0.50	327.6	91	355	180	0.356	14.0	1.1	0.15	0.38	2.8
IV-A-16	NASA IIb-11	OFHC Copper and Type 6061 Aluminum	− 25	0.40	−1500	0.48	50.4	14	383	230	0.127	5.0	2.5	0.36	0.41	3.1
IV-A-17	NASA IIb-11	OFHC Copper and Type 6061 Aluminum alloy	− 25	0.40	−1500	0.50	61.2	17	389	240	0.279	11.0	1.7	0.24	0.39	2.9
			0	0	−1500	0.44	100.8	28	375	215					0.37	2.7
IV-A-18	NASA IIb-11	OFHC Copper and Type 6061 Aluminum alloy	− 25	0.42	−1500	0.45	381.6	106	NM	NM	0.711	28.0	1.8	0.26	0.32	2.4

NOTES:

[1] All depositions performed with triode discharge.

NM − Not Measured.

TABLE XIX. COMPOSITION[1] OF TARGET AND SPUTTERED Ti-5Al-2.5Sn DEPOSIT[2]

Element	AMS 4966 Specification	Target[3] (A)	(B)	Deposit From Run IV-1	IV-2	IV-3	IV-4	IV-5	IV-6	IV-7	IV-8
Al	4.0-6.0	4.5	5.4	5.4	5.4	5.0	5.0	4.9	4.5	4.2	4.0
Sn	2.0-3.0	2.6	2.6	2.5	2.6	2.0	2.0	2.0	2.1	2.2	2.1
Ti	Bal	Bal	Bal	Bal	Bal	Bal	Bal	Bal	Bal	Bal	Bal

NOTES:

[1] Composition in weight percent

[2] Analysis by atomic absorption spectroscopy

[3] Target analysis performed at two different times.

TABLE XX. COMPOSITION[1] OF TARGET AND SPUTTERED NASA IIb-11 DEPOSIT[2]

Element	NASA IIb-11 Specification	Target[3] (A)	Deposit From Run IV-A-16	Target (B)	Deposit From Run IV-A-18
Hf	0.75-1.25	1.05	0.83	0.70	0.90
Ti	0.50-1.00	0.80	0.90	0.80	1.10
Co	8.50-9.50	8.85	8.50	9.20	8.90
Mo	1.50-2.50	1.90	1.90	1.90	1.90
Cr	8.50-9.50	9.10	8.55	9.00	8.80
V	0.40-0.60	0.23	0.43	0.30	0.40
W	7.25-8.25	6.80	5.80	7.30	7.80
Zr	0.05-0.15	0.07	0.06	0.08	0.08
Ta	6.25-7.25	7.50	7.50	8.00	6.70
Al	4.20-4.80	4.50	4.00	4.80	3.50
Ni	Bal	Bal	Bal	Bal	Bal

NOTES:

[1] Composition given in weight percent

[2] Analysis by atomic absorption spectroscopy

[3] Target analysis (A) performed with Run IV-A-16 deposit; target analysis (B) performed with Run IV-A-18 deposit.

Representative dense deposits were chosen for tensile testing. The properties shown in table XXI were obtained from subscale, flat tensile specimens machined from the coated substrates. The substrates were removed from the gauge section by chemical etching in the cases of Ti-5Al-2.5Sn and NASA IIb-11 (copper substrates were dissolved in dilute HNO₃, aluminum substrates were dissolved in warm NaOH) or by machining in the case of aluminum and aluminum plus Al₂O₃.

The final evaluation was an interaction study between the expected substrate, Cu, and the candidate high strength materials at elevated temperatures.

RESULTS AND DISCUSSION

Ti-5Al-2.5Sn

The initial depositions in this task were made with Ti-5Al-2.5Sn targets as it was believed this material would present the most problems with cleanliness and substrate incompatibility. These beliefs were confirmed. Therefore, a large number of depositions were performed with Ti-5Al-2.5Sn and a relatively small number with aluminum and NASA IIb-11. The parameter development which was done on the Ti system was directly transferable to the other systems.

The first two depositions IV-1 and IV-2 were performed on grounded aluminum substrates at low temperature with a diode discharge. Both titanium deposits had an open columnar structure which was poorly bonded to the substrate, figure 66. Varying substrate bias, switching to a copper substrate and increasing temperature while maintaining a diode discharge in depositions IV-3, IV-4 and IV-5 resulted in a minor increase in density but the coating remained columnar and open as shown in figure 67. No mechanical tests could be performed with any of these deposits as the open structure precluded any possibility of mechanical strength.

When a triode discharge was employed in depositions IV-6 through IV-9, there was a dramatic density increase and effects of temperature and deposition rate were more noticeable. Deposits IV-6, performed at 2.3 nm/sec (0.33 mils/hr) and 750-790°K (522-594°F), and IV-7 performed at 4.3 nm/sec (0.6 mils/hr) and 900°K (792°F), were dense but brittle while deposit IV-8 performed at 3.3 nm/sec (0.47 mils/hr) at 880-900°K (756-792°F) and IV-9 performed at 5.1 nm/sec (0.72 mils/hr) at 970-980°K (918-936°F) were both dense and ductile to some extent. The typically dense structures illustrated in figure 68 also show potential problems inherent in the copper-titanium binary.

An acicular precipitate phase, present in high concentration in deposit IV-8 and to a lesser degree in IV-9 was identified as a titanium hydride, TiH₂, by X-ray diffraction and was presumed due to system outgassing. This embrittling phase can be decomposed by annealing in vacuum at about 800°K. An anneal such as this will, however, compound the second problem. A titanium copper reaction at the interface apparently forms TiCu₃, a brittle intermetallic phase which cannot be decomposed by heat treatment.

A series of experiments to explore low temperature deposition and substrate cleaning procedures was carried out using the two plate coater depositing Ti-5Al-2.5Sn with a triode discharge.

110
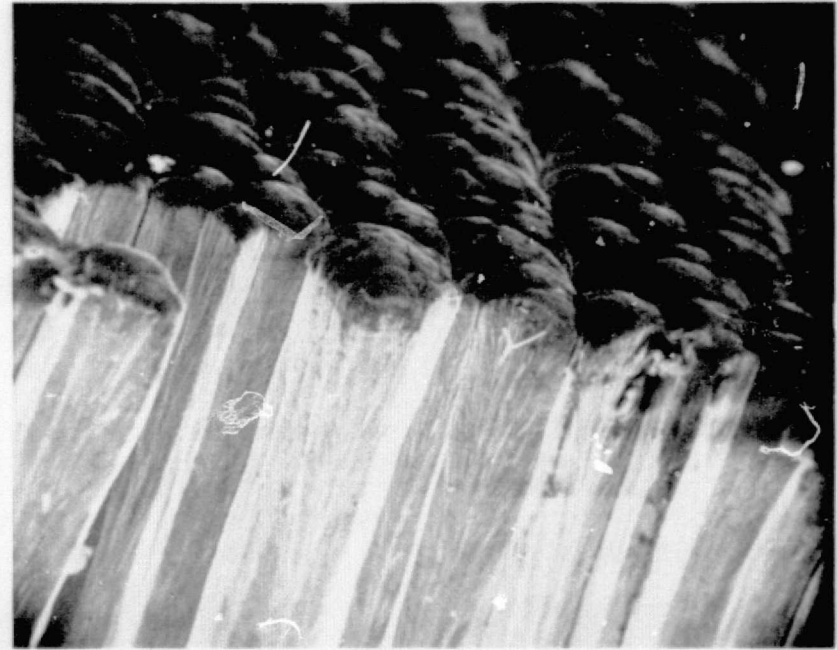
100X

250X

Mag: Left: 100X
Right: 250X

Figure 66. Microstructure of Sputtered Ti-5Al-2.5Sn Showing Open, Columnar Structure and Lack of Intercolumnar Bonding. (Run IV-1, Low Temperature Substrate)

FD 91430

111
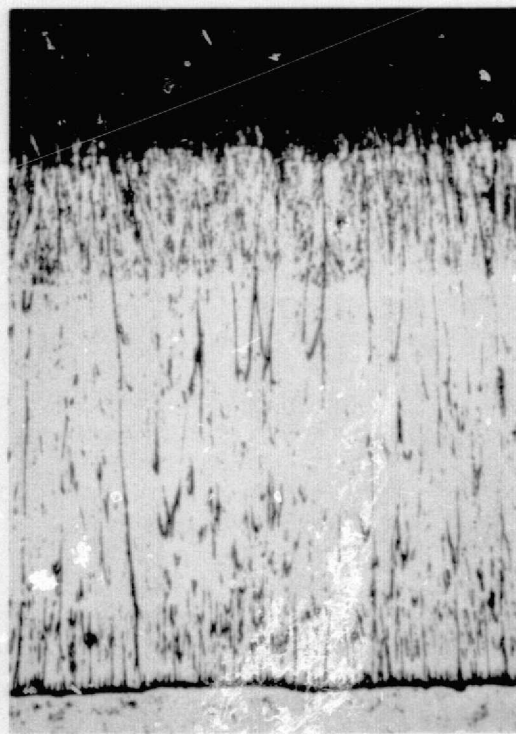
Run IV-3   50X   Run IV-4   100X   IV-5   200X
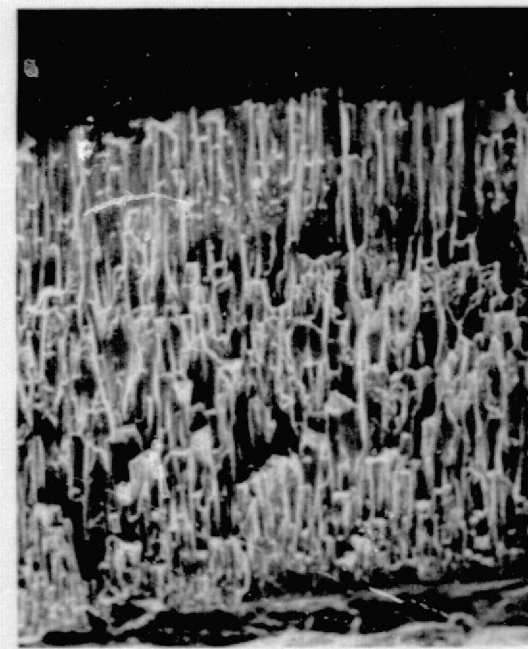
Figure 67.   Representative Microstructure of Ti-5Al-2.5Sn Deposited at Elevated Temperatures on   FD 91431
Copper Substrates in Diode Mode
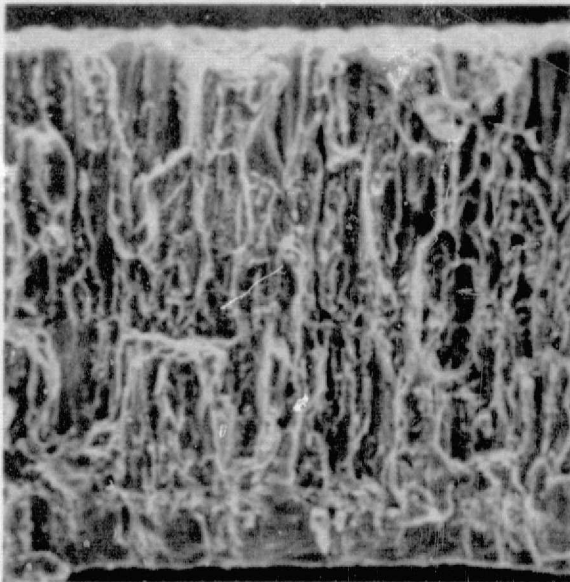
Run IV-8   550X
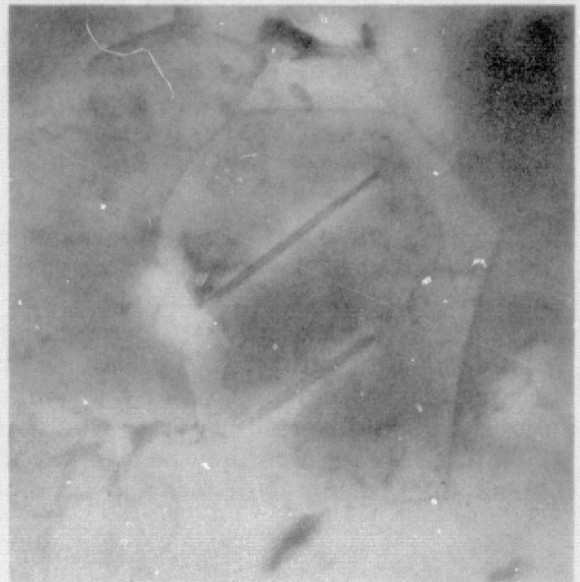
Run IV-8   10000X
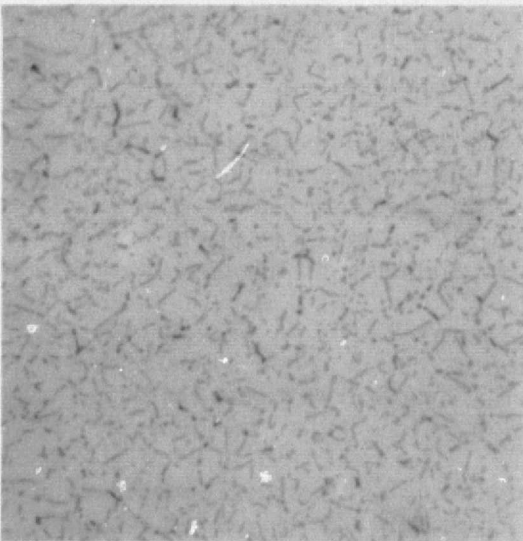
Run IV-8   500X
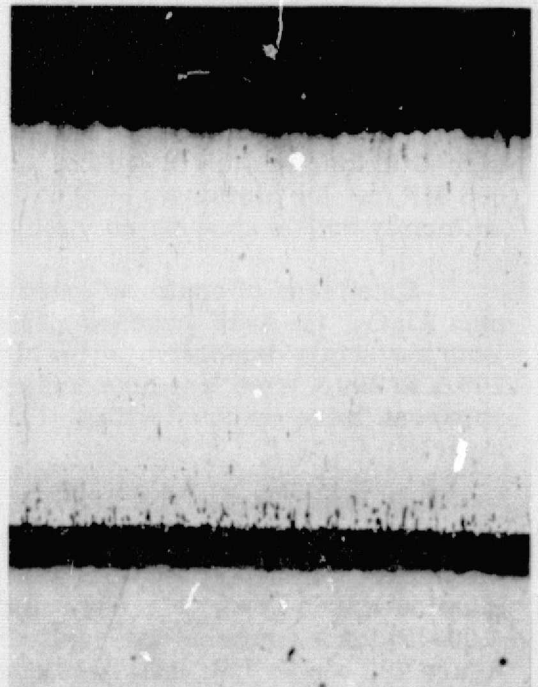
IV-9   200X

Figure 68.   Typically Dense Ti-5Al-2.5Sn Deposits   FD 91432
             and Ductile Appearing Fractures Resulting
             from High Temperature, Low Rate
             Depositions in the Triode Mode.   Note
             Especially the Fine Grain Size in the
             Transmission Photomicrography, the
             Acicular Hydride Phase and the $TiCu_3$
             Intermetallic at the Cu-Ti Interface

113

The optimum substrate cleaning procedure, for all substrate material investigated, was to sand with 600 grit SiC paper, scrub with Ajax® and rinse with ethyl alcohol prior to sputter cleaning in the coater. Vapor blasting prior to sputter cleaning, as was investigated in deposition IV-A-1, 2 and 3, left numerous abrasive particles imbedded at the substrate-coating interface, figure 69.

This series of experiments demonstrated that it is possible to deposit a dense coating of Ti-5Al-2.5Sn on various substrates if a trade-off of very low deposition rates is acceptable. These successful low temperature depositions indicate that the brittle $TiCu_3$ reaction layer at the Cu-Ti interface can be avoided. Unfortunately, as seen in table XXI the "as deposited" material is not strong and is very brittle. An anneal which could increase the effective strength and introduce limited ductility would also promote the formation of the $TiCu_3$ reaction layer which may negate any gains. Figure 69 illustrates typical structures and interfaces of these low temperature low rate deposits.

Aluminum and Al_2O_3-Al

Aluminum, with and without an Al_2O_3 dispersion, was also investigated as a high strength cylinder material. All of these depositions, IV-A-11 through IV-A-15 were performed in the two plate coater at low temperatures as shown in table XVIII. These depositions, on OFHC copper and type 6061 aluminum, were uniformly dense and adherent as shown by representative structures in figures 70 for pure aluminum and 71 for aluminum plus Al_2O_3 where relative hardness is also shown. Tensile testing, as reported in table XXI revealed a high ultimate tensile strength of 438 to 481 MN/m^2 for pure aluminum and 405 to 605 MN/m^2 for aluminum with oxide dispersion. However, all depositions were uniformly brittle showing no yield or perceptible elongation.

Specimens of sputtered pure aluminum, IV-A-11, and co-deposited aluminum plus Al_2O_3, IV-A-15 were examined by thin foil transmission electron microscopy. Both materials demonstrated an ultra-fine grain size, estimated to be between 100Å to 200Å from line broadening in selected area electron diffraction, and an apparent "wire texture" with a (111) fiber axis perpendicular to the deposited layer.

No aluminum oxide precipitate was resolved in the sputtered deposit from IV-A-15 and no evidence was seen in the electron diffraction patterns, although the microstructure of the codeposited material was different than the pure aluminum as may be seen from figures 70 and 71. After heat treatment at 813°K (1000°F) for 1 hour the codeposited microstructure showed a mottled background, figure 72, which may have been due to oxide precipitation. However, no evidence of Al_2O_3 was seen in electron diffraction patterns indicating that the oxide, if present, was a very fine precipitate. Unfortunately, the 813°K (1000°F) heat treatment dropped both materials to a 96.5 to 110.3 MN/m^2 (14 to 16 ksi) yield and 117.2 to 131.0 MN/m^2 (17 to 19 ksi) ultimate tensile strength. However, 8% elongation was achieved.
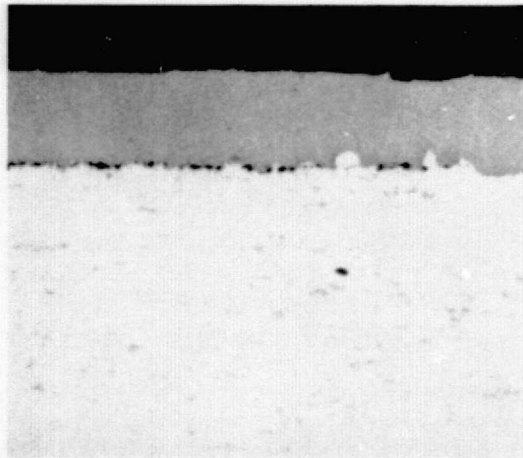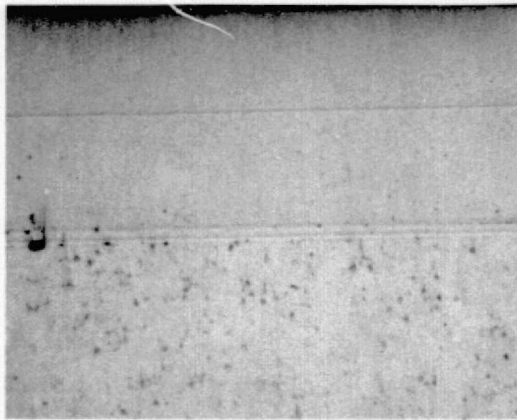
Run IV-A-2   200X   Run IV-A-4   200X   Run IV-A-4   1200X
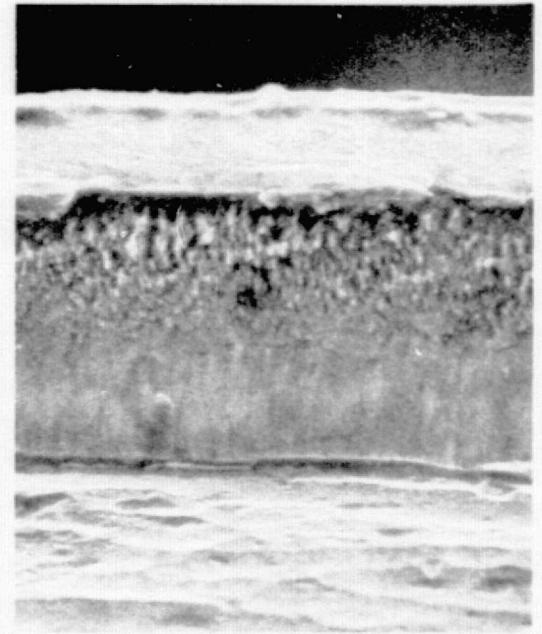
Figure 69. The Dense Structure of the Ti-5Al-2.5Sn Deposits and Ductile Appearing Fracture Were Typical   FD 91433 of Triode Depositions. Note the Abrasive Inclusions at the Interface of IV-A-2 Where the Substrate was Vapor Blasted Prior to Sputter Cleaning Compared to the Relatively Clean SiC Sanded Interface of Run IV-A-4

100X

Unetched

100X

Etched
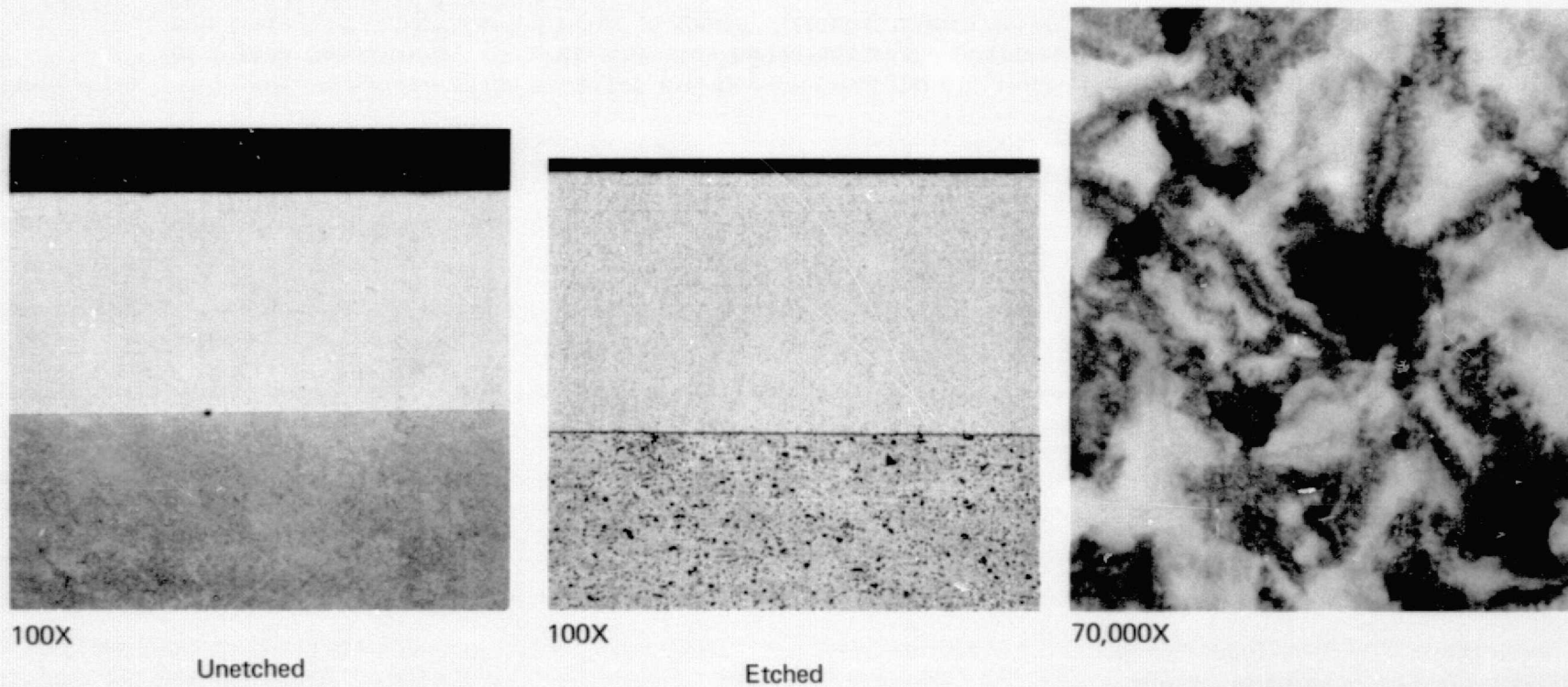
70,000X

Figure 70. Microstructure of Pure Aluminum As Sputtered in Deposition IV-A-11. Note the Dense Deposit, Clean Interface and Extremely Fine Grain Size

FD 91434
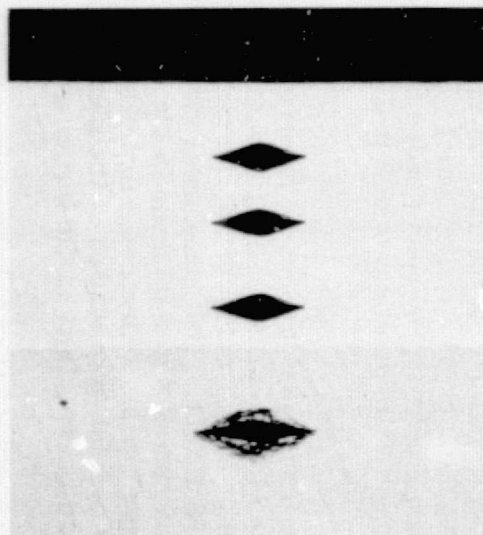
Aluminum
Run IV-A-13
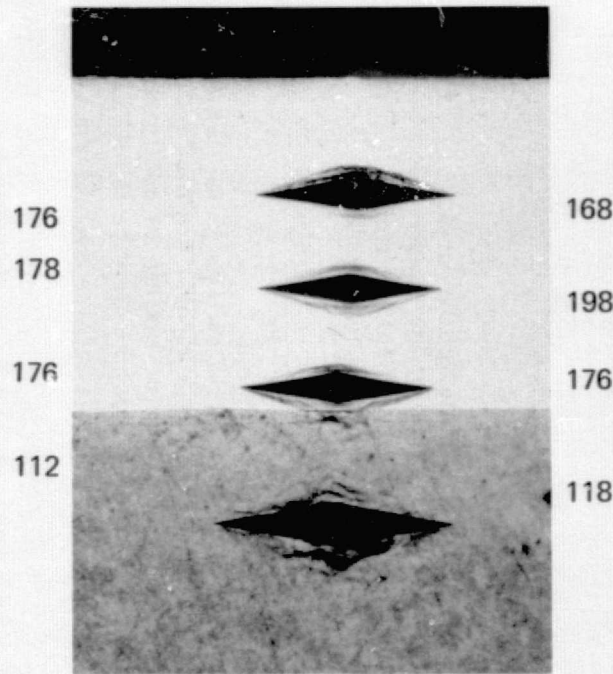
200X

Al-Al$_2$O$_3$
Run IV-A-14

70,000X

Al-Al$_2$O$_3$
Run IV-A-15

176
178
176
112

168
198
176
118
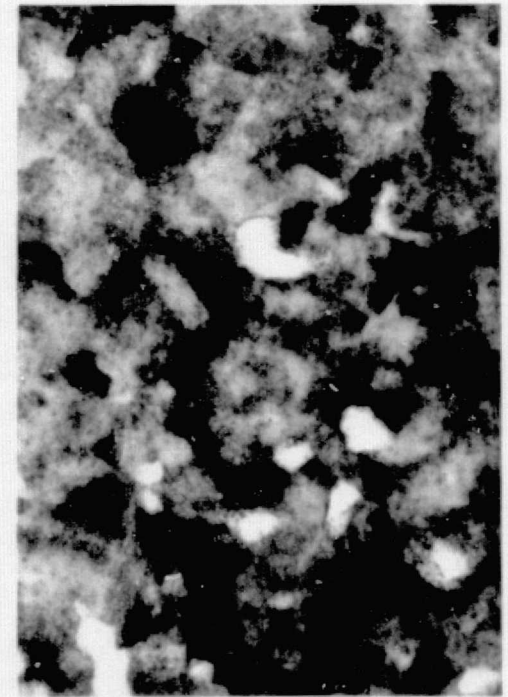
Figure 71.   Two Hundred Gram Knoop Microhardness Measurements Show the Slight Increase in Hardness   FD 91435
Realized in the Co–Deposited Al+Al$_2$O$_3$.   The Ultra Fine Grain Size is Evident from the
Transmission Photomicrograph
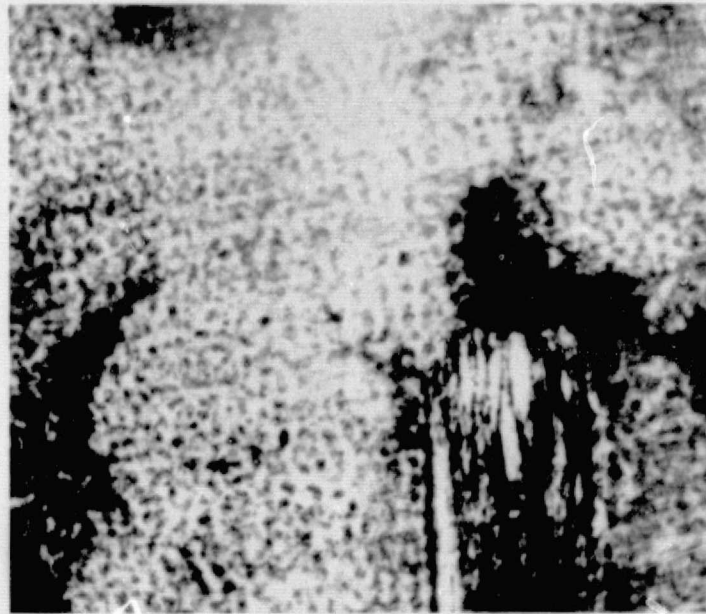
70,000X

Figure 72. Structure of Deposit from Run II-A-15.   FD 91436
(The Mottled Appearance of the Back-
ground is Probably Due to Al_2O_3 Pre-
cipitation from 813°K Heat Treatment)

NASA IIb-11

The last three depositions in Task IV, IV-A-16, 17 and 18 were performed
with NASA IIb-11 deposited on OFHC copper and 6061 aluminum alloy substrates
in the two plate coater. These deposits varied mainly in maximum thickness as
shown in table XVIII and were uniformly dense as may be seen in figure 73. All
were brittle as deposited.

Specimens from IV-A-16 were examined by transmission electron micros-
copy as-deposited and after heat treating at 1310°K (1900°F) for 1 hour in hy-
drogen. The as-deposited material had an estimated grain size of approximately
200Å and a strong (111) "wire texture" perpendicular to the deposit. The most
surprising observation was the lack of a visible second phase in the as-deposited
material. This observation means there was an enormous amount of γ' forming
elements as well as carbon in solid solution, which probably explains the 200 gram
Knoop hardness of 700 to 750.

Figure 74 shows the transmission electron microscopy microstructure of
the as-deposited NASA IIb-11 as well as the microstructure resulting from an
anneal at 1310°K (1900°F) for 1 hour compared to the microstructure of con-
ventionally processed NASA IIb-11. The post-anneal structure is duplex being
approximately 50% isolated grains 3 to 5 microns in diameter and 50% 0.1 micron
grains separating the larger grains. Electron diffraction showed remnants of
the (111) wire texture and careful examination of the photomicrographs shows
the beginnings of precipitation especially in the larger grains.

118
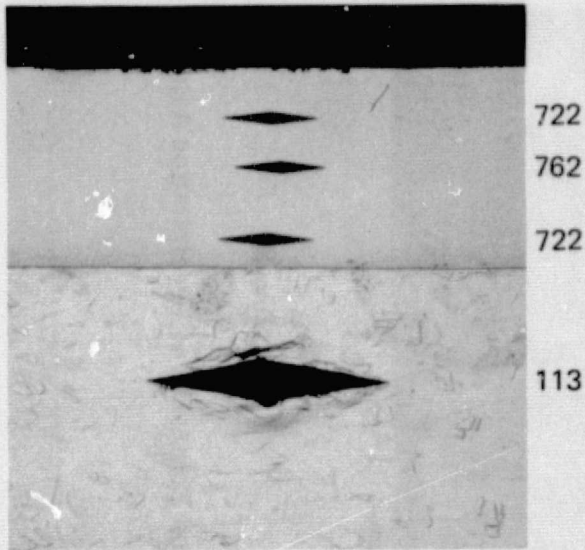
200X NASA IIb-11
Run IV-A-16
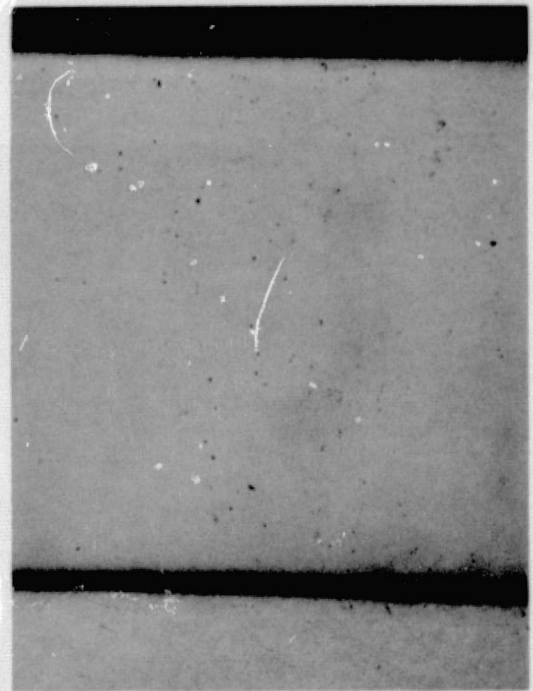
100X IV-A-18
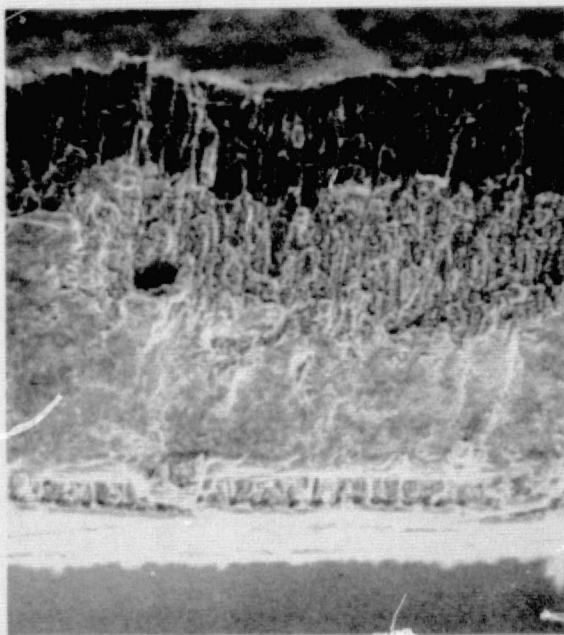
700X IV-A-16
As Deposited
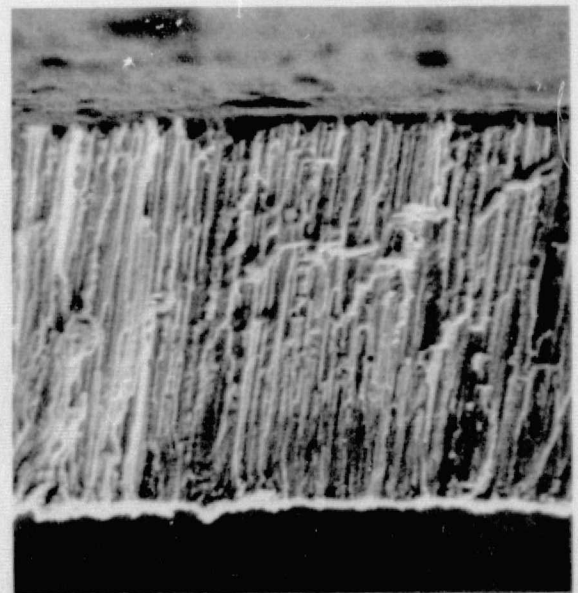
700X IV-A-16
Annealed
1900°F-1 hr

Figure 73. Typical Microstructure and 200 Gram   FD 91437
Knoop Microhardness of NASA IIb-11
Sputtered Deposits

70,000X

10,000X

As Deposited
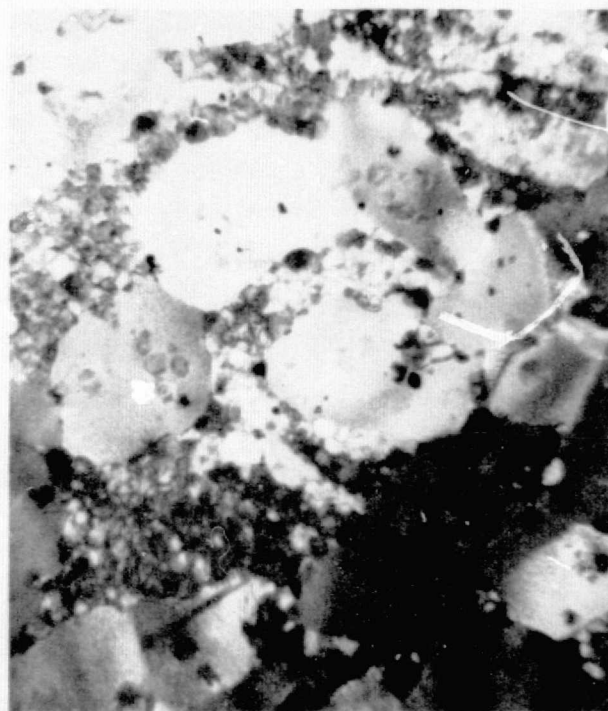
Annealed

Figure 74. Transmission Electron Micrograph Showing Grain Growth and Beginning of Precipitation After Annealing at 1311°K (1900°F) for 3.6 ks   FD 91438

Tensile tests on material from IV-A-17 showed the as-deposited alloy to be very strong but brittle. An anneal at 1250°K (1800°F) for 14.4 ks (4 hours) demonstrated the capability of promoting ductility in this alloy with essentially no loss of ultimate tensile strength. These results are presented in table XXI.

TASK IV

CONCLUSIONS

Four sputtered materials were evaluated in this task with respect to their use as outer jacket structures for strengthening regeneratively cooled rocket thrust chambers. From this task the following conclusions were drawn:

1. Of the materials evaluated, sputtered NASA-IIb-11 provided the highest tensile strength, 916 MN/m^2 (132,000 psi), and would provide the greatest effect in strengthening the outer close-out layer of regeneratively cooled thrust chambers. The as-sputtered strength obtained approached that of as-cast NASA IIb-11. The other benefit of this material was that interaction with the copper base chamber materials is minimal. The reaction zone is not brittle, which is desirable with respect to fatigue considerations. Furthermore, this alloy and reaction effect offer the greatest latitude of substrate temperature in sputter deposition.

2. The sputtered aluminum and co-sputtered Al$_2$O$_3$-aluminum materials provided the greatest strength-to-density of the materials evaluated in this task. The tensile strength obtained of sputtered aluminum, 481.6 MN/m^2 (69,900 psi), is over double that obtained with Grade 1100 aluminum.

3. High strength deposits of Ti-5Al-2.5Sn could be obtained in sputtering from a hollow cathode. To achieve strength and density, a -25V bias and sputter deposition from a triode discharge was required.

4. Of the materials evaluated, the aluminum and Al$_2$O$_3$-Al exhibited the greatest interaction with the copper substrate materials, while the NASA IIb-11 material showed the least interaction. Based on the extent of interaction, the NASA IIb-11 alloy offers the most stable couple with copper to provide the greatest latitude in substrate temperature range for deposition and the highest operating temperature for thrust chambers.

TABLE XXI. TENSILE PROPERTIES OF TASK IV SPUTTERED MATERIALS

Material	Run Number	Substrate Temperature °K	°F	Condition or Heat Treatment	Yield Strength MN/m²	psi	Ultimate Tensile Strength MN/m²	psi	Elongation Percent
TI-5Al-2.5Sn	IV-8	900	1160	As sputtered	–	–[1]	606.3	88,000	–
	IV-8	900	1160	813K-3.6ks-VAC	875.0	127,000	898.5	130,400	< 0.7
	IV-9	978	1300	As sputtered	–	–	785.5	114,000	–
	IV-9	978	1300	813K-3.6ks-VAC	–	–	819.9	119,000	–
Aluminum	IV-A-11	367	200	As sputtered	–	–	438.2	63,600	–
	IV-A-11	367	200	As sputtered	–	–	330.7	48,000	–
	IV-A-11	367	200	813K-14.4ks-Ar	106.1	15,400	123.3	17,900	8.0
	IV-A-12	400	260	As sputtered	–	–	478.2	69,400	–
	IV-A-12	400	260	813K-14.4ks-Ar	95.8	13,900	115.1	16,700	8.0
	IV-A-13	378	220	As sputtered	–	–	481.6	69,900	–
Al₂O₃-Al	IV-A-14	356	180	As sputtered	–	–	604.9	87,800	–
	IV-A-14	356	180	As sputtered	–	–	551.2	80,000	–
	IV-A-14	356	180	813K-14.4ks-Ar	106.8	15,600	119.9	17,400	8.0
	IV-A-15	356	180	As sputtered	–	–	405.1	58,800	–
	IV-A-15	356	180	As sputtered	–	–	516.8	75,000	–
NASA IIb-11	IV-A-17	383	230	As sputtered	–	–	865.4	125,600	–
	IV-A-17	383	230	As sputtered	–	–	916.4	133,000	–
	IV-A-17	383	230	1250K-14.4ks	606.3	88,000	906.0	131,500[2]	–

NOTES:

[1] Where yield and elongation not shown, specimen failed before yield with no measureable elongation

[2] Specimen did not break, failure in grip hole.

COATED OR REFURBISHED WALLS

The objectives of this task were to evaluate the sputtering parameters for refurbishing degraded chamber inner walls with OFHC copper and for applying ZrO_2 and graded $Cu-ZrO_2$ as thermal barrier coatings for lowering inner wall surface temperatures to extend thrust chamber life.

EQUIPMENT AND PROCEDURES

For the depositions performed in this task, a post cathode coater as described in Task III (figure 61) was used. In the deposition of OFHC copper, triode sputtering using a DC target voltage was employed. For diode sputtering of ZrO_2 and copper-ZrO_2, RF voltage was used. A summary of the preliminary substrate preparations and sputter cleaning parameters for each deposition is shown in table XXII. The deposition parameters are presented in table XXIII.

The OFHC copper target was machined from wrought OFHC copper rod. The ZrO_2 target was fabricated by plasma spraying ZrO_2 onto a 2.54 cm OD zirconium mandrel. In both cases, the targets were water cooled. Attempts to sputter from a ZrO_2 tube were unsuccessful; while sputtering at high current densitites, the target fractured. This problem promoted the use of the plasma sprayed targets.

The post cathode coater was used to fabricate targets for sputtering the graded OFHC copper-ZrO_2 coatings. The following unique approach was used to make the targets and graded coatings. First, a plasma sprayed zirconia post cathode was shadowed with a stainless steel screen. Then OFHC copper was sputtered from a hollow cathode cylinder onto the post, thus leaving an array of copper hills and valleys on the zirconia. RF sputtering from the post removed copper and formed the first layer of the graded coating. With continued sputtering, the thin layer of copper in the valleys was removed, exposing ZrO_2, which was co-sputtered with OFHC copper from the thicker deposit (hills) region. With continued sputtering, the extent of ZrO_2 increased as the copper was depleted. Eventually, pure ZrO_2 was sputtered to make the outer ZrO_2 layer of the coating.

For all depositions, the substrates were 2.54 cm high OFHC copper rings, 6.6 cm ID. Five rings per deposition were used. 5.08 cm high OFHC copper cylinders were placed below and above the 5 ring substrate stack. All substrates were fixtured on a water-cooled substrate holder.

The deposits generated in this task were evaluated by standard metallographic techniques for structure, bond integrity, surface topography, and thickness. On selected deposits of ZrO_2, quenching in water and liquid nitrogen from 813°K (1000°F) was used to determine deposit adherence. In this testing, 2.54 cm square sections from the coated substrate rings were heated in air for approximately 1800s and then quenched. The evaluation of adherence was based on visual examination.

TABLE XXII. SUMMARY OF TASK V CYLINDER PREPARATION AND SPUTTER CLEANING PARAMETERS

Run Number	Substrate Material	Finishing Treatment, Surface Preparation and Primary Cleaning	Voltage, V	Sputter Cleaning[1] Current, mA	Duration, ks	Pressure N/m²	μ
V-1	OFHC Copper (6.6 cm ID)	ID mechanically buffed with No. 600 grit paper, scrubbed with AJAX®, ethyl alcohol rinse	−25	900	0.30	0.45	3.4
V-2	OFHC Copper (6.6 cm ID)	ID mechanically buffed with No. 600 grit paper, scrubbed with AJAX®, ethyl alcohol rinse	−25	1800	0.30	0.63	4.7
V-3	OFHC Copper (6.6 cm ID)	ID mechanically buffed with No. 600 grit paper, scrubbed with AJAX®, ethyl alcohol rinse	−25	1850	0.30	0.56	4.2
V-4	OFHC Copper (6.6 cm ID)	ID mechanically buffed with No. 600 grit paper, scrubbed with AJAX®, ethyl alcohol rinse	−25	1750	0.30	0.77	5.8
V-5	OFHC Copper (6.6 cm ID)	ID mechanically buffed with No. 600 grit paper, scrubbed with AJAX®, ethyl alcohol rinse	−25	3000	0.30	0.55	4.1
V-6	OFHC Copper (6.6 cm ID)	ID mechanically buffed with No. 600 grit paper, scrubbed with AJAX®, ethyl alcohol rinse	−25	4000	0.30	0.59	4.4
V-8	OFHC Copper (6.6 cm ID)	ID buffed circumferentially with jewler's rouge, scrubbed with AJAX®, ethyl alcohol rinse	−25	3000	0.30	0.49	3.7
V-9	OFHC Copper (6.6 cm ID)	Segmented rings used with many preparations	−25	3200	0.90	0.37	2.7
V-10	OFHC Copper (6.6 cm ID)	Segmented rings used with many preparations	−25	3530	0.30	0.72	5.4
V-11	OFHC Copper (6.6 cm ID)	Segmented rings used with many preparations	−25	3130	0.39	0.70	5.3
V-12	OFHC Copper (6.6 cm ID)	Segmented rings used with many preparations	−25	3190	0.30	0.63	4.7
V-13	OFHC Copper (6.6 cm ID)	ID mechanically buffed with No. 600 grit paper, scrubbed with AJAX®, ethyl alcohol rinse	−25	5000	0.50	0.35	2.6
V-14	OFHC Copper (6.6 cm ID)	ID mechanically buffed with No. 600 grit paper, scrubbed with AJAX®, ethyl alcohol rinse	−25	5000	0.50	0.32	2.4

NOTES:

[1]Substrate cleaned simultaneously with target.

TABLE XXIII. SUMMARY OF TASK V DEPOSITION PARAMETERS[1]

Run Number	Target Material	Substrate Material	Substrate Voltage, V	Substrate Current, A	Target Voltage, V	Target Current, A	Time ks	Time hr	Substrate Temperature[2] °K	°F	Maximum Deposit Thickness nm	mils	Average Deposition Rate nm/s	mil/hr	Pressure N/m²	μ
V-1	OFHC Copper	OFHC Copper	- 25	0.9	- 25	0.52	0.29	0.08	350	170	0.18	7.0	4.3	0.61	0.45	3.4
			- 25	1.8	-500	1.35	15.3	4.25(3)	367	200					0.31	2.3
			- 25	0.9	- 25	1.12	0.29	0.08	nm	nm					0.43	3.2
			+ 12.5	0	-500	1.55	25.2	7.0	377	220					0.27	2.0
V-2	OFHC Copper	OFHC Copper	- 25	1.8	- 25	1.20	0.29	0.09	350	170	0.20	8.0	8.5	1.21	0.63	4.7
			- 25	2.2	-500	1.65	23.4	6.50	377	220					0.33	2.5
V-3	OFHC Copper	OFHC Copper	- 25	1.85	- 25	1.10	0.29	0.08	350	170	0.38	15.0	7.3	1.03	0.55	4.2
			0	0	-500	1.60	23.4	6.5	377	220					0.33	2.5
			0	0	-500	1.60	28.8	8.0	377	220					0.33	2.5
V-4	OFHC Copper	OFHC Copper	- 25	1.75	- 25	1.15	0.29	0.08	350	170	0.27	10.8	5.5	0.78	0.77	5.8
			- 50	1.90	-500	1.70	23.4	6.50	377	220					0.39	2.9
			- 50	1.90	-500	1.70	26.1	7.25	377	220					0.39	2.9
V-5	OFHC Copper	OFHC Copper	- 25	3.00	- 25	1.10	0.29	0.08	Water Cooled (350K–377K)	Water Cooled (170F–220F)	0.23	10.0	4.9	0.70	0.53	4.1
			- 25	3.10	- 25	1.15	0.29	0.08							0.55	4.1
			- 25	3.30	-500	1.50	25.2	7.0							0.37	2.7
			- 25	2.80	- 25	1.25	0.29	0.08							0.47	3.6
			- 25	2.80	- 25	1.20	0.29	0.08							0.47	3.6
			- 25	3.15	-500	1.45	25.2	7.0							0.29	2.2
V-6	OFHC Copper	OFHC Copper	- 25	4.00	- 25	1.25	0.29	0.08	Water Cooled (350K–377K)	Water Cooled (170F–220F)	0.17	6.75	3.4	0.48	0.59	4.4
			- 25	3.85	- 25	1.25	0.6	0.16							0.49	3.7
			- 25	3.50	- 25	1.12	0.29	0.08							0.53	4.0
			- 50	4.00	-500	1.45	23.4	6.50							0.35	2.6
			- 25	3.12	- 25	1.10	0.29	0.08							0.45	3.4
			- :	3.10	- 25	1.10	0.29	0.08							0.43	3.2
			- 50	4.10	-500	1.40	25.2	7.00							0.35	2.6
V-8	OFHC Copper	OFHC Copper	- 25	3.1	- 25	1.4	0.29	0.08	Water Cooled (350K–377K)	Water Cooled (170F–220F)	0.29	11.5	6.5	0.92	0.47	3.6
			- 25	4.5	-500	2.5	23.4	6.50							0.51	3.8
			- 25	2.9	- 25	1.15	0.29	0.08							0.41	3.1
			- 25	2.9	- 25	1.15	0.29	0.08							0.47	3.8
			- 25	4.6	-500	1.2	21.6	6.0							0.49	3.7

NOTES:

[1] Deposition performed in triode discharge

[2] Substrate water cooled

[3] System pumped to below 6.65 x 10^{-4} N/m² (5 x 10^{-7} torr) before each deposition step, sputter cleaned, and deposition continued.

[4] Depositions performed using RF discharge with applied magnetic field (2.8A through coils)

[5] Copper sputtered on ZrO_2 target.

TABLE XXIII. SUMMARY OF TASK V DEPOSITION PARAMETERS[1]
(Continued)

Run Number	Target Material	Substrate Material	Substrate Voltage, V	Substrate Current, A	Target[4] Voltage, V	Target[4] Current, A	Time ks	Time hr	Substrate Temperature[2] °K	Substrate Temperature[2] °F	Maximum Deposit Thickness nm	Maximum Deposit Thickness mils	Average Deposition Rate nm/s	Average Deposition Rate mil/hr	Pressure N/m²	Pressure μ
					Target RF Power (Watts)											
V-9	ZrO₂	OFHC Copper	− 25	3.2	150		0.9	0.25	nm	nm	−	−	−	−	0.37	2.7
			50 (RF)	−	800		72.0	20.0	nm	nm	−	−	−	−	1.60	12.0
			DC Ground													
V-10	ZrO₂	OFHC Copper	− 25	3.53	110		0.29	0.08	nm	nm	0.09	3.5	1.1	0.15	0.72	5.4
			− 50	3.53	110		0.29	0.08							0.45	3.4
			70 (RF)	−	900		86.4	24.0							0.37	2.7
			DC Ground													
V-11	ZrO₂	OFHC Copper	− 25	3.13	100		0.29	0.08	nm	nm	0.13	5.0	1.6	0.23	0.49	3.7
			− 50	3.10	100		1.2	0.33							0.17	1.3
			70 (RF) Floating	−	800		76.5	21.25							0.63	4.7
V-12	ZrO₂	OFHC Copper	− 25	3.19	100		0.29	0.08	nm	nm	0.08	3.0	1.0	0.14	0.63	4.7
			− 50	3.35	100		0.9	0.25							0.50	4.4
			−100	3.50	100		2.0	0.56							0.55	4.1
			Ground	0	850		74.7	20.76							0.27	2.0
V-13	Cu/ZrO₂[5]	OFHC Copper	82 RF Floating	−	800		1.4 86.4	0.40 24.0	nm	nm	0.24	9.4	2.9	0.39	0.35	2.6
V-14	Cu/ZrO₂[5]	OFHC Copper	~0 RF Floating	−	820		1.4 86.4	0.40 24.0	nm	nm	0.11	4.5	1.3	0.18	0.32	2.4

NOTES:

[1] Deposition performed in triode discharge

[2] Substrate water cooled

[3] System pumped to below 6.63×10^{-4} N/m² (5×10^{-7} torr) before each deposition step, sputter cleaned, and deposition continued.

[4] Depositions performed using RF discharge with applied magnetic field (2.8A through coils)

[5] Copper sputtered on ZrO₂ target.

To further evaluate the coating adherence and the effect of the coating on LCF properties, hoop type LCF testing was performed. The test used was identical to that used in Task III.

RESULTS AND DISCUSSION

OFHC COPPER REFURBISHMENT

For the deposition of OFHC copper from a post cathode using triode sputtering, the effects of deposition parameters, namely substrate bias, on the structure, hardness and LCF properties, were investigated.

The use of a -25V followed by a +12.5V bias (run V-1) resulted in areas of recrystallized copper within the deposit, figure 75. The recrystallized regions exhibited a hardness of 64-66 VPN while the other areas of the deposit exhibited higher hardness, 90-100 VPN, table XXIV. In the case where no bias was used, run V-3, with the substrate at ground potential, some recrystallization was observed in the deposit near the original interface and at the interface between the first and second layers, see figure 76. The hardness of this deposit was higher (118 to 137 VPN) than that obtained in the V-1 deposit.

In the other runs performed, the effect of a -25V bias (runs V-2, 5 and 8) and a -50V bias (runs V-4 and 6) was investigated. The representative structures for the -25V and -50V bias substrates are shown in figures 77 and 78, respectively. As with all other deposits in this task, the structure was extremely dense and columnar. In examining the structure in the transverse direction (perpendicular to to the cylinder length) the structure appeared equiaxed. However, in longitudinal sections (parallel to the cylinder length), the structure was columnar, figure 78. This difference in structure is attributed to the pre-coating surface finish resulting from the circumferential buffing operation.

It was apparent from the depositions performed that the 25V and 50V negative bias on the water-cooled substrates increased the effective surface temperature (not measured) to increase adatom mobility and effect deposit nucleation and growth.

Based on the hardness of the deposits produced in this task, the hardness decreased with increasing bias. Although the surface temperatures were not measured, it was apparent that since the substrate hardness also varied, the deposition temperatures must have been significantly different for each deposition, especially in the case of run V-4. In run V-3, where no bias was used, the deposit was significantly harder than the substrate.

The surface of all deposits exhibited a faceted topography, figure 79. Although deposition rate was varied between 3.5 to 8.5 nm/s (0.48 to 1.21 mils/hr), an effect of rate on structure and topography was not observed.
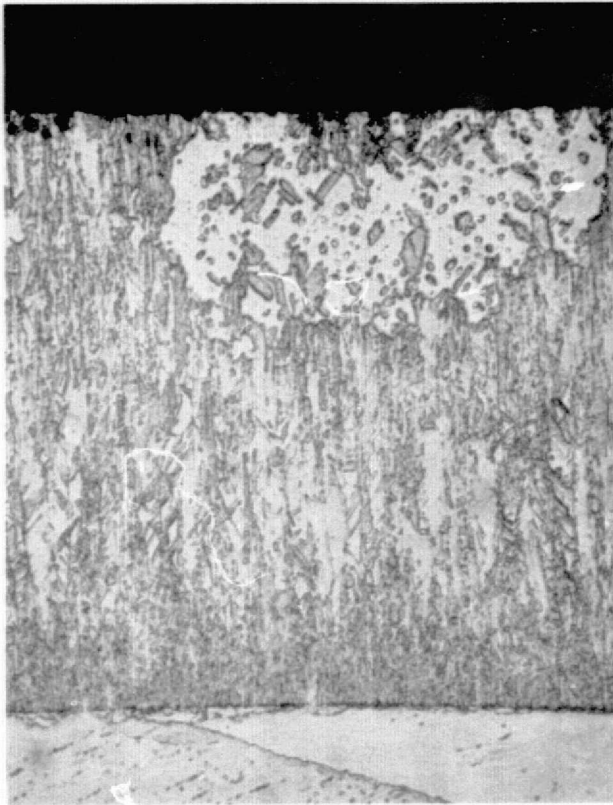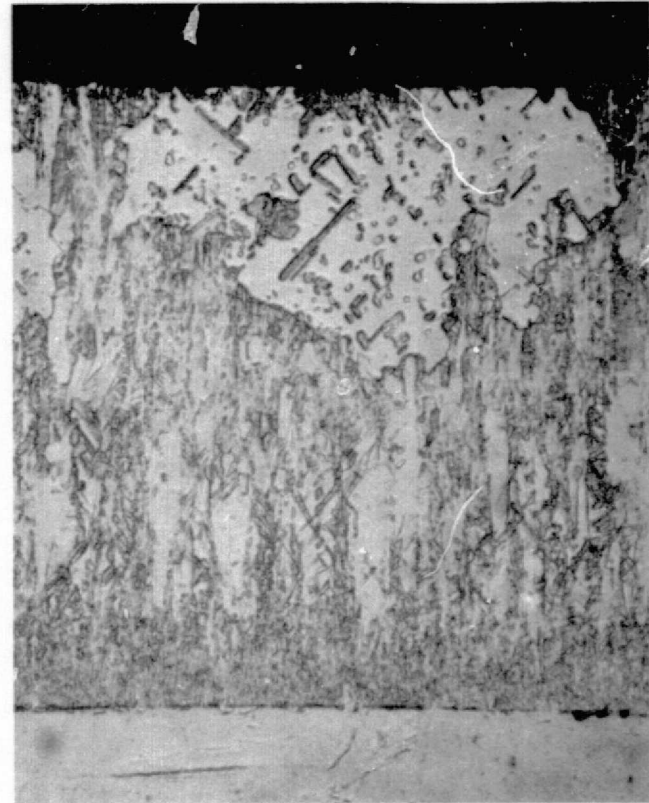
Longitudinal Section   Transverse Section

Mag: 500X

Figure 75.   Microstructure of OFHC Copper Sputtered With a Bias of –25V and +12.5V, Run V-1   FD 91439

TABLE XXIV. HARDNESS OF TASK V OFHC COPPER SUBSTRATE AND SPUTTERED DEPOSIT

Run Number	Substrate Bias	Hardness (VPN 0.2 Kg Load) Deposit			Substrate
		First Layer	Second Layer		
V-1	-25V, +12.5V	96	90	64*	96
		96	96	64	103
		100	96	66	110
V-2	-25V	88	—		90
		90	—		100
		100	—		103
V-3	No Bias (grounded)	118	132		83
		123	137		88
		123	137		88
V-4	-50V	61	59		50
		61	62		50
		70	62		51
V-5	-25V	75	70		90
		78	71		100
		88	73		103
V-6	-50V	80	80		103
		88	80		123
		85	75		103
V-8	-25V	74	80		83
		77	83		90
		80	83		96

*Recrystallized region of deposit
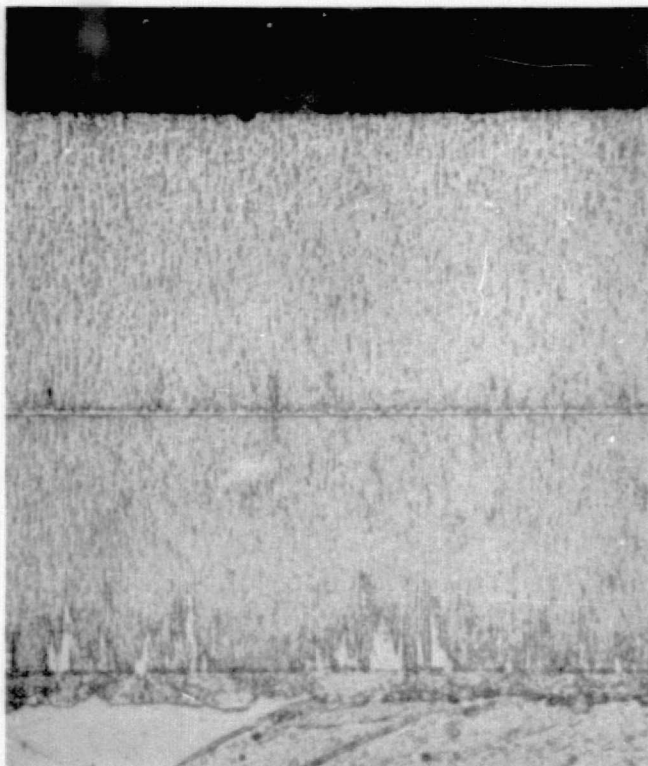
Mag: 250X

Figure 76. Microstructure of OFHC   FD 91440
            Copper Coating on ID of
            OFHC Copper Cylinder.
            Specimen Grounded During
            Deposition (No Bias),
            Run V-3
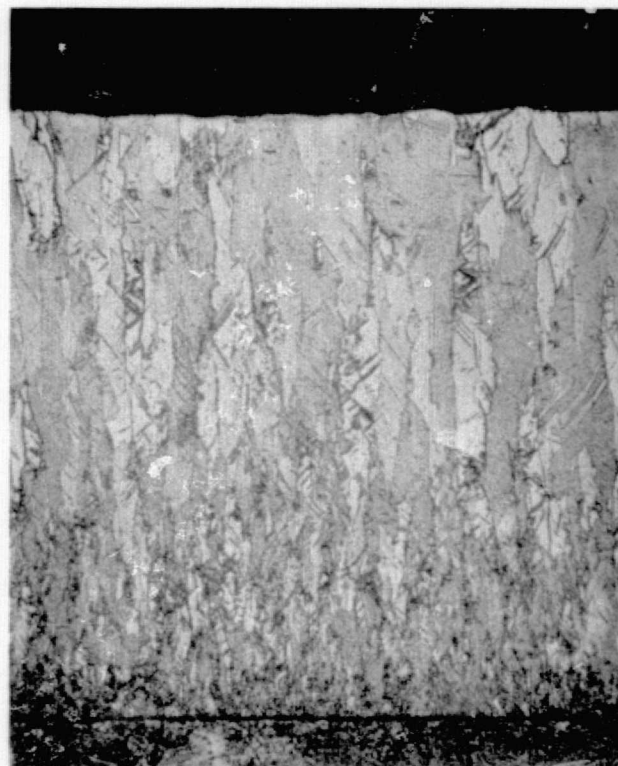
Mag: 250X

Figure 77. Microstructure of OFHC   FD 91441
            Copper Sputtered Using a
            -25V Substrate Bias,
            Run V-8
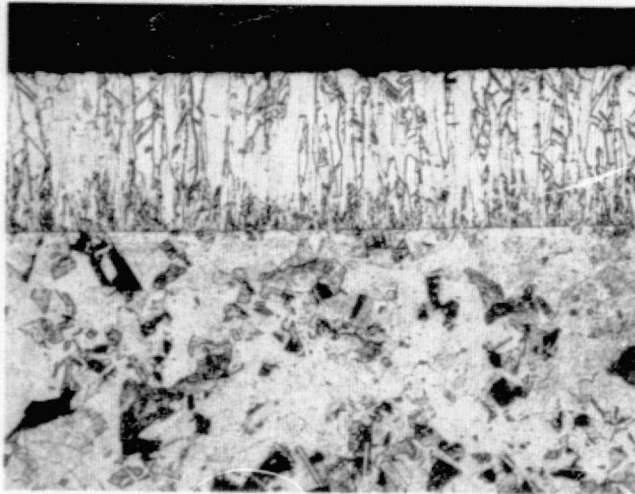
Longitudinal Section 100X   Transverse Section 100X
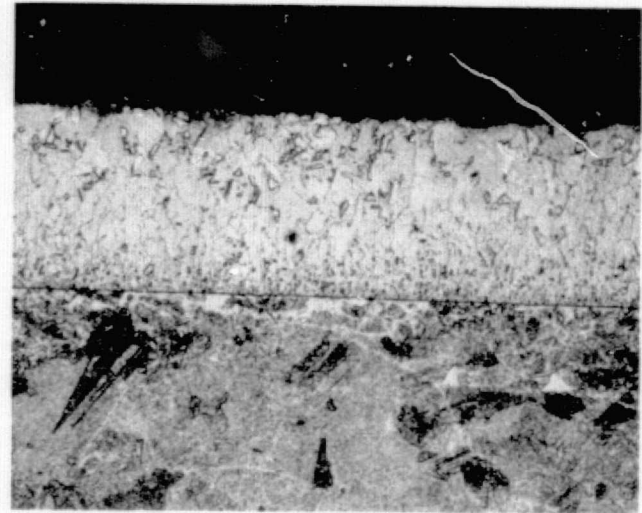
Figure 78.   Microstructure of OFHC Copper Deposited Using a -50V Bias, Run V-4

FD 91442
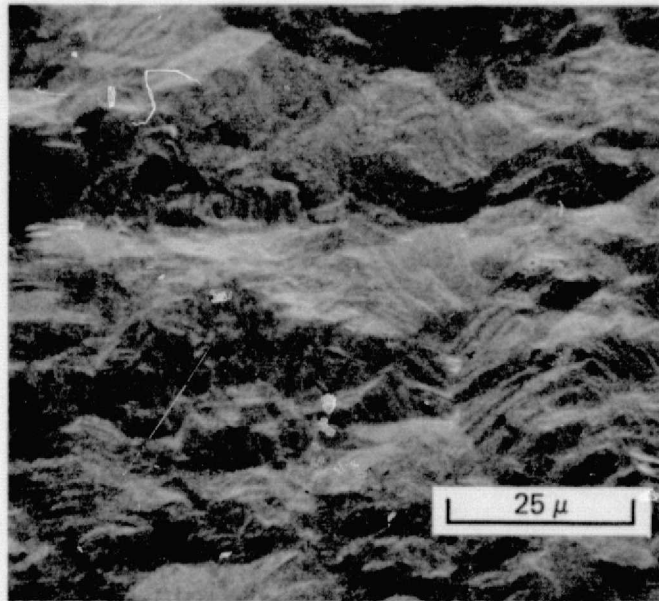
Figure 79. Typical Surface Topography of Task V   FD 91443
Sputtered OFHC Copper Deposits.
(Surface Shown from Run V-6 Deposit)

In comparing the coated to uncoated cylinders in low cycle fatigue testing
at 2% total strain, no decrease in fatigue life of the OFHC copper substrate was
observed due to the presence of coating, table XXV. However, cycles to crack
the deposit varied from 54 to 750. The difference in behavior could not be at-
tributed to deposition conditions or structure. Cracking however, was inter-
granular, occuring in the columnar grain boundaries. It is possible that a com-
bination of the columnar structure and deposit properties caused the variation.
However, with the limited testing a structure-property-fatigue relationship could
not be formulated.

ZrO_2 Coating

RF sputtering from a post cathode was used in the application of the
zirconia (ZrO_2) coating to the inside surface of the 2.6 ID OFHC copper cylinder
segments in runs V-9 to 12.

The overall appearance of the coated substrates and the typical micro-
structure is shown in figure 80. All deposits exhibited a black color which is
indicative of the low temperature monoclinic form of ZrO_2.

In the direct sputtering of ZrO_2 the primary parameters studied were sub-
strate surface finish and substrate bias. Preliminary testing showed that a
surface roughened by vapor blasting made a stronger bond with the ceramic
than did surfaces prepared by chemical etching, polishing with buffing compound,
or hand sanding with 600 grit SiC. The bond region of the vapor blasted, buffed
and polished finishes is shown in figure 81.

132

TABLE XXV. RESULTS OF ROOM TEMPERATURE LCF TESTING OF TASK V SPUTTERED OFHC DEPOSITS

Run Number	Strain Range (%)	Cycles to Deposit Crack[1]	Cycles to Substrate Crack	Cycles to Failure
V-2	-0.8 to +1.2	54	341	701
V-3	-0.8 to +1.2	225	400	640
V-5	-0.8 to +1.2	344	427	961
V-6	-0.8 to +1.2	60	160	817
V-6	-0.8 to +1.2	367	447	668
V-8	-0.8 to +1.2	54	341	701
V-8	-0.8 to +1.2	750	871	923
Base Line[2]	-1.0 to +1.2	-	300	438
Base Line[2]	-0.8 to +1.2	-	400	697

NOTES:

[1] Cracking determined by visual observation

[2] OFHC copper segment, no internal coating, baseline data.

134
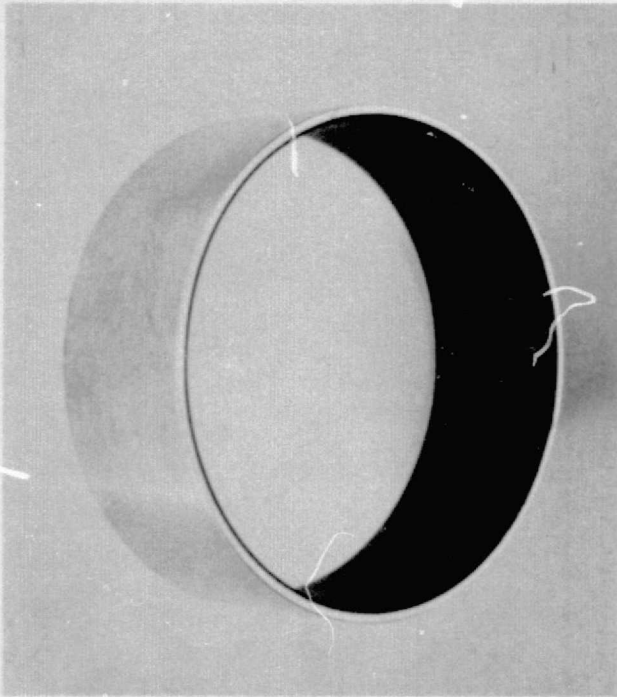
Mag: 1X
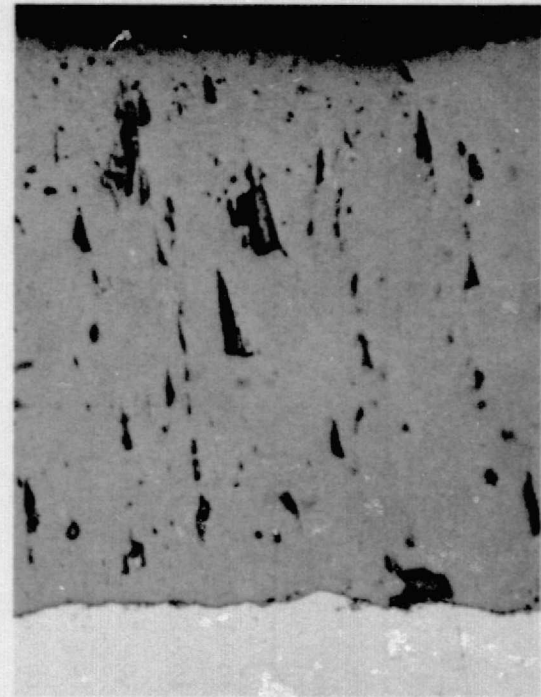
Mag: 1000X

Figure 80. Visual Appearance and Microstructure of ZrO$_2$ RF Sputtered on ID of Cylindrical OFHC
Copper Sample (Surface Prepared by Vapor Blasting), Run V-11

FD 87945

Mounting Material →

ZrO$_2$ →
Bond Region →

OFHC Copper Substrate →

Mag: 100X   Mag: 100X   Mag: 100X

Chemically Etched   Mechanically Buffed   Vapor Blasted

(Poor Adherence)   (Poor Adherence)   (Good Adherence)
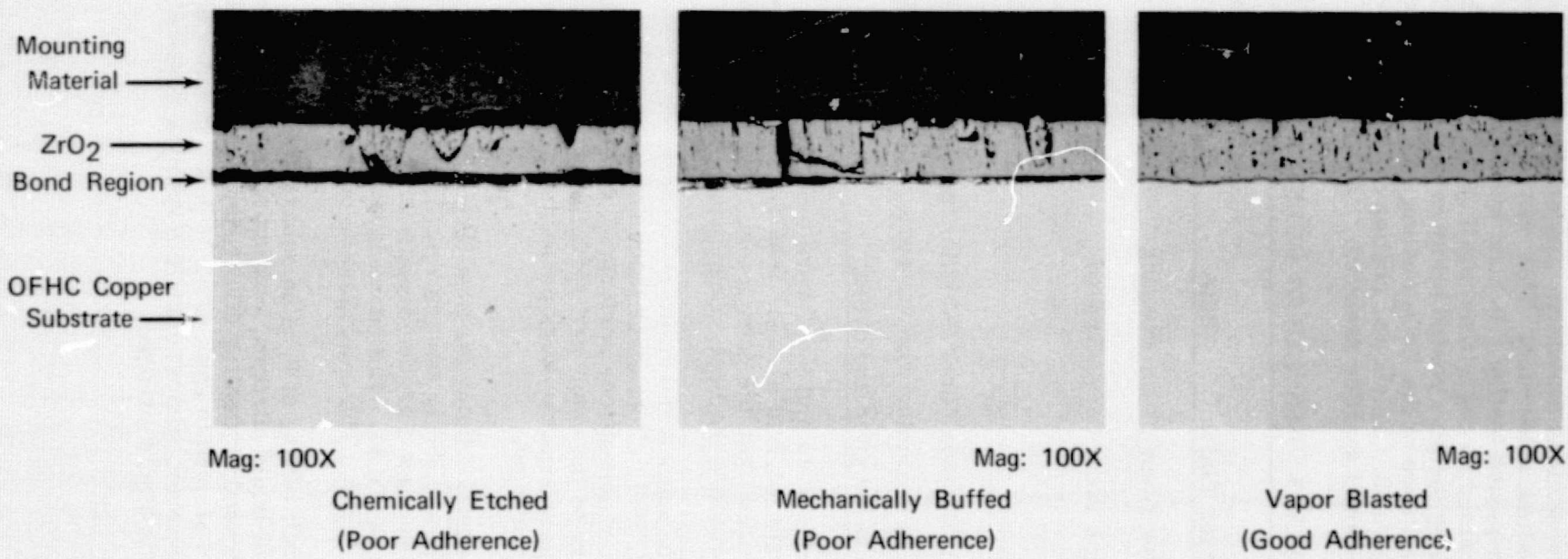
Figure 81. Effect of Substrate Surface Finish on Bonding of RF Sputtered ZrO$_2$ on ID Surface of   FD 87946
OFHC Copper Cylinder (Note Substrate Grounded During Deposition), Run V-12

Of the two bias conditions evaluated, grounded and floating, the floating (-70 RF) bias gave the best adherence. This was observed in bend testing coated samples and in quench testing. In bend testing, the bias-coated 2.6 inch ID rings could be deformed 90 deg without coating spalling. In both water and liquid nitrogen quenching the bias coated samples gave the best adherence, table XXVI. The appearance of the ZrO_2 coating (run V-11) after 10 quench cycles is shown in figure 82. As shown, coating cracking of both samples occurred. However, minimal spalling resulted.

TABLE XXVI. RESULTS OF QUENCH TESTING[1]

Run Number	Surface Finish	Bias	Cycles to Failure LN$_2$	H$_2$O
V-11	Vapor Blast	Floating	6[2]	6[2]
V-12	Vapor Blast	Ground	2[3]	2[3]

NOTES:

[1] One cycle - 813K/180s (1000°F-3 min) immersed in quenchant

[2] Partial spalling beginning with 6th cycle, run to 10 cycles

[3] Completely spalled after 2nd cycle.

Samples from runs V-11 and V-12 were tested for coating adherence in LCF testing at 2% total strain (-0.8 to +1.2%). The results of testing are given in table XXVII. As expected from the quench testing results, the vapor blast surface preparation provided the best coating adherence.

In general, all deposits were similar in structure. Of the sputtering parameters evaluated, little effect other than adherence improvement was obtained. In the limited depositions performed, the feasibility of sputtering adherent ZrO_2 coatings to the inner wall surfaces of thrust chambers was demonstrated. Certainly from the work performed, the parameters for increased adherence were not optimized.

Graded Copper-ZrO_2 - Using the post target as previously described, two depositions, runs V-13 and V-14, were made. The sputter fabricated target was successfully used to generate a graded copper-ZrO_2 coating. The resultant structure is shown in figure 83. The initial layer was OFHC copper, followed by a Cu-ZrO_2 graded layer. The outer portion of the deposit was ZrO_2.

Based upon quench testing of 2.54 on square coated samples from 813K (1000°F) into water and liquid nitrogen, coating adherence was not as good as that produced by the biased or floating direct sputtered ZrO_2. The graded coating from run V-14 started to spall after 3 cycles in water and after 4 cycles in liquid nitrogen. However, almost complete spalling resulted after 4 cycles in water and 5 cycles in liquid nitrogen.

Mag: 3X

H_2O
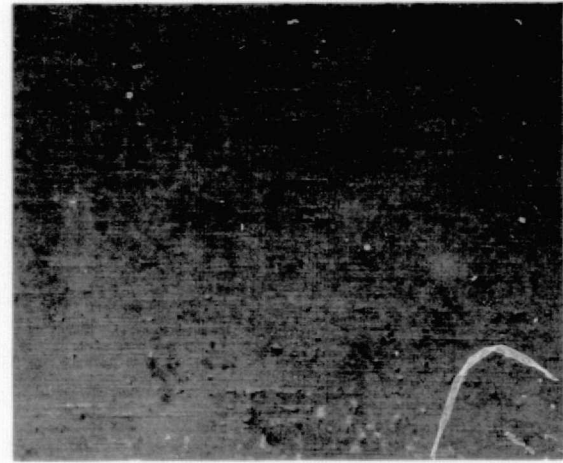
Mag: 3X

LN_2

Figure 82. Appearance of ZrO_2 Coating on OFHC Copper Segments After 10 Quench Cycles from 813°K (Air) Into Water and Liquid Nitrogen, Run V-11

FD 87944

TABLE XXVII. RESULTS OF ROOM TEMPERATURE LCF TESTING OF
ZrO$_2$ AND GRADED Cu-ZrO$_2$ DEPOSITS

Run Number	Substrate Surface Preparation	Strain Range (%)	Cycles to Coating Crack[1]	Cycles to Metal Crack	Cycles to Failure	Coating Adherence at Fracture Area[2]
V-11	Buffed	-0.8 to 1.2	2	46	474	Gross deposit spalling.
V-11	Vapor Blasted	-0.8 to 1.2	195	227	543	Spalled 0.42 cm (0.125 in.) from fracture.
V-12	Vapor Blasted	-0.8 to 1.2	43	100	221	No spalling.
V-13[3]	-[4]	-0.8 to 1.2	27	92	354	No spalling
V-13[3]	-[4]	-0.8 to 1.2	15	257	497	Spalled 0.84 cm (0.250 in.) from fracture, one side only.
V-14[3]	-[4]	-0.8 to 1.2	93	181	411	Spalled 0.42 cm (0.125 in.) from fracture, one side only.

NOTES:

[1] Cracks determined by visual observation

[2] Visual observations

[3] Graded Cu-ZrO$_2$ deposits

[4] Substrate sputtered to make target.
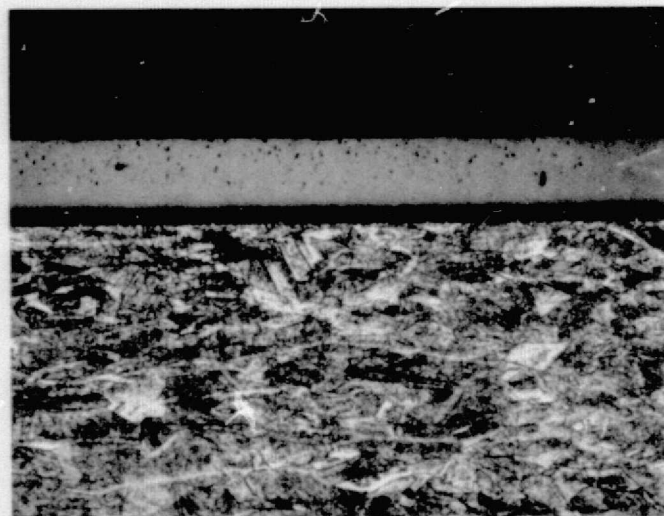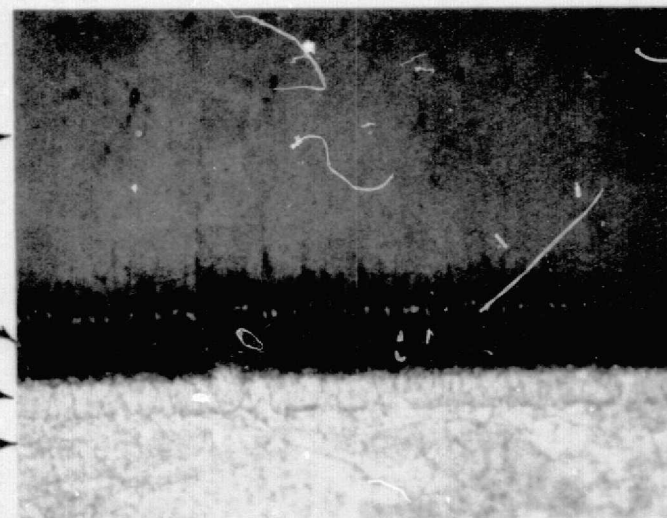
Figure 83. Microstructure of Graded OFHC Copper ZrO_2 Coating on Inner Surface of 2.6 inch ID OFHC Copper Cylinder (Applied by RF Sputtering; Etched), Run V-14

FD 87947

The graded Cu-ZrO$_2$ coatings from runs V-13 and V-14, were evaluated in LCF testing. The LCF behavior and adherence of graded deposits showed little difference from the ZrO$_2$ coated samples, table XXVII. In the areas that did spall the spalling resulted at the interface between the sputtered copper and Cu-ZrO$_2$ graded layers.

With the work performed the viability of making a graded coating by sputtering was demonstrated. However, with the limited depositions performed, the graded Cu-ZrO$_2$ performance was not optimized.

TASK V

CONCLUSIONS

Based on the depositions and evaluations performed in this task, the following conclusions were made:

1. Sputtering from a post cathode in a triode discharge was successful in generating dense deposits of OFHC copper to the inner walls of 6.6 cm ID OFHC copper segments. Increasing substrate bias decreased the deposit hardness, probably as a result of increased surface temperature.

2. The results of low cycle fatigue testing (2% total strain) showed that sputtered OFHC copper (of the structure and properties deposited) on the inner wall did not decrease OFHC copper substrate fatigue life. Based on the work performed, refurbishment of degraded thrust chambers can readily be performed by sputtering.

3. In direct RF sputtering of ZrO$_2$, an adherent ZrO$_2$ coating on inner wall surfaces of 6.6 cm ID OFHC copper cylinders was obtained. With the parameters evaluated a self-biased or floating substrate and a vapor blast surface preparation gave the best adherence.

4. A sputter fabricated target was successfully used to generate graded OFHC copper-ZrO$_2$ coatings. However, with the limited depositions performed, an improvement in adherence over the direct sputtered ZrO$_2$ was not obtained. Improvements in adherence possible, through additional parameter studies warrant further investigation.

PROGRAM SUMMARY

In this program techniques and materials were developed and evaluated for the fabrication and coating of advanced high performance regeneratively cooled thrust chambers.

The successful use of sputter deposition in the fabrication of the regeneratively cooled thrust chambers was found to be most dependent on the application of a suitable filler material. Of the five materials evaluated as fillers in Task I, aluminum was found to provide the highest bond strength and be most desirable for chamber fabrication. The methods of filling with aluminum by flame spraying and slurry techniques were found to be unacceptable. The filler porosity associated with these deposition techniques contributed to extensive outgassing during sputter cleaning and deposition. The aluminum filler is attractive since it does not promote rib contamination during sputter cleaning and can readily be removed by leaching with sodium hydroxide. Application of a dense aluminum filler by sputtering offers potential and should be investigated in future work.

In filler evaluation an OFHC copper closeout layer was deposited to filled ribbed wall cylinders using a hollow (cylindrical) cathode and a diode discharge. With the configuration of substrate and target, the diode mode was found to be unacceptable for generating a dense high quality closeout layer structure Further analysis of bulk OFHC copper deposits sputtered from a hollow cathode (Task II), using a diode discharge, showed a relationship of deposit structure to deposition rate and substrate temperature. At conditions of low substrate temperature, crystallite size and openness of the structure increased with increasing deposition rate. At elevated temperatures it was possible to produce an equiaxed, ductile structure, but only at low deposition rates. At higher deposition rates an open structure resulted having recrystallized, equiaxed grains within large, poorly bonded crystallites. Similarly 0.15Zr-Cu alloy, sputtered from the hollow cathode using a diode discharge, exhibited open type structures for all conditions evaluated. Low deposition rates significantly reduced the openness of the structure as did increasing substrate temperatures.

The use of triode discharge with the higher degree of ion bombardment with biasing was successful in generating dense, high strength structures of 0.15 Zr-Cu at low substrate temperature and at basically equivalent conditions to those employed in sputtering from a diode discharge. Although not investigated, the use of triode discharge for closeout layer application should provide a significant improvement over diode sputtering.

In investigating other bulk sputtered materials for inner wall structures (Task II) co-sputtering of Al_2O_3-Cu and SiC-Cu were found to yield deposits of high strength. Co-sputtered deposits of both systems resulted in deposit strength over twice that of OFHC copper, and the highest of the copper materials evaluated. However, in the co-sputtered Al_2O_3 and Cu or SiC-Cu, it was not apparent that a true dispersion strengthened alloy was formed. The strengthening of the Al_2O_3-Cu and SiC-Cu was attributed to solid solution strengthening mechanisms. As an alternate to bulk sputtered inner wall structures, layered deposits of OFHC copper and 0.15Zr-Cu were investigated as means of improving chamber fatigue life (Task III). Deposits having four layers, with increasing

hardness from substrate to surface, were produced by sputtering from a post cathode. With the structures evaluated, the OFHC copper layered structure did not affect low cycle fatigue properties over unlayered wrought OFHC copper. With the four layer 0.15Zr-Cu structure of varying hardness, low fatigue properties resulted. A 100% sputtered 0.15Zr-Cu, comprised of 13 layers of constant hardness, exhibited excellent fatigue properties. Post cathode sputtering produced dense deposits at all deposition conditions investigated.

For evaluating alternate means of strengthening thrust chambers, sputtered Ti-5Al-2.5Sn, NASA IIB-11, aluminum and Al_2O_3-Al alloys were evaluated as high strength chamber outer jackets (Task IV). Of the materials evaluated, the NASA IIb-11 provided the highest tensile strength as deposited. The aluminum and Al_2O_3-Al materials as sputtered exhibited tensile strength over double that of wrought aluminum. With the properties obtained, these materials (NASA IIb-11, aluminum, or Al-Al_2O_3) would be effective as outer chamber jackets.

Techniques for refurbishing degraded thrust chambers with OFHC copper and coating thrust chambers with protective ZrO_2 and graded ZrO_2-copper thermal barrier coatings were developed (Task V). No decrease in substrate fatigue strength was observed with OFHC copper sputtered to the inner wall surface of simulated chamber segments. Adherent ZrO_2 coatings were obtained in sputtering from a post cathode using a floating RF bias and a vapor blast surface preparation. Using sputter fabricated targets, techniques were developed to apply graded ZrO_2-copper coatings. However, with the limited depositions performed, the properties and adherence of the direct sputtered and graded Cu-ZrO_2 were not optimized.

ACKNOWLEDGMENTS

REFERENCES

1. McClanahan, E. D., R. Busch, and R. W. Moss, "Property Investigation and Sputter Deposition of Dispersion-Hardened Copper for Fatigue Specimen Fabrication," Final Report, Contract NAS3-17491, 12 November 1973.

2. McCandless, L. C., and L. G. Davies, "Development of Improved Electroforming Technique," NASA CR-134480, November 1973.

3. American Metal Climax, Inc., New York, New York.

4. AIRCO, Inc., Riverton, New Jersey.

5. Cerro Copper and Brass Company, Bellefonte, Pennsylvania.

6. Hysol Division, Dexter Corporation, Olean, New York.

7. Teleflex, Inc., Sermetel Division, North Wales, Pennsylvania.

8. Gill, W. D., and E. Kay, "Efficient Low Pressure Sputtering in a Large Inverted Magnetron Suitable for Film Synthesis," Review of Scientific Instruments, Vol. 36 (1965) 277.

9. Thornton, J. A., "Influence of Apparatus Geometry and Deposition Conditions on the Structure and Topography of Thick Sputtered Coatings," presented at the American Vacuum Society Conference on Structure – Property Relationships in Thick Film and Bulk Coating, 28-30 January 1974, San Francisco, California.

10. Movchan, B. A., and A. V. Demchishin, "Structure and Properties of Thick Vacuum Condensates," Fiz. metal. metalloved., 28 (1969) 653.

11. Spalvins, T., and W. A. Brainard, "Nodular Growth in Thick Sputtered Metallic Coatings," J. Vac. Sci. Technol. 11 (1974) 1186.

12. Silicone Products Dept., General Electric Co., Waterford, New York.

13. Ceradyne Inc., Chatsworth, California.

14. Metal Powder Division, Federal-Mogul Corporation, Detroit, Michigan.

15. Reactive Metals Inc., West Hartford, Conn.

16. Alcan Sales, Division of Alcan Aluminum, New York, New York.